The Role of Peroxidasin in Basement Membrane Physiology and Human Disease

By

Abraham Scott McCall

Dissertation

Submitted to the Faculty of the

Graduate School of Vanderbilt University

in partial fulfillment of the requirements

for the degree of

DOCTOR OF PHILOSOPHY

in

Pharmacology

August, 2015

Nashville, Tennessee

Approved:

David G. Harrison, M.D.

Sean S. Davies, Ph.D.

Ambra Pozzi, Ph.D.

Dan M. Roden, M.D.

Billy G. Hudson, Ph.D.

PHARMACOLOGY

The Role of Peroxidasin in Basement Membrane Physiology and Human Disease

Abraham Scott McCall

Dissertation under the direction of Professor Billy G. Hudson

Basement membranes are a distinct form of extracellular matrix responsible for signal transduction and mechanical integrity throughout development, in mature tissues, and during wound healing. The collagen IV scaffold of basement membranes relies on a sulfilimine crosslink (S=N) between methionine and lysine for its essential function of maintaining basement membrane architecture. The sulfilimine crosslink is formed by the heme peroxidase, peroxidasin. The precise mechanism by which peroxidasin forms sulfilimine crosslinks, or if this crosslinking process is involved in disease, remains largely unknown. Biochemical investigation of peroxidasin-catalyzed formation of the crosslink found that bromide (Br^-) appeared to be the preferred enzymatic cofactor through its conversion to hypobromous acid (HOBr). Through my development of Br-free salts, purified proteins, and *in vitro* cell culture models of basement membranes, Br^- was shown to be essential to the formation physiologically observed levels of sulfilimine crosslink. I further investigated the underlying mechanism of sulfilimine formation with chemical crosslinking, mass spectrometry analysis, and modeling. These approaches cumulatively supported the presence of a S-Br^+ (bromosulfonium-ion) intermediate by the crosslinked methionine of the NC1 domain of collagen IV as the key reaction intermediate and energetic basis for bromines role in sulfilimine crosslinking. The essentiality of Br was therefore tested *in vivo* in *Drosophila* by developing novel Br-free culture techniques. I found that dietary Br-deficiency is lethal in *Drosophila* while Br-replenishment restores viability, demonstrating a physiologic Br^- requirement. Importantly, through electron and fluorescence microscopy, I was also able to show that Br-deficient flies phenocopy the developmental and basement membrane defects observed in peroxidasin mutants which indicates a functional connection between Br^-, collagen IV, and peroxidasin. These data collectively established that Br^- is required for sulfilimine crosslinking of collagen IV, an event critical for basement membrane assembly and tissue development. Thus, bromine is an essential trace element for animals through the enzymatic activity of peroxidasin, and Br-deficiency may be relevant to basement membrane alterations observed in patients undergoing dialysis, receiving total parenteral nutrition, and in some smoking related disease. I also sought to test the hypothesis that anti-peroxidasin autoantibodies occur in a specific rapidly progressive glomerulonephritis known as Goodpasture's disease (GP). Goodpasture's Disease is characterized by anti-collagen IV NC1 antibodies and the sulfilimine crosslink is thought to modulate immunogenicity of the collagen IV epitopes. Many GP patients have concurrent autoantibodies which recognize myeloperoxidase (MPO), a structurally related heme peroxidase to peroxidasin. Through testing multiple independent patient cohorts by immunoassay, I found anti-peroxidasin autoantibodies in GP patient sera, both before and at the time of clinical presentation. Unexpectedly, the anti-peroxidasin specific antibodies cross-react with coated, but not native MPO, accounting for a subset of the historically characterized dual-positive (anti- collagen IV and anti-MPO) patients. I also found that anti-peroxidasin antibodies inhibited HOBr production, suggesting a possible contribution of these antibodies in GP pathogenesis within this subset of anti-peroxidasin positive patients. These studies demonstrate chemical, biochemical, and tissue level evidence for the role of peroxidasin and Br^- in the assembly of sulfilimine-crosslinked collagen IV scaffolds in basement membranes and peroxidasin's potential role in disease, including as a novel autoantigen in a subset Goodpasture's disease patients.

Acknowledgements

I would first like to thank my mentor Billy G. Hudson. During my time in the lab, he pushed me to excel both experimentally and intellectually in a way no one had before. I'm incredibly grateful for the opportunities he provided me while I was under his guidance; they made my time in graduate school everything I could have hoped. The constant pursuit of novelty from truly fundamental biology, especially with chemical detail, is the biggest lesson I will carry forward from our time working together.

Next, I would like to sincerely thank my committee, Drs. David Harrison, Ambra Pozzi, Sean Davies, and Dan Roden. My path through graduate school would charitably be described as unorthodox, and their willingness to work with me through this process has meant a great deal. The flexibility, time given, and generosity shown was genuinely appreciated. I am excited for these mentoring relationships to extend beyond graduate school.

I would like to explicitly acknowledge and thank 'Team Bromine' for their contributions to the final manuscript and to my training in the process. Dr. Gautam Bhave and I worked closely on many aspects of the project, including the design of Br-free Chloride purification apparatus and subsequent experimental designs of all Br-free purification and production methods for proteins, media, and *Drosophila* culture conditions. Dr. Bhave's previous fundamental work on peroxidasin, both in terms of its biochemistry and the establishing the laboratory techniques required for its study, enabled this work to proceed at the astounding speed it did. The technical advances required with Br-free materials in this work were substantial, and while I conducted the experiments, it was our ability to work together that really brought the Br-free experimental concept to fruition. Dr. Chris Cummings performed initial experiments on peroxidasin cofactor preference which initiated our group's collective interest in Br as a cofactor. He kindly allowed me to present our collaborative work in Figure 6A and D, and an experiment he performed in Figure6B to facilitate my explanation of the progression of the experiments. The drafting of the manuscript was a long process, but working with Dr. Cummings on many of the drafts was a great experience. Dr. Roberto Vanacore and I worked together on the mass spectrometry analysis, which would not have been possible without his expertise. The time he took to teach me how to conduct the analysis which ultimately appeared in the paper was a foundational piece of my training in the lab. Our work proved to be the backbone of my ability to quantify the mechanistic aspects of the sulfilimine crosslinking. Dr. Andrea Page-McCaw was instrumental in guiding the *in vivo* fly work, working closely with Dr. Bhave and me to develop the Br-free culture techniques, genetics, and assays which we ultimately used. Since I performed all of *Drosophila* work in her lab, I genuinely appreciated her hospitality, concern for my success, and mentorship in a field of science to which I was completely new. It was a privilege to be able to work this group of people.

Dr. Vadim Pedchenko, Dr. Stephen Olson, Dr. Agnes Fogo, and Ms. Ellen Donnert also deserve recognition for their resources, assistance, and insight, with the anti-peroxidasin antibody project. I am also grateful to K.L. Rose at Vanderbilt Mass Spectrometry Resource Center; J. Clanton, X. Wang, and E. Shannon for assistance with Drosophila in the Page-McCaw lab; J. Williams for assistance with Electron Microscopy and sample preparation, performed with use of the VUMC Cell Imaging Shared Resource; and the Bloomington Drosophila Stock Center, Yale FlyTrap, and the VDRC for fly stocks; and S. Vaughn in the VUMC Hormone Assay and Analytical core for her assistance with cytokine assays.

My other colleagues in the Hudson lab, C. Jones-Paris, A. Fidler, K. Brown, C. Darris, S. Chetykrin, I. Ero-Tolliver, S. Colon, N. Danylevych were exceptional resources, friends, and support throughout my time in the lab. The technical assistance and advice of P. Todd and M. Rafi was invaluable.

Dr. Terry Dermody, Dr. Larry Swift, and Ms. Melissa Krasnove in the Medical Scientist Training Program have provided important guidance, advice, and kindness throughout my training. It is deeply appreciated. I also am grateful for the support of Dr. Joey Barnett, Dr. Vsevolod Gurevich, Dr. Christine Konradi, and Ms. Karen Geig in the Department of Pharmacology.

Finally, I would like to thank my family, my fiancée Natalie, and my past mentors (S. Kraft and G. Conrad), without whom none of this would have been possible nor would it mean so much.

Sources of Funding: This work was supported by NIH R01 DK18381, NIH F30 DK100094, NIGMS T32 GM07347 to the Vanderbilt Medical-Scientist Training Program and the Canby Robinson Society of the Vanderbilt University Medical Center.

Table of Contents

List of Figures

List of Tables

Chapter I

Introduction

Basement membrane architecture

Basement membranes are a conserved, unique, and specialized form of extracellular matrix responsible for signal transduction and mechanical integrity in epithelial and endothelial tissues (Bissell, 1997; Daley and Yamada, 2013; Morrissey and Sherwood, 2015). Through the ability to bind and control growth factor gradients such as bone morphogenic proteins (Wang et al., 2008) as well as constrain the physical growth of cells as part of tissue development (Haigo and Bilder, 2011), and even guide the differentiation of stem cells into functional organs such as kidneys and lungs (Song et al., 2013), the basement membrane possess a unique functional niche across all animal tissue types (Figure 1A). Another essential feature is the critical role re-establishment of the basement has in appropriate wound healing after injury, which seems to represent the bifurcation between scarring and regeneration of a wound (Thorning and Vracko, 1977; Vracko, 1974). These features collectively support the idea that the basement membrane serves as a key nexus in tissue development and homeostasis.

The main constituents (by mass) of the basement membrane are collagen IV, laminin, perlecan, nidogen, and several other glycosaminoglycans. (Hynes and Naba, 2012; Yurchenco, 2011)(Figure 1B). Based on the particular demands of the tissue,

additional components can be doped into the matrix to aid in organ specific function. For example, the heparan sulfates in the glomerular basement membrane(GBM) of the kidney assist in providing an inherent negative charge to the GBM and endowing some filtration specificity which helps the kidney exclude albumin from the urine (Groffen et al., 1999) (Figure 1C).

Basement membrane properties are also fine-tuned through the step-wise secretion and subsequent selection of subunits for the main integral basement membrane proteins. For example, during development, laminin is deposited as the initial and indispensable component of the basement membrane and then followed by collagen IV when additional integrity is required during organogenesis (Poschl et al., 2004). In addition to the change in protein content, different gene products yielding different isoforms of integral membrane proteins can be expressed through development before forming the mature basement membrane network. In the glomerular basement membrane for example (Figure 1C), the ubiquitous α112 predominant network of collagen IV (composed of two α1 and one α2 chain of collagen IV as a α112 protomer) is replaced by the α345-predominant network in the mature basement membrane (Abrahamson et al., 2013). While the exact reasons these different collagen chains are incorporated is unclear, the tissue specific expression patterns of basement membrane proteins have profound end-organ functional effects and contribute to multiple conditions. (Boudreau et al., 1995; Hudson et al., 2003)

Covalent crosslinking is another consistent and foundational feature of basement membranes.(Figure 1B) Collagen IV, crosslinked at multiple places along the length of the molecule, requires at least two enzymes, peroxidasin (PXDN) and lysyl oxidase

family members (LOX) to be fully integrated in the matrix (Bhave et al., 2012; Bignon et al., 2011). The recent discovery of the sulfilimine bond (S=N) as the crosslink within the carboxy terminus non-collagenous 1 domain (NC1) of collagen IV, and the ensuing discovery of peroxidasin as the enzyme responsible, has thrown this post-translational modification into sharp relief as fundamental to collagen IV function within the basement membrane. Laminin shares the need for crosslinking to achieve its optimal function within the basement membrane, with another unique enzyme (QSOX- quiescin sulphydryl oxidase) required for the formation of different disulfide mediated crosslinks (Ilani et al., 2013). The overall degree of crosslinking strongly influences the mechanical properties of the basement membrane, its biologic activity, as well as its longevity *in vivo* (Chaudhuri et al., 2014; Levental et al., 2009).

The extracellular, insoluble, and highly crosslinked nature of the basement membrane necessitates that the turnover of these networks is at a different pace from intracellular proteins. While the typical intracellular protein has a half-life of hours to days (Eden et al., 2011), tissue to tissue variability of basement membrane half-life can vary from weeks to decades, with high tissue specificity.(Walker, 1972b, 1973) Through designed experiments in rats and inadvertent experiments (silver toxicity) in humans, the colonic basement membrane appears to have a half-life measured in weeks (likely around 1-2 weeks)(Walker, 1972a; Walker, 1972b), while the glomerular basement membrane appears to have half-life on the order of several months

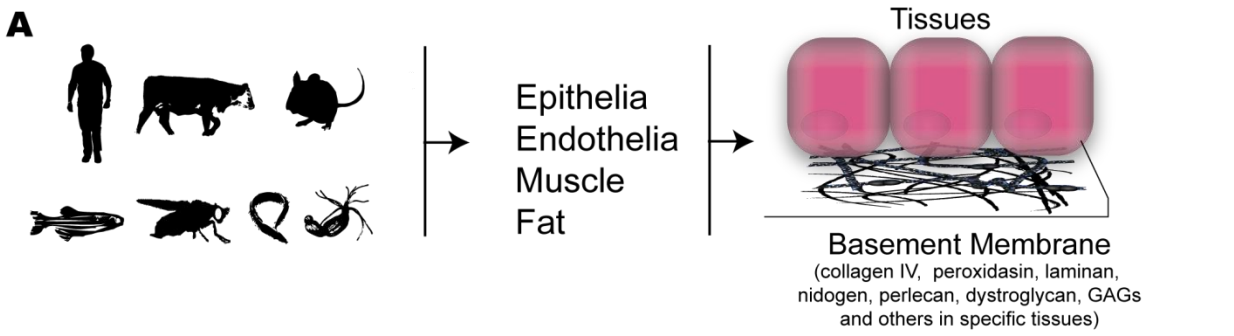
A
Tissues
Epithelia
Endothelia
Muscle
Fat
Basement Membrane
(collagen IV, peroxidasin, laminan, nidogen, perlecan, dystroglycan, GAGs and others in specific tissues)

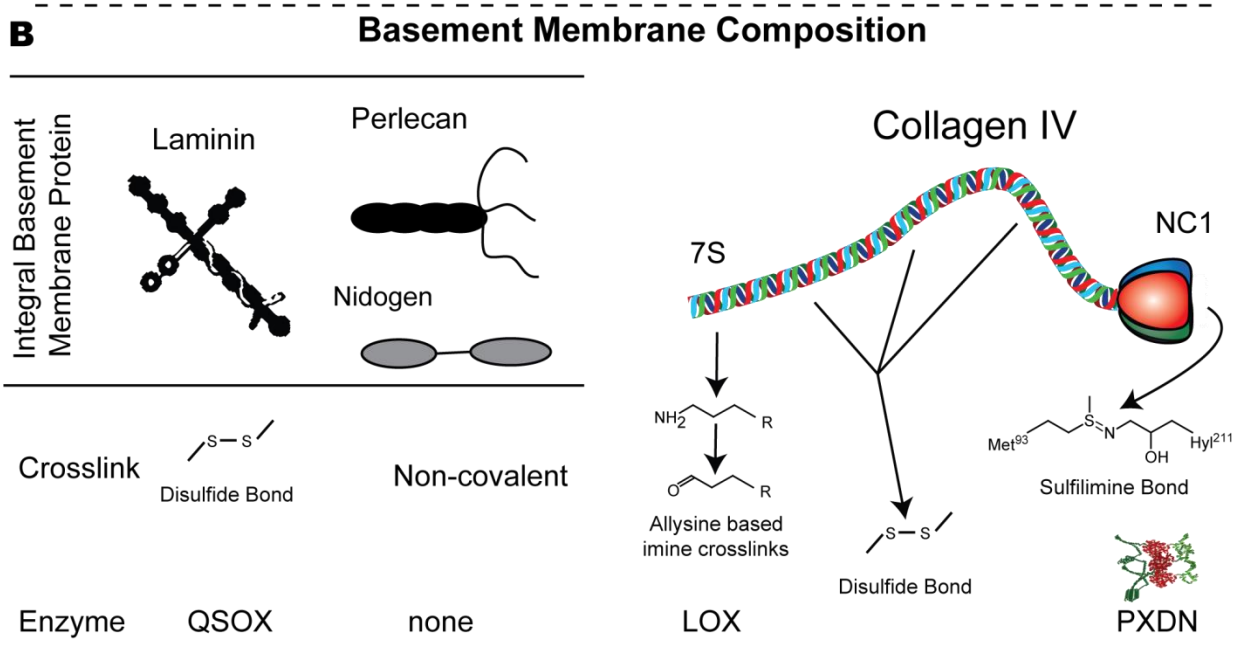
B
Basement Membrane Composition
Integral Basement Membrane Protein
Laminin
Perlecan
Nidogen
Collagen IV
7S
NC1
Crosslink
Disulfide Bond
Non-covalent
Allysine based imine crosslinks
Disulfide Bond
Sulfilimine Bond
Enzyme
QSOX
none
LOX
PXDN

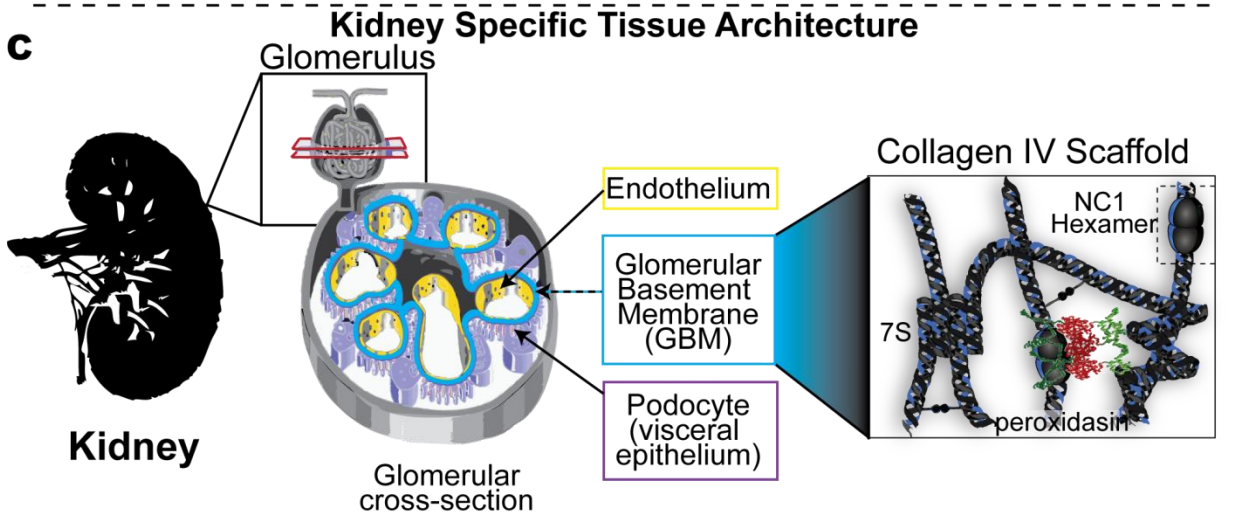
C
Kidney Specific Tissue Architecture
Glomerulus
Kidney
Glomerular cross-section
Endothelium
Glomerular Basement Membrane (GBM)
Podocyte (visceral epithelium)
Collagen IV Scaffold
NC1 Hexamer
7S
peroxidasin

Figure 1. Tissues architecture and basement membrane composition and crosslinking

Figure on Previous Page

(**A**)An overview of tissue organization in animals, focusing on the interaction of cell layers with the underlying basement membrane

(**B**) The major protein components, their crosslinking, and the enzymes responsible for that crosslinking. The integral membrane components, defined as those protein with an intrinsic structural role in the basement and the crosslinks found within those proteins. The enzymes responsible for crosslinking are noted below the respective location of the crosslink in the protein. The collagen protomer showing the 7S N-terminal region, locations within the triple helical portion of the collagen protomer responsible for disulfide formation with other collagen IV protomers once in the matrix, and the c-terminal NC1 domain (Non-Collagenous 1 domain) which binds another NC1 domain to form a collagen IV NC1 hexamer in the basement membrane. The sulfilimine crosslink in the NC1 hexamer occurs between a juxtaposing lysine and methionine. QSOX (Quiescin-sulfhydryl oxidase), LOX (Lysyl-oxidase family members including the LOX-like enzymes), PXDN (peroxidasin). The enzyme responsible for collagen IV disulfide crosslinking is unknown.

(**C**) An overview of the glomerular basement membrane (GBM) within the glomerulus and its surrounding cell types. A simplified model of the mature collagen IV network within basement membrane and peroxidasin localization to facilitate sulfilimine crosslinking. The 7S domain

(approximately 100 days (Price and Spiro, 1977)). These widely variable rates of basement membrane turnover suggest an additional level of regulation for the basement membrane and the corresponding epithelial cell layer responsible for its deposition.

The interplay of composition, crosslink status, and half-life of the basement membrane couples with the ability of the cell to sense its mechanical environment to appropriately drive differentiation during development and tissue homeostasis. In an important example of all the aforementioned features, the environment facilitated by the basement membrane (both in terms of mechanical strength and composition) is essential to maintaining an appropriate intestinal stem cell niche (Amcheslavsky et al., 2009; Watt and Huck, 2013). As part of this overall picture of basement membrane synthesis and architecture, collagen IV is an essential structural role with important signaling contributions.

Collagen IV composition and function in the basement membrane

Collagen IV, in its final form in the basement membrane, is composed of two protomers joining head to head via the carboxy terminus NC1 domains, and four protomers associating as part of the amino terminus 7S domain (Figure 1B-C). These two separate points of attachment facilitate the “network forming” behavior of collagen IV. Each promoter is the combination of three individual α chains. The most ubiquitous protomeric form, and therefore network, found within all basement membranes in the human body is α112.(Khoshnoodi et al., 2008) As mentioned earlier, other collagen IV networks are expressed in a tissue specific manner. In total, collagen IV genes (COL4A1-6) encode six distinct chains for which the products are referred to as α-

chains (e.g. α1-6), expressed differentially, with specific stoichiometries for final protomers. The typical composition of a protomer is two α chains derived from α1, 3, or 5 and one chain from α2, 4, or 6 to produce the common forms of protomeric collagen IV α112 and α345 . The specific chain compositions are thought based on recognition of α2 NC1 domain for the conjugate NC1 domain in α1 (and likely α4 chain selecting α3 and α5 by homology) to limit the number of permutations observed within the matrix. (Khoshnoodi et al., 2006). While α112 is ubiquitous and the main collagen IV expressed early in development, the other networks identified, such as α345 (expressed in the glomerular basement membrane, lung, testes, eye and ear), and the recently identified α112556 (found in the aorta) appear in the final, functionally mature basement membranes. (Hudson, 2004; Robertson et al., 2014). The specific role of the collagen IV chains in the basement membrane has been dissected through the use of genetic knockout of α1 and α2, which somewhat surprisingly did not prevent basement membrane deposition, however did result in early embryonic lethality in mice through an apparent disruption of basement membrane integrity at later developmental stages (Poschl et al., 2004). Gene mutations within α1 chain (COL4A1) in humans produce a range of phenotypes, with the common themes of small vessel/microvessel fragility (resulting in hemorrhagic stroke) and porencephaly depending on the severity of the mutation. (Gould et al., 2005; Gould et al., 2006; Weng et al., 2012) Genetic defects mainly in COL4A5 result in Alports syndrome, characterized by hematuria, hearing defects, and ultrastructurally, a thickened GBM, corresponding exquisitely with the site specific expression of the α345 network. (Hudson, 2004; Hudson et al., 2003) These differences in collagen IV mutation phenotypes highlight the specificity of collagen IV

chains in the different basement membranes in the body and multiple functional roles demanded of a collagen IV network.

Sulfilimine crosslink within the NC1 hexamer of collagen IV

The Non-Collagenous 1 domain (NC1 domain) of collagen IV molecule is unique in both its biochemistry and role within the overall collagen IV molecule. Typically, basement membrane components are studied through their liberation from the insoluble matrix via detergents and bacterial collagenase digestion. The globular conformation of the NC1 domain makes it immune to proteolysis by the standard bacterial collagenases which target the triple-helical portion of the collagen IV molecule. This feature of the NC1 domain results in it being the most soluble and easily accessible portion of matric derived collagen IV to study. For these reasons, the early study of collagen IV recognized post-translational heterogeneity in the NC1 domains derived from many primary tissue sources, with multiple seemingly dimeric NC1 bands identified by SDS-PAGE which varied significantly based on the tissue source of the basement membrane preparation (Langeveld et al., 1988; Weber and Pullig, 1992). These studies led eventually to the publication of competing crystal structure publications of the NC1 hexamer by the Hudson and Than groups (Sundaramoorthy et al., 2002; Than et al., 2002). Analysis of these crystal structures indicated that the basis for the dimerization of the NC1 domain by SDS-PAGE was not a supposed disulfide linkage (Weber et al., 1988), but rather that a linkage between methionine and lysine was possible (Sundaramoorthy et al., 2002; Than et al., 2002). After purification of the putative crosslinked peptide by high-performance liquid chromatography, high resolution mass spectrometry identified the S=N crosslink through the absence of 2 proton equivalents

in the crosslinked peptide and the identification of an olefin elimination product and a methyl-sulfenamide fragment on CID (collision induced dissociation) MS^3 analysis (Vanacore et al., 2009) (Figure 2A). These data represented the first known instance of a sulfilimine crosslink in biology. After the initial identification, both the salient residues (Met^{93} and Hyl^{211} (or Lys^{211} in α2-like collagen IV chains)) as well as the S=N bond itself were found to be almost completely conserved in all true animals, suggesting that the S=N crosslink is essential for collagen IV function (Fidler et al., 2014).

Peroxidasin forms the sulfilimine crosslink

Given the discovery of a novel biological bond, the next natural question was to identify which enzyme was responsible for sulfilimine formation. Through the use of azide click chemistry and mass spectrometry, peroxidasin was identified as a basement membrane peroxidase. With the additional evidence of peroxidase inhibitors (phloroglucinol, methimazole, and 3-aminotriazole) ability to block S=N crosslinking, peroxidasin appeared to be the most likely candidate. (Bhave et al., 2012) Recombinant expression of peroxidasin revealed that it was capable of forming S=N crosslinks in isolated NC1 hexamer and producing hypohalous acids (HOCl and HOBr) in a hydrogen peroxide dependent manner. Both hypohalous acids were also shown to chemically be sufficient to form varying degrees of S=N crosslink. Through *in vitro* and *in vivo* methods in *drosophila melanogaster*, peroxidasin was identified as the enzyme necessary and sufficient for the formation of the S=N bond (Bhave et al., 2012) (Figure 2A).

Originally discovered in drosophila (Nelson et al., 1994), peroxidasin is a 500KDa trimeric heme peroxidase with a complex multidomain structure including IgG-like, Leucine Rich Repeat (LRR), Von Willebrand factor type C-like domain. (Figure 2B) The

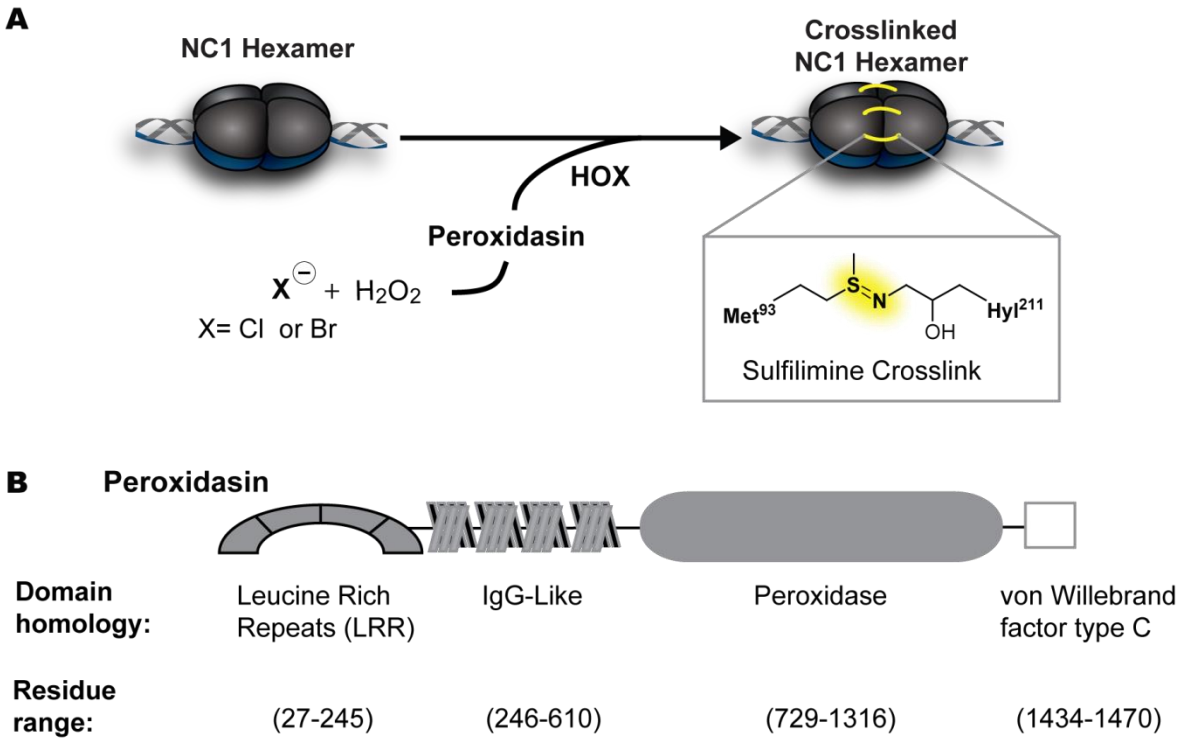

Figure 2. Peroxidasin forms the sulfilimine crosslink in the collagen IV NC1 domain

(**A**)Peroxidasin mediated crosslinking of the NC1 hexamer based on the data of Bhave *et al.* (Bhave et al., 2012) showing the unresolved identity of the halide cofactor and resulting hypohalous acid species involved in sulfilimine formation.

(**B**) The domain structure of peroxidasin

peroxidase domain, having the strongest similarity to LPO (Lactoperoxidase), and appearing to be one of the oldest evolutionary peroxidases, corresponds well over evolutionary time to collagen IV. (Fidler et al., 2014; Soudi et al., 2012) Recent interest has shown peroxidasin to be a heavily N-glycosylated protein with key disulfide links as part of each of the four domains. (Lázár et al., 2015; Soudi et al., 2015) Consistent with data generated by Bhave et al. (Bhave et al., 2012), the homotrimeric structure was confirmed by mass spectrometry. Additional mutagenesis work by Peterfi's group showed that Cys1315 was essential for the homo-oligimerization observed in the protein. (Lázár et al., 2015)

The *in vivo* function of peroxidasin has this far been studied through the hypomorphic drosophila allele (*Pxn*^{f07229}) as the genetic loss of function model for peroxidasin; however there are also several consanguineous families who have homozygous truncation mutations at multiple points within the gene. These mutants manifest mainly with anterior eye segment dysgenesis phenotypes, including corneal opacity, cataracts, and in the worst cases, mircopthalmia (Choi et al., 2015; Khan et al., 2011; Yan et al., 2014). It is notable here that no further interrogation into the phenotypes of these individuals was carried out, leaving significant room for our understanding of peroxidasin-null humans and their physiology. However, several additional mouse knockout models (C1272X homozygous truncation mutants) have similarly demonstrated ophthalmologic phenotypes resembling the human homozygous mutants (Lázár et al., 2015; Yan et al., 2014). Beyond the eye manifestations, there has also been evidence in *Caenorhabditis elegans* suggesting a role for peroxidasin in functional axon guidance through development (Gotenstein et al., 2010; Lee et al.,

2015). In addition to the mounting developmental evidence of peroxidasin function, a unilateral ureteral obstruction model of kidney injury in mice demonstrated elevation in peroxidasin content in the injured kidney, suggesting potential involvement in the response to injury and its potential resolution (Peterfi et al., 2009). The knowledge of peroxidasin's key role in the formation of the S=N bond coupled with the growing knowledge of what its physiologic absence can mean for an organism, underscores the need for deeper knowledge about the mechanism of action of peroxidasin both *in vitro* and *in vivo* to understand its contribution to basement membrane function.

Goodpasture's disease and collagen IV

Goodpasture's disease (GP) is a rapidly progressive autoimmune glomerulonephritis with concurrent alveolar hemorrhage which can result in death if left untreated. Within the kidney, the glomerulus is the functional filtration unit responsible for organ function. Glomerular architecture relies on the vascular endothelium, glomerular basement membrane (GBM), and visceral epithelial cells known as podocytes to maintain optimal filtration efficacy and selectivity (Figure 1C). The kidney and lung injury which are pathognomonic for Goodpasture's disease are driven through inflammatory responses against the specific type of collagen IV networks in those specific basement membranes. The autoimmune response in Goodpasture's disease is directed against the NC1 domain of α3 and α5 collagen IV (Pedchenko et al., 2010). The α345 collagen IV network, as previously mentioned, has a very confined tissue expression window predominately limited to the glomerular basement membrane and alveolar basement membrane. The pathogenicity of α3 autoantibodies can then be very rationally

understood because of the localization of the α345 collagen IV network to these tissues. The localization of IgG to the glomerular basement membrane in these patients creates hallmark linear staining of the GBM by indirect immunofluorescence of kidney biopsies. (Pedchenko et al., 2010) The spatial proximity of the S=N crosslink to the autoimmune epitope in GP has led to the intuitive thought that the two features might be linked in disease pathogenesis. In fact, the overall recognition of the NC1 hexamer by patient autoantibodies is influenced by the relative degree of S=N crosslinking (measured as dimerization of the NC1 domain in this study) in the target α345 hexamer. (Borza et al., 2005; Pedchenko et al., 2010)

Independent of any perturbation of S=N crosslink status, GP autoantibodies isolated from patient's serum and nephrectomies were some of the first autoantibodies shown to be uniquely pathogenic in a passive transfer to non-human primates. (Lerner et al., 1967) These data have formed the foundation or the understanding of GP autoantibody pathogenicity. Epidemiologically, GP occurs in two distinct temporal groups: young individuals in their early 20's or older individuals in their mid-50's, with the latter group having significant percentages with concurrent Anti-MPO (myeloperoxidase) autoantibodies at the time of diagnosis (Yang et al., 2007a). While the overall significance of the coincidence of Anti-MPO and Goodpasture's disease is controversial, it is clear that there is a meaningful overlap in these two serologic findings amongst this patient cohort. (Levy et al., 2004a) Other epidemiologic clues come from a strong contribution of HLA-DRB1*15:01 to the development of Goodpasture's disease, suggesting multiple potential contributing immunologic pathways to the final clinical picture. (Ooi et al., 2013) Despite the genetic predisposition, a dwindling $CD4^+$ T-cell

population and Anti-GBM antibody load after the acute disease episode potentially accounts for the very infrequent disease recurrence, a rarity amongst autoimmune conditions which are normally life-long (Salama et al., 2001). The multi-factorial suppression of B-cells observed in bone marrow for the suppression of autoreactive α3NC1 B-cells bolsters the idea of complex regulatory mechanisms. (Clark et al., 2011) One potential explanation for the changes in cellular immunity toward α3NC1 is differential antigen processing by antigen presenting cell lysosomes. Typically, the autoreactive T cell epitopes in α3NC1 are quickly degraded in the early endosomal pathway by Cathepsin D, (Zou et al., 2007) however, a change in the classically oxidizing endosomes could change antigen processing significantly enough to enable a robust $CD4^+$ T Cell response. Given our limited knowledge of how a sulfilimine crosslink would behave in an oxidizing endosomal compartment, the potential contribution of the sulfilimine crosslink to differential T-cell epitope display remains open-ended. As a whole, the epidemiologic and immunologic evidence about Goodpasture's disease is complex and conspicuously multifactorial

The molecular determinants and epitopes of the α3 and α5 NC1 domains' recognition by Goodpasture autoantibodies is well understood, however many lingering questions exist about Goodpasture's disease pathogenesis. The major questions are threefold: 1) Is the S=N involved in altered antigen presentation? 2) What changes occur in the autoimmune milieu that facilitates the development and then regression of such a robust autoimmune process? 3) is the coincidence with Anti-MPO antibodies important in disease pathogenesis?

Major questions addressed by this work

The recently discovered S=N crosslink between a methionine and a (hydroxy)lysine within the NC1 domain has emerged as an essential component of collagen IV function across all phyla of animals. Peroxidasin, as the enzyme required to form the S=N crosslink, is similarly conserved (Fidler et al., 2014). However, the precise mechanism and terminal oxidant manufactured by the enzyme is unclear. While peroxidasin is known to be important for basement membrane function and sulfilimine crosslinking (Bhave et al., 2012), we have thus far not been able to demonstrate directly that S=N crosslink deficiency within collagen IV causes changes in the ultrastructure of the basement membrane.

Thus, peroxidasin has recently emerged as an important enzyme with key unresolved questions about the mechanism of crosslink formation within normal basement membrane physiology and any potential involvement in disease. Because of the potential role of the S=N crosslink in Goodpasture's disease, this condition offers a potentially unique window into the peroxidasin-collagen IV functional complex.

Within this context, we sought to address the following questions:

- What is peroxidasin's cofactor for crosslinking collagen IV?
- How is S=N formation occurring in the NC1 with that cofactor?
- Based on cofactor identity, what is the underlying chemistry driving S=N bond formation chemistry within the NC1 domain?

- Once the cofactor is identified, what are the biologic consequences of its perturbation and what direct effects on the basement membrane will this cause?
- Based on the coincidence of Anti-MPO and the interaction of S=N crosslink with GP recognition, is peroxidasin involved in GP disease?

Chapter II

Materials and Methods

The following chapters of this work contain many experiments which rely on shared techniques, materials, and analytical methods. To avoid redundancy and provide an easily accessible resource for the comprehensive materials and methods used, they have been assembled here.

These materials and methods were published in part here: McCall, A.S., Cummings, C.F., Bhave, G., Vanacore, R., Page-McCaw, A., and Hudson, B.G. (2014). Bromine is an essential trace element for assembly of collagen IV scaffolds in tissue development and architecture. Cell *157*, 1380-1392.

Materials

Chemicals: Reagent grade chloride salts were purchased from Thermo Fisher Scientific (Whaltham, MA), cell culture reagents from Mediatech (Manassas, VA), and all other chemicals from Sigma-Aldrich (St. Louis, MO) except where specified.

Br-Free Salt Purification: All reagents were used as supplied, without further purification. The glass reaction Chamber was designed by Gautam Bhave and built by Adams and Chittenden Glass Company (Berkeley, CA http://www.adamschittenden.com/). All dishware and Teflon was acid washed and then rinsed with Millipore purified H_2O. This method was adapted from a similar method published previously (Joy et al., 1973).

Ultrapure Br-Free NaCl Preparation: 210 ml of 50% w/w NaOH solution (J.T. Baker, 4.014 mols, 1.0 eq) was measured using a polypropylene graduated cylinder and decanted into a 250 ml Teflon beaker (Chemglass Inc.) containing a large caliber Teflon coated stir-bar. Separately, 1710 ml of 37.25% w/w HCl solution (Macron Chemicals, 20.07 mols, 5.0 eq) was carefully poured into the outer moat of the reaction chamber. Silicon high-vacuum grease (DuPont Chemicals) was then spread uniformly along the top rim of the reaction container. The Teflon beaker containing the NaOH solution was placed into the holder in the reaction chamber and the lid sealed (Figure 6). The assembled reaction chamber was then placed into an oven pre-equilibrated to 30^{o}C with a magnetic stir-plate inside set to vigorously stir the NaOH solution. The reaction was allowed to proceed for 48 hrs. without removal of the sealed lid. At this point, the chamber was removed from the oven, lid removed, and pH of the solution in the Teflon beaker was tested using litmus paper. If the stir bar was trapped by precipitation of NaCl, a Teflon-coated magnetic rod was used to pulverize the accumulated salt and enable stirring. The pH was retested after mixing; if still above pH 7.0, reaction was placed back into the oven in 24hr increments until neutralization occurred. If the stir bar had stopped, only the pH measured after the breakup of accumulated salt was used to determine reaction progression because a pH gradient can develop without active stirring. Total reaction times were typically 96 hours. Extreme caution was used to ensure no liquid in the outer mote spilled into the Teflon beaker.

Once neutralization of the NaOH solution occurred via vapor diffusion of HCl, that solution was filtered through a Buchner funnel (crude yield: 202.8 g NaCl wet weight). The crude precipitate was then re-dissolved in 18 MΩ Millipore purified H_2O (100ml/40g

crude precipitate) and hot filtered again through a Buchner funnel after boiling. After filtering, the volume of the water was reduced by heating to an approximate volume of 85 ml with vigorous stirring, then removed from heat and allowed to cool slowly to room temperature. This recrystallized NaCl was filtered with a glass-frit, and placed under high vacuum with heating to 100^{o}C to completely dry the sample. Overall Yield: 156.7 g NaCl (2.681 mols, 66.8% yield). Final NaCl purity was tested by ICP-MS showing a Br concentration of <11nM/100mM NaCl solution, below the lower detection limit for this method (see Table 1) .

Ultrapure Br-Free KCl Preparation: The reaction and purification were performed exactly as above with 210 ml of 45% w/w KOH solution. Yield: 87.2 g (1.124 mols, 47.0%). Purity of the KCl was tested by ICP-MS showing a Br concentration of <11nM/100mM KCl solution, below the lower detection limit for this method of analysis (see Table 1).

Collagen IV Production, Isolation of Collagen IV Matrix, and Purification NC1 Hexamer:

Matrix Production: PFHR9 cells were plated at high density and maintained at confluency for 5-8 days in the presence of 50µg/ml ascorbic acid, with media changes every 24-36 hours. If desired, S=N bond formation was inhibited by the sustained presence of 1mM KI or 50 µM phloroglucinol (PHG), with inhibitor treatment being initiated upon confluency (typically 24hours after plating). Cultured cells and matrix were washed in 1x PBS before being scraped in 1% (w/v) sodium deoxycholate lysis buffer. The lysate/matrix mixture was sonicated to sheer genomic DNA, the insoluble material

was pelleted by centrifugation (20,000xg), washed in 1M NaCl plus 10 mM Tris HCl , again pelleted via centrifugation, and ultimately washed (by addition of buffer and vortexing for 30 sec., followed by centrifugation) into the experimentally indicated buffer twice. *NC1 Hexamer Purification:* If purification of NC1 domain was desired, the matrix was washed into 50 mM Tris HCl pH 7.4. NC1 hexamers were excised from the collagenous matrix by digestion of purified matrix with bacterial collagenase (Worthington Biochemical Corporation) in a buffer containing 5 mM $CaCl_2$, 5 mM Benzamidine, 25 mM 6-aminocaproic acid, and 0.4 mM phenylmethylsulfonyl fluoride (PMSF). The supernatant from the collagenase digest was dialyzed against 50 mM Tris HCl followed by separation by DEAE chromatography in 50mM Tris-HCl (pH 7.5). NC1 hexamers remain unbound in this condition, and were collected in the flow-through fractions. DEAE-purified NC1 was further refined by gel filtration (Superdex^{TM} 200, 10/300GL, GE Healthcare) to isolate purified NC1 hexamers. If Br-Free hexamers were needed, the S200 column was equilibrated in a 10 mM Phosphate buffer with 100 mM Br-Free NaCl. Table 1 contains the ICP-MS analysis of phosphate buffer demonstrating the absence of Br contamination.

Purification of Recombinant Human Peroxidasin (hPXDN): Peroxidasin was purified from stably transfected HEK293 as described previously (Bhave et al., 2012) and adapted to obtain purified peroxidasin free of bromide contamination with only the changes noted below to the protocol. Buffers used in the purification protocol were made with Br-Free NaCl. The mono-Q anion exchange column (GE Life Sciences) was washed for 10 column volumes in 0.3 M sucrose, 0.1 M NaCl(Br-Free), 20 mM Tris

Acetate (pH 8.5). The sucrose gradient for ultracentrifugation was poured from 5% and 20% sucrose solutions of 50 mM NaCl(Br-Free), 3 mM hexadecyltrimethylammonium chloride, and 10 mM phosphate buffer (pH 7.5).

Preparation of Hypohalous Acids: 10mM reagent hypochlorite (OCl-) (Sigma Aldrich) was used alone after dilution into required reaction buffer (concentration of HOCl confirmed spectrophotometrically ε_{292} = 350 $M^{-1}cm^{-1}$) or mixed with and equal volume of 12mM NaBr or KBr, and allowed to react for 60 seconds at high pH before being diluted into the reaction buffer at pH 7.4. HOBr was always prepared less than 15 minutes before use and concentration quantified spectrophotometrically (ε_{329} = 332 $M^{-1}cm^{-1}$).

Phytagel Purification: In order to limit any bromide contamination present in commercial Phytagel (Gellan), we decided solubilize the phytagel to liberate any trapped bromide. Phytagel (7.5 g) (Sigma Aldrich) was added to 500 ml of 5mM EDTA (1.5% w/v final) solution at 60^{o}C with stirring. Concentrated NaOH (268 µl, 5.5 mmol) was added drop wise resulting in a complete solubilization of the Phytagel. [Doner and Douds demonstrated that 1.1 mmol OH^- was needed to solubilize 1.5g of Phytagel(Doner and Douds, 1995) in the absence of divalent cations]. Concentrated H_3PO_4 (300 µl) was then added (final pH 5.5) and the flask removed from heat. 2 volumes (1L) of isopropanol were added and the mixture was shaken vigorously. A stringy precipitate was visible immediately upon addition of the isopropanol. The

solution and precipitate were allowed to stand until cool, filtered over a glass frit, and washed with another volume of isopropanol, then left under high vacuum for 24 hours. 6.81g (90.8% yield) of a stringy white solid (Sodium Gellanate) was recovered, and stored at room temperature. Bromide content in the purified phytagel was tested by Neutron Activation Analysis and found to be less than the detection limit afforded by this method (<0.06 ppm, <0.8 μM).

Biochemical Methods

Determination of Sulfilimine Crosslink Number and Oxidation State of Methionine in NC1 Dimeric Subunits: To determine the number of S=N crosslinks in NC1 dimers, NC1 hexamers (native and chemically oxidized) from HR9 matrix were fractionated on 12% SDS-PAGE. After staining with BioSafe Coomassie (BioRad), gel images were acquired and analyzed in a ChemiDoc^{TM} XRS+ imaging system using Image Lab 2.0 software. Dimeric NC1 subunits D_1 and D_2 showing equal intensities were excised out of the gel and prepared for “in-gel” trypsin digestion protocol(Vanacore et al., 2009). To establish the oxidation state of methionine 89, 91, and 93 in NC1 domains after oxidation with HOBr or HOCl, gel bands corresponding to the monomeric subunits of each sample were excised out of the gel and processed by “in-gel” trypsin digestion as described above. Peptides were dried and stored at -20 ˚C until MS analyses were performed.

High-Resolution Mass Spectrometry: For mass spectrometric analysis of tryptic digests of NC1 subunits, dry samples were reconstituted in 0.1% formic acid and loaded

onto a capillary reverse phase analytical column (360 µm O.D. x 100um I.D.) using an Eksigent NanoLC Ultra HPLC and autosampler. The analytical column was packed with 20 cm of C18 reverse phase material (Jupiter, 3µm beads, 300 Å, Phenomenex), equipped with a laser-pulled emitter tip. Peptides were gradient-eluted at a flow rate of 500 nL/min, and the mobile phase solvents consisted of 0.1% formic acid, 99.9% water (solvent A) and 0.1% formic acid, 99.9% acetonitrile (solvent B). A 90-minute gradient was performed and consisted of the following: 0-10 min, 2% B; 10-50 min, 2 - 35% B; 50-60 min, 35-90% B; 60-65 min, 90% B; 65-70 min 90-2% B; 70-90 min, 2% B. Upon gradient-elution, peptides were mass analyzed on a LTQ Orbitrap Velos mass spectrometer (Thermo Fischer Scientific, San Jose, CA), equipped with a nanoelectrospray ionization source. The instrument was operated using a data-dependent method in which full scan (m/z 400-2000) spectra were acquired with the Orbitrap as the mass analyzer (resolution 60,000), and the three most abundant ions in each MS scan were selected for fragmentation in the LTQ. These were followed by data-dependent MS^3 analysis of the three most abundant ions in each MS^2 scan. An isolation width of 2 m/z, activation time of 30 ms, and 35% normalized collision energy were used to generate MS^2 and MS^3 spectra. The MSn AGC target value was set to 1e4 or 2e4, and the maximum injection time was either 150 ms or 250 ms, respectively. For MS^2 scans, a minimum threshold of 500 was used to trigger data-dependent spectra, while a threshold of 500 or 100 was used to trigger MS^3 spectra. Dynamic exclusion was enabled, with an exclusion duration time of 60 ms.

Peptide identification and Bioinformatics: Two strategies were followed for the identification of sulfilimine-cross-linked peptides. First, raw data files were manually searched for sulfilimine-cross-linked peptides using the QualBrowser of Thermo Xcalibur 2.1 software. To calculate the monoisotopic mass of the sulfilimine-cross-linked peptides, the mass of two hydrogen atoms was subtracted from the sum of the masses for Met^{93}-containing peptide and Lys^{211}-containing peptide, each generated using GPMAW version 8.00sr1 (Lighthouse Data, Denmark), as previously shown by Vanacore *et al(Vanacore et al., 2009)*. Second, sulfilimine-cross-linked peptides not found manually were identified by searching the mouse subset of the Uniref100 database (www.uniprot.org) using either SEQUEST™ (Thermo Electron, San Jose, CA) on a high speed, multiprocessor Linux cluster in the Advanced Computing Center for Research & Education at Vanderbilt University or using Myrimatch algorithm on a 2 six-core Intel Xeon processor HP Proliant DL160 G6 server running Windows server 2008 R2 enterprise using the Bumbershoot suite(Tabb et al., 2007). The search files were adapted for the identification of peptides that included the dynamic amino acid modifications of interest (i.e. –48.0034 on Met, +45.9877 or +61.9826 on Lys as well as and oxidation of methionine to sulfoxide (+15.9949) and/or sulfone (+31.9898)) and the static modification of cysteine by carbamidomethylation (+57.021). The resulting files obtained from Sequest™ and/or Myrimatch were assembled on IDPicker(Holman et al., 2012; Tabb et al., 2007) and/or Scaffold (Proteome Software, Portland, OR). MS^3 spectra matching peptides containing modified Lys^{211} or Met^{93} were either confirmed by manual evaluation or by processing the raw data files through ScanRanker(Ma et al., 2011), and the spectra annotated with IonMatcher(Tabb et al., 2007).

The abundance of S=N cross-linked and Met oxidized peptides was quantified by generating extracted ion chromatograms (XICs) for precursors (all ionic forms) within each data set using Xcalibur software. The area of the peak containing modified peptide(s) was normalized to the total ion current over the entire chromatographic separation.

Cell Culture Screening of Halides: PFHR-9 cells were grown in the presence of halide salts for up to 7 days-post confluency. NC1 domains were biochemically isolated as above, and visualized by SDS-PAGE. Densitometry was conducted using ImageJ software (NIH), and dose-response curves fit in GraphOad Prism 5.1 using non-linear regression.

In Vitro Isolated Matrix Reactions: Collagen IV matrix was grown under 1mM KI for inhibition of crosslinking, and purified with 1% deoxycholate and 1M NaCl washes. Insoluble pellets were then subjected to five washes in the appropriate reaction buffer to remove contaminating endogenous halides. Reactions were initiated upon addition of 1mM H_2O_2, stored at -20° post-reaction. The collagenous matrix was digested with collagenase prior to separation of the soluble NC1 domains by non-reducing SDS-PAGE.

Reactions of Purified Human Peroxidasin and other peroxidases with the NC1 Hexamer under Br-Free Conditions: Peroxidasin (27.25 nM) and NC1 hexamer(1.3 μM) [both prepared Br-Free *vide supra*] were reacted in the presence of either reagent grade phosphate buffered saline (PBS) or Br-Free PBS composed 136 mM NaCl(Br-

Free), 2.68 mM KCl(Br-Free), 10 mM Na_2HPO_4, 2 mM KH_2PO_4 [NAA analysis of these PBS mixtures appears in Table 4, which demonstrated a Br concentration of <2.5 µM, the detection limit for the analysis, and each component was individually demonstrated to have <11 nM Br contamination by ICP-MS(Table S1)]. The reaction was initiated when H_2O_2 (10 µM) was added and the mixture placed at 37^{O}C for 10 minutes. The reaction was quenched by the simultaneous addition of 5 mM phloroglucinol, 0.2 mg/ml Bovine catalase, and 10 mM methionine in a premixed solution.

The dose response of purified peroxidasin to Br^- was accomplished in an identical way with Br-Free PBS as the buffer. For the reactions involving Myeloperoxidase (MPO), Eosinophil peroxidase (EPO), (purchased from Calbiochem), each enzyme was obtained commercially, and dialyzed against 10000 volumes of Br-free PBS to ensure minimal Br contamination.

Chemical oxidation of NC1 domains with HOCl and HOBr:

Dose response: HOCl and HOBr, prepared as noted above, were added to uncross-linked purified NC1 hexamer (833 nM) and reacted for 5 minutes at 37^{O}C and quenched by adding methionine to 1 mM. Preoxidation: For the HOCl preoxidation experiment, HOCl (in indicated concentrations) was added to 1.3 µM purified NC1 hexamer in 1x Br-Free PBS for 1 minute at 37^{O}C, at which point 8.5 mol eq HOBr (66 µM final concentration) was added and the solution reacted for 1 additional minute at 37^{O}C. Methionine was added to 20 mM to quench the reaction. For the H_2O_2 preoxidation, NC1 Hexamer (1.3 µM) in Br-Free PBS was mixed with H_2O_2 in indicated concentrations and incubated at 37^{O}C for 14 hours. After incubation, a 0.02 mg/ml final

concentration of catalase was added to consume residual H_2O_2 for 10 minutes at 37^{O}C, followed by treatment with 8.5 mol eq HOBr (66 µM final concentration) for 1 minute at 37^{O}C. Reactions were then quenched with 20 mM methionine.

Stoichiometric Oxidations for S=O and S=N product comparisons: 1.3 µM purified NC1 hexamer in 1x Br-Free PBS was oxidized with 10.7 mol eq (83.3 µM) of HOBr or HOCl for 1 minute at 37^{O}C then immediately quenched with 20 mM methionine. All NC1 domains were then subjected to non-reducing SDS-PAGE on a 12% gel and Coomassie stained (50% Methanol, 10% Glacial Acetic acid, 0.01% Coomassie Brilliant Blue) for 30 minutes, rinsed with distilled water, and destained for 1 hour (15% methanol, 10% Glacial Acetic acid) enabling consistent quantification between experiments.

***Br-Free cell culture of PFHR-9 cells*:**

Serum Dialysis: 27.5 ml Fetal Bovine Serum (Atlanta Biologicals, Norcross, GA) was dialyzed (10,000 MW cutoff dialysis tubing) against Br-Free HBSS (

Table 3) twice (2.5L/dialysis) for 12 hours each at 4^{o}C.

Media Preparation: The components listed in Table 2 were combined and the dialyzed serum was added. The final Br-Free media (DMEM +5% FBS) was sterile filtered (0.22 µm pore) and stored at 4^{o}C until use.

Culture Method: Passage 9-14 PFHR-9 cells, grown to confluency in a 15cm culture dish were trypsinized, centrifuged at 1000xg to form a pellet, and the supernatant removed. Br-Free DMEM was used resuspend and wash the cell pellet twice(10

ml/rinse), and then the cells split 1:4 into 10 cm culture dishes containing 12 ml of either standard media (commercial DMEM + normal 5% serum) as the control, Br-free media + 5% Br-Free Dialyzed FBS , or 100 µM NaBr +Br-free media + 5% Br-free Dialyzed FBS (Br-added). 24 hours after plating, 50 µg/ml ascorbic acid was added to the cultures. Media was changed every 24 hours and the cells were cultured for 5 days at 37^{o}C in 10% CO_2. After 5 days, the plates were harvested for matrix. Cells were rinsed with ice cold PBS with 50µM PHG followed by the application of a 1% deoxycholate, 10 mM Tris HCl, 1 mM EDTA lysis buffer with 50µM PHG, 0.5 mM PMSF, and Aprotinin, Leupeptin and Pepstatin (Sigma) (10µg/ml) added. The insoluble matrix and this buffer were scraped and then sonicated until mostly homogenous, then centrifuged (20000xg for 20 minutes). The supernatant was removed and the pellet washed by vortexing in a 1M NaCl, 50 mM Tris (pH 7.4), 0.5 mM PMSF, 50µM PHG solution for 10 minutes. The sample was re-pelleted and a collagenase digestion was performed as explained above (collagen NC1 purification) with the addition of 0.5 mM PMSF and 50µM PHG to the collagenase buffer. The supernatant following the collagenase digestion was subjected to SDS-PAGE (12% gel) and Coomassie blue staining.

Each media used for culture, including 5% Serum, was analyzed by NAA for Br content (Table 4). Standard commercial media contained 1.00±0.011 ppm (12.5±0.1 µM), Br-free Media contained < 0.2 ppm (<2.5 µM, the detection limit of the analysis), and Br-added contained 7.0 ±0.252 ppm (87.6 ±3.2 µM).

Drosophila Methods

Yeast Culture in Br-Free Conditions: Yeast were cultured in an adapted Yeast Nitrogen Base (YNB) media. Once the solution was made, it was sterile filtered and

stored at 4^{o}C until use. Yeast were started by placing active dry pellets (~ 30 pellets) of *Saccharomyces cervesea* (Type II)(Sigma Aldrich, St. Louis, MO) in 5 ml sterile distilled water and inoculating in 50 ml Br-free YNB starter cultures at 30^{o}C and 230 rpm for 26 hours. From this starter culture, 500 µl was used to inoculate 500 ml of the same Br-free YNB. These 500 ml flasks were grown under the same conditions as above until an OD_{600}=1.5 was observed (~27 hours). The yeast was then harvested in a series of centrifugations at 4000xg for 25 minutes at 4^{o}C. Once pelleted, the yeast was re-suspended in 25 ml Br-Free PBS and re-centrifuged, and the supernatant was removed. The yeast pellet was the re-suspended in 15 ml of Millipore distilled water and transferred to a lyophilization chamber where the yeast paste was snap frozen around the periphery of the chamber in a dry ice/ethanol bath, followed by a 48 hour lyophilization process. The yeast powder was then stored at room temperature until use. Total dry yield was 6.47 g/ 6 L culture media (1.08g Dry Yeast/L).

Phytagel Semi-Solid Plate Preparation: Dishes were prepared in sizes appropriate for either larval rearing (35 mm dish, 2 ml phytagel mixture) or for egg deposition/adult feeding (55 mm dish, 10 ml phytagel mixture). To prepare the phytagel mixture, a solution was formulated to mimic the bulk salts present in grape juice (as the standard source of nutrients and salts) as well as to provide sufficient divalent cations to enable phytagel polymerization. This polymerization solution consisted of Br-free KCl (5 mM), Br-free NaCl (5 mM), KH_2PO_4 (1 mM), and MgSO4 (5 mM). To the polymerization solution, 18.1% w/v sucrose and 0.5% w/v purified sodium gellanate (prepared as described in Materials) were added to the desired final volume and the suspension vortexed and microwaved in 15 second intervals until boiling. Once the phytagel had

completely solubilized, the solution was placed in an 80° C water bath to enable multiple solutions to be prepared simultaneously.

Final solution preparation occurred after removal of the phytagel from the 80° C water bath and cooling to 60° C. Once at 60° C, Tegocept (final conc. 4 mM), Ampicillin (final conc. 64 µg/ml), and the Vitamin Mixture (1X) (recipe in Table 6-made as a 10x stock and stored at 4° C) were added. For dietary conditions containing either supplemental Br^- or high Br-free Cl^-, NaBr was added to 15 or 100 µM and Br-free NaCl to 70 mM when appropriate. Once these components were added, the yellow solution was vortexed carefully avoiding bubble formation, and then poured into dishes. Upon cooling to room temperature (~15 minutes), the phytagel was completely transparent with a yellow hue. These plates were wrapped in aluminum foil to preserve vitamin activity and stored at 4° C for up to one month.

Fly Husbandry: Fly stocks and experimental cohorts were maintained at 25^{o}C and 65% humidity. When necessary, adults were collected over light CO_2. For the temperature sensitive RNAi experiments, crosses were performed at 18° C and flies were moved to 29° C conditions when indicated.

Larval Rearing and Survival Rates: Eggs from mothers maintained on experimentally indicated diets were collected during a timed laying and moved to dishes containing experimentally indicated phytagel mediums, with 50 µl yeast paste (composed of 200 mg lyophilized Br-free yeast in 500 µl Millipore water) for 1st and 2nd instar larvae, and 100 µl of yeast paste for the laying cages and 3rd instar larvae. For the conditions with

supplemental Br^-, both the phytagel medium and Br-free yeast paste contained 15 or 100 μM NaBr added to ensure consistent Br exposure through both the yeast and phytagel for the given condition. 48 hours after egg deposition, the number of hatched eggs and 1^{st} instar larvae counted. Following this time point, larvae were counted and transferred to a new plate every 24 hours until pupariation or death of all larvae.

To induce accelerated halide flux (Br-free^{DEP} conditions) , total salt concentration in all portions of the diet were raised to 80 mM using Br-free NaCl. The increased salt concentration shortens the half-life of Cl^- in the fly to ~5hours (Fairbanks and Burch, 1970); this increased total halide flux enables greater depletion of Br^- in a manner analogous to high-salt bromide wash-out in mammals (Pavelka et al., 2005).

Aspect ratio determination and hatching rate: Adult flies were maintained on the experimental diets for the indicated amounts of time. For every experimental interval, eggs were laid in 55 mm dishes until the desired time point, after which the flies were transferred to a fresh food source. The dish containing eggs deposited during the experimental interval were assed randomly by dividing the dish into equal sections containing at least 30-50 eggs per section. For aspect ratio determination, all eggs from individual sections were transferred to a fresh phytagel surface and oriented with dorsal appendages facing the surface. Eggs were imaged with a Zeiss AxioCam mounted on a Zeiss SteREO Lumar dissecting microscope and the egg diameter and the anterior-posterior axis length was digitally measured using Axiovision software (versions LE and 4.8.2, Carl Zeiss Microimaging GmbH). Aspect ratio was calculated by dividing the axis length by the diameter. Hatching rate was assessed 48 hours after the conclusion of egg collection and aspect ratio calculation.

Anti-NC1 Antibody: Polyclonal antibodies were raised against linear peptides corresponding to the C-terminal portions of the NC1 domains of both *Drosophila* collagen IV proteins (*Cg25c* [(1742)Ac-CMYNLESSQPFERPQQQTIKAGERQSHV-amide(1768)] and *vkg* [(1701)Ac-CLTVIEEQDQFVQPRQQTLKADFTSKI-amide(1726)]) simultaneously in the same rabbit by Green Mountain Antibodies (Burlington, VT). Whole sera was diluted to 50% with sterile ethylene glycol and stored in aliquots at -20° C until use.

Biochemical isolation and western blotting of NC1 domains: Sulfilimine crosslinks in collagen IV were analyzed in vkg^{454}-$GFP^{+/-}$ larvae reared on experimental diets. A single collection of vkg^{454}-$GFP^{+/-}$ parents were divided into distinct cohorts that were placed on separate experimental diets and treated exactly as the cohorts depicted in Fig. 5E. Female flies were exposed to Standard, Br-free^{DEP}, or Br-free^{DEP} +100 μM NaBr for 3-5 days, and eggs deposited on days 3,4,and 5 were transferred to fresh plate of new food and allowed to hatch. Plates every 24 hours and maintained at a density of ~80 larvae/ 55cm dish. After 4 days of growth, larvae were harvested by snap-freezing and divided into two groups for NAA analysis of Br-content (see Table 7 and Figure 13F) as well as biochemical analysis. For NC1 isolation, larvae were ground to a fine frozen powder using a liquid nitrogen chilled mortar and pestle, then suspended in an appropriate volume (5 ml/g larval pellet) of deoxycholate lysis buffer (1% DOC, 10 mM EDTA, 10 mM Tris HCl, 100 μM phloroglucinol, 1 mM PMSF, 2 μg/ ml Leupeptin, and 1 μg/ ml Pepstatin). This suspension was sonicated (75% power for 10x1 second pulses), incubated on ice for 15 minutes, then centrifuged at 20000xg for 30 minutes. The resulting pellet was subjected to a high salt wash (5 ml/g original pellet)

(1M NaCl, 50 mM Tris HCl, 100 µM phloroglucinol, 1 mM PMSF), vortexed and let stand 15 min. , centrifuged (20000xg), the supernatant removed, then subjected to a hypotonic wash (5 ml/g pellet) (10 mM Tris HCl, 50 µM phloroglucinol, 0.5 mM PMSF). The pellet was digested with collagenase (24 hours at 37° C), as described above in the purification of collagen NC1 domains, with 0.5 mM PMSF and 100 µM PHG being added to the collagenase buffer (5ml/g original larval pellet) and in dark conditions to prevent bleaching of the liberated GFP. The digested suspension was then centrifuged at 20000xg for 30 min. at 4° C. The supernatant was immediately removed and filtered through a 0.2 µ pore mini-syringe filter (Millex).

Because of the *vkg*^{454}*-GFP*$^{+/-}$ genotype of the larvae used in the study, and the specificity of collagenase for triple-helical structure, 1 mol of GFP should be liberated per mol of NC1 hexamer with complete digestion. Flourimerty was then performed on these samples using the collagenase buffer with collagenase to dissolve recombinant GFP (Life Technologies) to generate a standard curve, enabling calculation of the molar content of NC1 hexamer within the digest supernatant. The samples were then lyophilized and resuspended to a normalized concentration. 200 ng of NC1 hexamer was loaded per lane for non-reducing SDS-PAGE on a 12% gel. Prior to transfer, the gel was reduced in a solution of transfer buffer with 2% β-mercaptoethanol at room temperature, to linearize primary antibody epitopes and thereby enhance normalized recognition of dimers and monomers. After reduction, the gel was transferred to a 0.2 µ pore PVDF membrane for blotting. 5% milk in 0.1% Tween-20/TBS was used to block and dilute the Anti-NC1 1^{o} (1:500 dilution) and 2^{o} (1:10000) Goat Anti-Rabbit-HRP (Promega).

As a consequence of quantifying the about of NC1 hexamer liberated as part of the collagenase digestions, we were also able to calculated a mass of recovered collagen IV content per mg wet body weight in the original larval pellets.

Immunohistochemistry on posterior midgut: Larvae from the experimentally indicated conditions and genotypes were placed in ice-cold PBS and the gut was dissected from the surrounding tissue while leaving the malpighian tubules attached to the gut as a midgut-hindgut landmark for imaging purposes. Immediately after dissection, the gut was transferred into a 4% formaldehyde/PBS fixing solution for 20 minutes at room temperature using a Pasteur pipette. The gut was washed 3x with PBS (RT) and then blocked for at least 12 hours (Non-permeablizing Block solution: 5% Normal Goat Serum, 5% Bovine Serum albumin, 0.05% NaN_3 , in PBS, 0.22μ filtered). For *vkg*^{454}*-GFP*$^{+/+}$ larvae, the blocking solution was supplemented with 0.1% Triton X-100 before treatment with a 1:40 solution of flourophore-conjugated Phalliodin (Alexa Flour 647, Life Technologies), and incubated for 2 hours at room temperature. For all the *Pxn* hypomorphic larvae, a 1:50 dilution of Anti-NC1 antibody was prepared in non-permeablizing block and incubated for 12 hours at 4^{o} C to visualize collagen IV. Following incubation in Anti-NC1 primary, the gut was washed 3x for 1 hour at room temperature with PBS. In the same block solution, secondary antibody (Cy3-conjugated Donkey anti-Rabbit, Jackson Immunoreseasch, West Grove, PA, 1:150 dilution) and 1:20 dilution of florophore-conjugated Phalliodin (Alexa Flour 647, Life Technologies) were applied to the guts for 12 hours at 4^{o} C, and then washed 3x for 1 hour at room

temperature in PBS. All preparations were dehydrated in mounting media (Vectashield, Vector Laboratories, Burlingame, CA) and mounted after at least 3 hours.

Immunohistochemistry on Ovaries: *vkg*^{454}*-GFP*$^{+/-}$ females were collected from the indicated experimental and control diets after 7 days of exposure. Ovaries were dissected according to standard protocols and fixed for 20 min. in a 4% formaldehyde/PBS solution. Ovaries were then washed 3x 15 min. in PBS and placed in DAPI containing mounting media (as above).

Quantitation of Collagen IV content of Stage 8 egg chambers: All images were acquired on a Zeiss Axio Imager.M2 equipped with an Apotome under 40x oil magnification on the same day with identical exposure and microscope settings. Z-stacks were acquired of Stage 8 egg chambers from the top of the chamber to the equatorial plane with a Z section thickness of 0.58 µm. Using ImageJ, the Z-stack was summed to create a flattened projection. An area of the central egg was selected, and an integrated pixel density over that area was determined, as well as 3 background areas outside the egg area. An average of the background was calculated, and subtracted from the egg region based on area. The total integrated density was then divided by the area measured to obtain the fluorescent intensity per area (µm).

Transmission Electron Microscopy: Specimens were processed for TEM and imaged in the Vanderbilt Cell Imaging Shared Resource-Research EM facility.

Embedding: *Drosophila* (experimental diets: vkg^{454}-$GFP^{+/+}$, peroxidasin hypomorphs: $Pxn^{MI01492+/+}$, $Pxn^{f07229+/+}$) guts were dissected in and fixed with 2.5% gluteraldehyde in 0.1M cacodylate buffer, pH7.4 at room temperature (RT) for 1 hour then transferred to 4ºC, overnight. The samples were washed 3 times (5 minutes) in 0.1M cacodylate buffer then incubated for 1 hour in 1% osmium tetraoxide RT then washed with 0.1M cacodylate buffer. Subsequently, the samples were dehydrated through a graded ethanol series: 30%, 50%, 70%, 80%, 95% and then 3 exchanges of 100% ethanol. Next, the samples were incubated for 5-minutes in 100% ethanol and propylene oxide (PO) followed by 2 exchanges of pure PO. Samples were then infiltrated with 25% Epon 812 resin and 75% PO for 35 minutes at RT. Next, they were infiltrated with 50% Epon 812 resin and 50% PO for 1 hour at RT then exchanged with new 50% Epon 812 resin and 50% PO and incubated overnight at RT. Next day, the samples went through a 75%: 25% (resin: PO) exchange, then exchanged into pure epoxy resin for 3-4 hours, then incubated with pure epoxy resin overnight. Next, the resin was exchanged with freshly made, pure epoxy resin and incubated for 3 hours, then embedded in epoxy resin and polymerized at 60º C for 48 hours.

Sectioning and Imaging: 70-80 nm ultra-thin sections were then cut from the block and collected on 300-mesh copper grids. The copper grids were post-section stained at room temperature with 2% Uranyl acetate (aqueous) for 15 minutes and then with Reynold's lead citrate for 10 minutes. Samples were subsequently imaged on the Philips/FEI Tecnai T12 electron microscope at various magnifications.

Quantitation and fitting of gut basement membrane thickness: Images of the basolateral basement membrane of the distal posterior midgut of the experimentally indicated conditions were acquired at 42000x zoom and analyzed in ImageJ after adjusting the image scale to the superimposed scale bar. Measurement of basement membrane thickness were taken at 100 nm intervals across the field of view from at least 15 independent sections per experimental condition only where the basement membrane was clearly defined at the basal aspect of the enterocyte. A Box-Cox transformation (optimal lambda value for each distribution was calculated using the SigmaXL (SigmaXL Inc., Toronto, ON) plugin for Microsoft Excel) was then performed to enable the fitting of a normal distribution for each condition, as well as distribution testing between conditions using the F test in GraphPad Prism 5. To obtain 95% confidence interval measurements on the parameters for the different conditions and test the overall stability of the data, bootstrapping was performed using 1000 resamples.

Drosophila *Genetics*: The following fly lines were used: Wild-type flies were genotype w^{1118}, *Pxn* hypomorphic mutants (obtained from the Bloomington Stock Center and rebalenced)w^{1118};*PBac[WH]Pxn*^{f07229}/TM3,armGFP., w*; Mi{MIC}PxnMI01492/TM3,arm-GFP. RNAi lines were obtained from the Vienna Drosophila RNAi Stock Center: Ch.2 *Pxn*^{RNAi} w; P{KK108816}VIE-260B/CyO mCherry, and X chr. *Pxn*^{RNAi} w^{1118} P{GD5987}v15277 / (FM7c). collagen IV visualized by y w *vkg* P{GFP, w+}454. RNAi expression was driven by w; P{w[+mC]=tubP-GAL4}LL7, P{w[+mC]=tubP-GAL80^{ts}}2/TM6B, Tb.

Experimental Genotypes (by panel)
Figure 13
A-E) w^{1118}
F, N-P) y; vkg^{454}-GFP

G-J) y ; vkg^{454}-GFP
K,Q) y; *Pxn*^{MI01492}
L) y w *Pxn*^{MI01492}/ *Pxn*^{f07229}
M, R) w *Pxn*^{f07229}
Figure 14
B-C) *w*^{1118}
D) Freshly ecclosed *w*^{1118}males were cross with the following female**s**
Experimental: w UAS::*Pxn*^{RNAi} KK108816; Tub::GAL4, Tub::GAL80^{TS}
Control: Tub::GAL4, Tub::GAL80 ^{TS}
E) Freshly ecclosed *w*^{1118}males were cross with the following females
Experimental w UAS::*Pxn*^{RNAi} GD5987; Tub::GAL4, Tub::GAL80
Control: w UAS::*Pxn*^{RNAi} GD5987
F) *w*^{1118}
G) y *vkg*^{454}-GFP/+
Figure 15
A) y *vkg*^{454}-GFP/+
B-D) *w*^{1118}
E) y; *Pxn*^{MI01492}
F) w *Pxn*^{f07229}
H) Freshly ecclosed *w*^{1118}males were crossed with the following females
Experimental: w UAS::*Pxn*^{RNAi} KK108816; Tub::GAL4, Tub::GAL80 ^{TS}
Control: Tub::GAL4, Tub::GAL80 ^{TS}
I) Freshly ecclosed *w*^{1118}males were crossed with the following females
Experimental w UAS::*Pxn*^{RNAi} GD5987; Tub::GAL4, Tub::GAL80 ^{TS}
Control: w UAS::*Pxn*^{RNAi} GD5987

Bromine Content Analysis: Analysis of Br content was performed using three independent methods, as denoted in the main text. Ion Chromatography-Inductively Coupled Mass Spectrometry (IC-ICP-MS) was performed on solution not containing proteinacous material by Applied Speciation and Consulting, LLC, of Bothell, WA. For bulk complex samples, Neutron Activation Analysis (NAA) was performed by Elemental Analysis Inc, Lexington, KY. For limited quantities of complex biologic samples, epiboron neutron activation analysis (EINAA) was performed by the University of Missouri-Research Reactor Center, Columbia, MO. A brief outline of the methods used follows:

Bromide Quantitation by IC-ICP-MS: Aliquots of each sample are injected onto an anion exchange column and eluted isocratically. The eluting bromine species are then introduced into a radio frequency (RF) plasma where energy-transfer processes cause desolvation, atomization, and ionization. The ions are extracted from the plasma through a differentially-pumped vacuum interface and separated on the basis of their mass-to-charge ratio (m/z) by a mass spectrometer. A solid-state detector detects ions transmitted through the mass analyzer and the resulting current is processed by a data handling system. Retention times for each eluting species are compared to known standards for species identification. The estimated method detection limit (eMDL) for bromide was generated from replicate analyses of the lowest standard in the calibration curve.

General procedure for Bromine quantitation by EINAA: Upon receipt, samples were held in a -20°C freezer. Samples were transferred to pre-cleaned high-density polyethylene irradiations vials and weighed. The samples were analyzed for bromine by epiboron neutron activation analysis (samples irradiated 5 times for 15 seconds each, decayed for 7.5 minutes and counted for 15 minutes). The bromine was quantified using the peak area of the 616 keV gamma-ray from the decay of ^{80}Br ($t_{1/2}$ = 17.68 m) which was produced via the neutron capture reaction on ^{79}Br. A minimum detectable amount (MDA) for Br was calculated to be 15 nanograms/g sample.

Bromide Quantitation by NAA: Methods for NAA were generally similar to that of EINAA, except that samples were not surrounded in a boron-nitride shield during irradiation.

Human Antibody Methods

Cohort Acquisition

Vanderbilt Goodpasture Disease Cohort- The Goodpasture disease cohort at the time of active disease was collected and handled exactly as previously described (Pedchenko et al., 2010). Samples were either serum collected within the first 72 hours of hospitalization or the earliest available plasmapheresis fluid. Samples were de-identified after collection, used and stored according to approved uses by Vanderbilt University Medical Center's Institutional Review and use Board.

Department of Defense Serum Repository Cohort- A unique cohort was obtained from the DoDSR essentially as previously described (Olson et al., 2011). Briefly, to perform a matched-case control study on serial samples pre-dating the onset of clinical Goodpasture's disease, patients were identified from the military database with an International Classification of Diseases, 9th Revision, Clinical Modification (ICD-9-CM) code for (Goodpasture's disease) anti-GBM disease (446.0) between January 1990 and October 2008. Only current or previous active duty members were included. One inpatient or two separate outpatient GP codes were required for inclusion. Additional ICD-9 codes were queried and assembled into a de-identified database as a surrogate for chart review to obtain additional clinical course insight when possible. For each case identified, three separate age, gender, race, and age of serum-matched healthy controls (as determined by lack of ICD-9- coded disease) were pulled to generate the final cohort of 6 patients and 18 matched controls with four pre-diagnosis samples. The assembled samples (~500 µL serum per time point per patient) were then shipped to Vanderbilt where all additional experimentation was performed. Researchers at

Vanderbilt (A.S.M) were blinded to specimen identity for the initial screen of peroxidasin, MPO, a3, and a5 collagen IV NC1 domains. The coded data was returned to S. Olson for case-control assignment as per the stipulations if the institutional review board of Walter Reed Army Medical Center.

Preparation of Antigens for ELISA- Recombinant human peroxidasin (hPXDN) was expressed in HEK293 cells and purified as described previously (Bhave et al., 2012; McCall et al., 2014). Human Myeloperoxidase was purchased from Athens Research and Technology (Athens, GA), reconstituted, aliquotted, frozen in liquid nitrogen, and stored at -80^{o}C until use. Both peroxidasin and MPO were checked for activity upon thawing by using a Tetramethylbenzidine (TMB) peroxidase assay (1µg enzyme in 100 µL TMB-ELISA Substrate Solution [Thermo-Fischer Scientific]) in the presence of 3mM NaBr and compared to pre-freezing values for each batch to ensure internal consistency. α3, and α5 collagen IV NC1 domains were recombinately expressed in HEK293 cells and purified exactly as described (Pedchenko et al., 2010).

Detection of Antigens by ELISA-All assays were run in 384 well format with 50 µL volumes for coating, incubation with human sera, and development. 100 µL volumes were used for blocking and wash steps. Peroxidasin (4 nM- 2.5 µg/ml), MPO (4 nM- 0.8 µg/ml), a3(IV) , and a5(IV) NC1 were applied immediately following dilution of the antigen in TBS and coated overnight at 4^{o}C on polystyrene 384 well plates (Nunc). Wash steps were then performed on a BioTek ELx50 plate washer using TBS with 0.05% v/v Tween-20 . Plates were blocked with 1% bovine serum albumin (Fraction V-RIA grade-Sigma Aldrich, St. Louis, MO) in TBS for 1hr at 37^{o}C. Human sera or plasmapheresis fluid was then diluted as defined in each experiment (1:100 for primary

screen, 1:500 for most subsequent experiments) in 0.1% BSA in TBS with 0.05% v/v Tween-20. After washing, secondary antibodies (Goat Anti-Human IgG (Fc specific)−Alkaline Phosphatase conjugate)(Sigma Aldrich, St. Louis, MO) was diluted 1:2000 in in 0.1% BSA in TBS with 0.05% v/v Tween-20 and applied for 1hr at 37^{o}C. After another wash, wells were developed using p-nitrophenyl phosphate (pNPP) as the AP substrate and the absorbance at 405nm was determined (SpectraMax Plus 384 Microplate Reader, Molecular Devices, Sunnyvale, CA). All samples run in duplicate. Initial screen of the DoD cohort run on the same day in four consecutive plates with control samples repeated across plates to insure internal consistency. Blank wells which were coated in BSA and received no primary antibody or sera were used as blanks.

Competition ELISA-Antigens were coated and plates blocked as described above. Sera were diluted 1:500 in 0.1% BSA in TBS with 0.05% v/v Tween-20 with varying amounts of MPO or peroxidasin (0 to 100 nM competing antigen) and allowed to pre-incubate for 12hrs at 4^{o}C before application to plates for 1hr 10min at 37^{0}C before a double wash (6 total volume changes per well). Secondary antibody and development proceeded as previously detailed.

Multiplex Cytokine Assay-Cytokine analysis on serum samples from the DoDSR cohort were assayed using the 30-plex MILLIPLEX MAP Human Cytokine/Chemokine Magnetic Bead Panel (EMD Millipore, Billerica, MA) as per manufacturer instructions with a reduction serum volume added for the assay to 20µL. Samples were run in

duplicate. The assay was developed on a Luminex MAGPIX system and analyzed using MILLIPLEX® Analyst 5.1 software. The lower limit of detection was set to 3.2 pg/ml of each cytokine as the lowest level present in the standard curve.

Immunofluorescence of Normal and Goodpasture kidney biopsies-2 µ frozen section were cut and acetone fixed from Normal and GP kidney. Sections were rehydrated in PBS and blocked for 1hr at RT with 10% normal goat serum. Block was incompletely removed and primary antibody was applied in PBS with 0.01% Triton-X100. Collagen IV NC1 domains were stained with JK2 (1:250), peroxidasin was stained with a peptide purified polyclonal antibody raised in Rabbit against an epitope within the peroxidasin domain. Specificity of the antibody was confirmed by western blot against MPO, EPO, and peroxidasin before immunofluorescence experiments. After washing, secondary antibodies were mixed in 5% NGS (Goat Anti-Rat 647, Goat Anti-rabbit 555, Donkey Anti-human IgG 488; numbers refer to conjugated fluorophore excitation maximum; Abcam, Cambridge, MA) in PBS-X and incubated at RT for 30 minutes. Samples were washed 3x and mounted in DAPI (4',6-diamidino-2-phenylindole**)** containing medium (Vectashild, Vector Laboratories, Burlingame, CA). Fluorescence images were acquired on a Zeiss Axio Imager.M2 equipped with an Apotome under 20x air magnification on the same day with identical exposure and microscope settings to enable quantitative comparison for all images acquired.

Peroxidasin inhibition kinetics- Peroxidasin was prepared as previously described (Bhave et al., 2012; McCall et al., 2014). Antibodies from patient sera were isolated using size exclusion chromatography on an Superdex 200 10/300 GL (GE Healthcare Life Sciences) in Phosphate Buffered Saline (PBS). Antibodies and peroxidasin were

premixed (500 pM peroxidasin, 218 µM whole patient IgG (437.5-fold mol excess), 100µM NaBr, 140mM NaCl) and added to a 96 well black-walled plated for fluorimetry. Using a GloMax® Discover fluorimeter equipped with a sample injector (Promega Corporation), APF (aminophenyl fluorescein) (AAT Bioquest, Sunnyvale, CA) (10µM APF final concentration) was injected and an initial time point measured. Because hypohalous acids react with APF to form fluorescein, an excitation wavelength was set to 470-490nm with an emission filter set between 500-500nm. Next, initial rates were measured after the addition of 7.5 µM H_2O_2 (final concentration) using the sample injector with serial readings every 30 seconds. All patient and control samples were run on the same plate, at the same time, with the same reagent batches to ensure maximum consistency in the rate measurement.

Statistical analysis: Analysis performed in this work was completed in either GraphPad Prism version 5.00 for Windows (GraphPad Software, San Diego California USA) or SPSS v. 22 (IBM). Broadly, all statistical tests between groups were analyzed using the non-parametric measures indicated unless the data being compared was found to have a normal distribution.

Table 1. ICP-MS analysis of reagent grade and purified salts used experimentally.

Sample	Bromide	
	µg/L	µM
1xPBS (reagent grade)	521	6.520
1xTBS (reagent grade)	510	6.380
10mM KBr	$1.1x10^6$	1376.7
100mM KCl (reagent grade)	472	5.907
100mM NaCl (reagent grade)	188	2.353
10mM Phosphate buffer (pH 7.4)	<4.6	<0.0576
H_2O (Millipore)	<4.6	<0.0576
100mM KI	5.32	0.0666
100mM KSCN	67.3	0.0842
100mM KF	5.60	0.0701
100mM KCl (pure)	<0.91	<0.0114
100mM NaCl (pure)	<0.91	<0.0114

Table 2. Components of Br-Free Dulbecco's Modified Eagle Media

Component	Sigma Cat No.	Final Concentration (mM)	Molecular Weight	mg/L
Neutral Amino Acid				
Glycine	G7126	0.4	75.07	30.0
L-Arginine	A8094	0.4	174.2	69.7
L-Cystine	C7602	0.2	240.3	48.1
L-Glutamine	49419	4	146.14	584.6
L-Histidine	53319	0.2	155.15	31.0
L-Isoleucine	W527602	0.8	131.17	104.9
L-Leucine	61819	0.8	131.17	104.9
L-Lysine	L9037	0.8	164.2	131.4
L-Methionine	64319	0.2	149.21	29.8
L-Phenylalanine	P5482	0.4	165.19	66.1
L-Serine	S4311	0.4	105.09	42.0
L-Threonine	89179	0.8	119.12	95.3
L-Tryptophan	93659	0.08	204.23	16.3
L-Tyrosine	93829	0.4	181.19	72.5
L-Valine	V0513	0.8	117.15	93.7
Vitamin				
Choline Citrate	C2004	0.03	295.29	8.9
D-calcium pantothenate	P5155	0.008	238.27	1.9
Folic Acid	F8758	0.009	441.4	4.0
Niacinamide	PHR1033	0.033	122.12	4.0
Pyridoxine (neutral)	P5669	0.02	169.18	3.4
Riboflavin	R4500	0.001	376.36	0.4
Thiamine Nitrate	CDS000474	0.012	327.36	3.9
Myo-inositol	57569	0.04	180.16	7.2
Bulk Salts/Minerals				
Sodium Chloride (Br-Free)		110	58.44	6428.4
Potassium Chloride (Br-Free)		5.4	74.55	402.6
Sodium bicarbonate	S6014	44	84.007	3696.3
Calcium lactate	L4388	1.8	218.22	392.8
Ferric nitrate	254223	0.001	404	0.4
Magnesium sulfate	63138	0.8	246.47	197.2
Sodium Phosphate Monobasic	71492	0.4	119.98	48.0
Sodium Phospahte Dibasic	71629	0.3	141.96	42.6
D-Glucose	G7021	25	180.16	4504.0
Sodium Pyruvate	P2256	1	110.04	110.04
Antibiotic				
Penicillin	P3032	100U/ml final	356.3	60.45mg/L
Streptomycin	S1277	100ug/ml final	728.69	100mg/L

Table 3. Br-Free Adapted Hanks Buffered Saline Solution

Final Composition	final conc(M)	formula weight	g/L
137 mM NaCl (Br-Free)	0.137	58.44	8.006
5.4 mM KCl (Br-Free)	0.0054	74.55	0.402
1.3 mM Ca-lactate	0.0013	218.22	0.284
1 mM MgSO4 (x7 H_2O)	0.001	246.47	0.246
0.3 mM Na_2HPO_4(Dibasic)	0.0003	141.96	0.043
0.4 mM NaH_2PO_4 (Monobasic)	0.0004	119.98	0.048
5.5 mM D-glucose	0.0055	180.16	0.991
8 mM HEPES	0.008	238.3	1.906
4.2 mM $NaHCO_3$	0.0042	84.007	0.351

Table 4. Neutron Activation Analysis of Media and Fly Diet Components

Sample	**Bromide**		
	ppm	µM	Method
1x PBS (reagent grade)	0.6 ±0.09	7.5 ±1.1	NAA
1X Br-free PBS	<0.2	<2.5	NAA
100 mM NaCl (Br-free)	<0.2	<2.5	NAA
Post-Culture Media for Br-free cell culture (See figure 2E)			
Commercial DMEM	1 ±0.011	12.5 ±0.1	NAA
Br-free DMEM	<0.2	<2.5	NAA
100 µM Br-added 'Br-free' DMEM	7.0 ±0.252	87.6 ±3.2	NAA
***Drosophila* Food Componants**			
Fleishmann's Active Dry Yeast	<0.3	<3.8	NAA
Standard Diet Grape Agar	1.2 ±0.061	15.0 ±0.76	NAA
Purified Phytagel	<0.06	<0.8	NAA
Br-free YNB yeast growth media	<0.09	<1.1	NAA
Br-free Yeast (lyophilized)	<1	<12.5	NAA
Whole Assembled Diets (includes vitamin mixture)			
Br-free^{DEP} whole food	<0.015	<187 nm	EINAA
Br-free^{DEP} + 100 µM NaBr whole food	7.958	98.6	EINAA

Chapter III

Bromide is a required cofactor for peroxidasin mediated collagen IV sulfilimine bond formation

These data appear as part of McCall, A.S.*, Cummings, C.F.*, Bhave, G.*, Vanacore, R., Page-McCaw, A., and Hudson, B.G. (2014). Bromine is an essential trace element for assembly of collagen IV scaffolds in tissue development and architecture. *Cell 157*, 1380-1392. *Co-first authors. I generated all data in this chapter except the explicitly noted collaborative panels as part of Figure 6.

Abstract

The peroxidasin generated sulfilimine bond crosslinks the collagen IV NC1 domain to varying degrees depending on the tissue from which the basement membrane is isolated. Yet, it is still unknown how the difference in observed dimer content from those tissues relates to quantitative differences in sulfilimine bond content or what halide cofactor peroxidasin employs to generate these observed sulfilimine contents in tissues, two key areas at the core of normal basement membrane physiology. Through mass spectrometry, we quantified the S=N content of the different dimer bands, finding that the doubly crosslinked NC1 domain dimer has a higher electrophoretic mobility. Screening of possible halide cofactors found that Bromide enhanced crosslinking, while Iodide and thiocyanate, a metabolite related to smoking could inhibit crosslinking. However we were unable to deconvolute the crosslinking role of Cl and Br because of Br contamination of commercial Cl salts. We therefore purified Br-free NaCl (<11nM Br contamination) and tested then *in vitro* behavior of peroxidasin, finding that Br was required for S=N crosslinking at physiologic levels for both the purified enzyme and in a cell culture model of basement membrane synthesis. Overall, peroxidasin uses Br^- to catalyze formation of sulfilimine crosslinks with at least 50,000-fold greater efficiency compared to Cl^-. These data firmly establish that peroxidasin requires Br as its cofactor to generate sulfilimine crosslink at physiologically observed levels. The interaction of smoking and peroxidasin crosslinking suggest the potential reduction in crosslinking by almost half in 1-pack per day smokers because of the functional Br-deficiency caused by thiocyanate accumulation in smokers, raising the possibility of a role for functional inhibition of peroxidasin crosslinking in smoking related disease. Because Br has not to date had any required biologic role, these data represents the first essential function of the element Br is biology.

Introduction

Assembly of the collagen IV scaffold is an intricate process of organization and covalent reinforcement. Triple-helical protomers self-assemble extracellularly into insoluble lattices, and nascent scaffolds are stabilized via the enzymatic formation of sulfilimine crosslinks between the NC1 domains of two juxtaposed protomers at residues methionine-93 (Met^{93}) and hydroxylysine-211 (Hyl^{211})(Vanacore et al., 2009)(Figure 3A). Peroxidasin, a heme peroxidase embedded within basement membranes, catalyzes the formation of sulfilimine crosslinks which confer critical structural reinforcement to collagen IV scaffolds, as seen in nematodes, flies, and zebrafish, where loss of peroxidasin causes basement membrane dysfunction(Bhave et al., 2012; Fidler et al., 2014; Gotenstein et al., 2010) .

Peroxidasin forms hypobromous acid (HOBr) and hypochlorous acid (HOCl) from bromide and chloride, respectively, both of which can mediate crosslink formation (Fig 1A). *In vitro* studies point to a preference for Br^- during enzymatic sulfilimine formation but its role within the *in vivo* reaction is unknown, particularly in light of the vast excess of Cl^- over Br^- in most animals (Weiss et al., 1986). Despite its ubiquitous yet trace presence within animals, Br^- is without a known essential function. Bromide is a cofactor for eosinophil peroxidase (EPO) following eosinophil activation (Mayeno et al., 1989; Weiss et al., 1986) but the relevance of this is unclear as EPO preferentially oxidizes SCN^- over Br^- (Nagy et al., 2006). Thus, the definitive identification of Br^- as a cofactor for peroxidasin-mediated crosslink formation would represent the first essential function for the element bromine. Moreover, the effects of potential cofactors on

peroxidasin derived sulfilimine content within tissues is a potentially critical linkage between functional collagen IV networks and the overlying tissues they support.

Results

Structural basis for sulfilimine crosslink heterogeneity in the collagen IV scaffold

Sulfilimine crosslinks connect the NC1 domains at the interface of two adjoining triple helical protomers within the collagen IV scaffold, forming a globular hexameric structure. Following isolation via collagenase digestion and SDS-PAGE analysis, NC1 hexamers dissociate into crosslinked dimers, designated D_1 and D_2 and uncrosslinked monomers (Figure 3A). The structural distinction between D_1 and D_2 is unknown and is of long-standing interest (Langeveld et al., 1988; Weber et al., 1984). The electrophoretic pattern of HOBr-reacted hexamers closely resembled that of hexamer isolated from native placental and glomerular basement membranes (PBM and GBM, respectively) (Langeveld et al., 1988). Since the NC1 domain has not been shown to have any phosphorylation or glycosylation, we hypothesized that the presence of multiple dimer bands could be the result of differential S=N crosslinking. In a manner analogous to circular vs. linear DNA, we expected that a doubly S=N crosslinked dimer would form a large cyclic structure and have higher electrophoretic mobility when compared to a mostly linear singly crosslinked dimer of the same sequence (Aaij and Borst, 1972). We hypothesized that D_1 and D_2 differed by the number of crosslinks, D_1 having one and D_2 with two crosslinks. Because a difference in S=N content would be expected in this scenario, we purified NC1 hexamer from murine PFHR-9 basement membrane cell-culture model, isolated D_1 and D_2 by electrophoresis, performed an in-gel trypsin digest, and analyzed the abundance of S=N crosslink peptides by liquid

chromatography- mass spectrometry(LC-MS). D_2, the band with higher electrophoretic mobility, was found to have 1.95-times more sulfilimine-containing peptides than D_1 (Figure 3B-C, Figure 4A-E), indicating that D_2 has two and D_1 has one sulfilimine crosslink. We thus used the relative abundance of D_1 and D_2 on SDS-PAGE analysis of NC1 hexamers to assess sulfilimine crosslink content (Figure 3D). The ability to accurately quantify sulfilimine content via SDS-PAGE electrophoresis was pivotal to mechanistically understanding the chemistry underpinning sulfilimine crosslinking in later studies as well. Re-quantification of tissue derived NC1 demonstrated that HOBr, but not HOCl, was able to mimic the tissue derived crosslinking content (Figure 5A-B). This observation prompted deeper investigation of the halide cofactors used by the enzyme.

Bromide is required for sulfilimine formation

Since our work thus far has been limited to Cl^- and Br^- in vitro, we screened the halides (F^-, Cl^-, Br^-, I^-) and thiocyanate (SCN^-, "pseudohalide") in cell culture to probe their effects on sulfilimine formation. SCN^- and I^- inhibited the reaction while Br^- enhanced crosslink formation (Figure 6A). Since F^- proved cytotoxic and testing of Cl^- was precluded by background levels in media, we moved to an isolated PFHR-9 *in vitro* model of collagen IV matrices. In this model, peroxidasin is reversibly inhibited during matrix deposition by the addition of KI to generate an uncrosslinked matrix that is harvested for study. The subsequent addition of H_2O_2 to the matrix drives crosslink formation by peroxidasin (Bhave et al., 2012). F^- was inert to crosslink formation, so we used 100 mM KF as an ionic control while titrating either Cl^- and Br^- (Figure 6B). Br^-

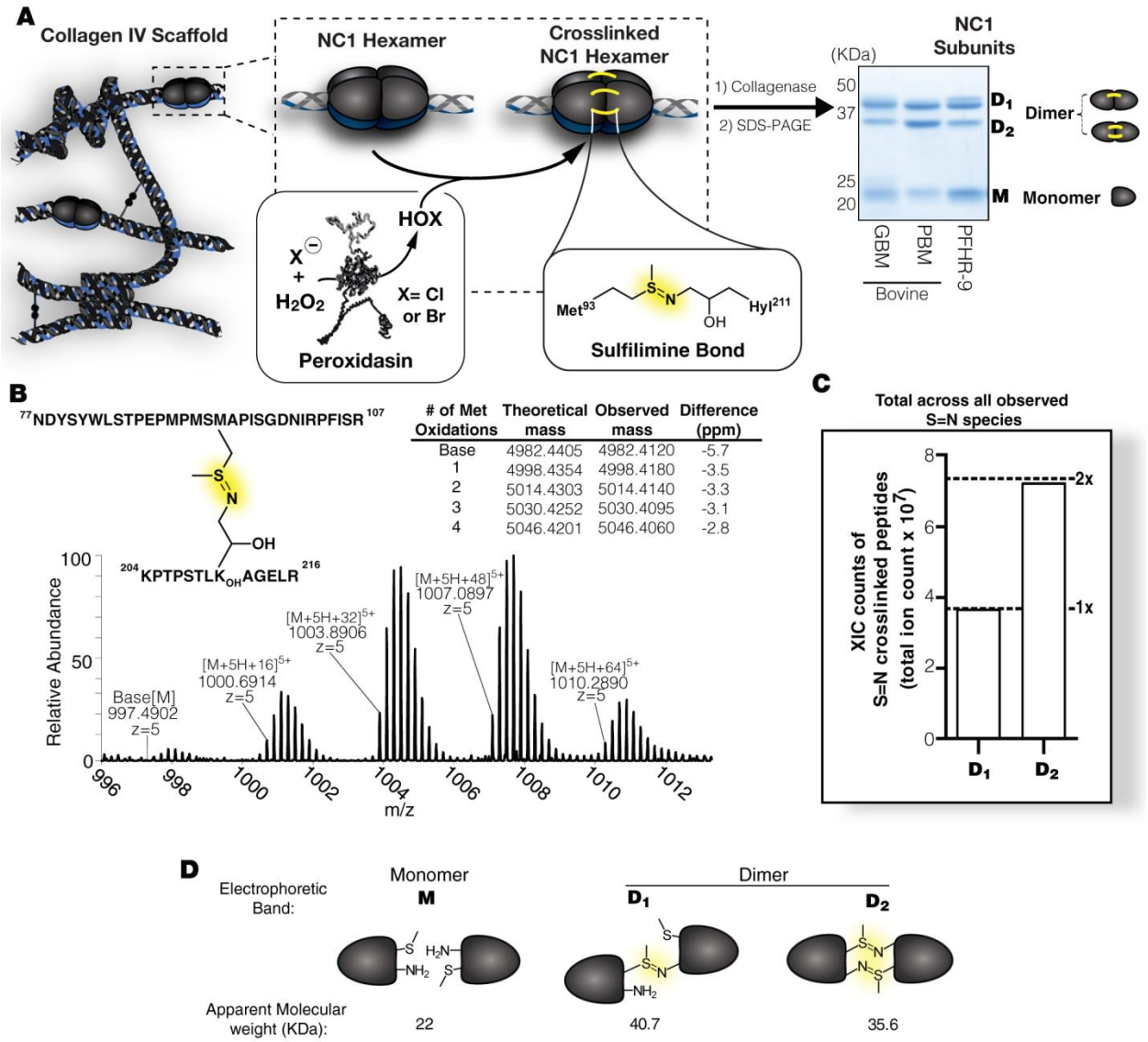

Figure 3. Measurement of sulfilimine crosslink content within NC1 domains of collagen IV scaffolds

(A) Diagram of the collagen IV scaffold, showing the relationship of NC1 hexamers sulfilimine crosslinks, peroxidasin (PXDN), and hypohalous acids (HOX). Inset shows resolution of dimeric (D_1 and D_2) and monomeric (M) NC1 domains by SDS-PAGE. Representative NC1 domains are shown from bovine placental basement membrane (PBM), bovine glomerular basement membrane (GBM), and murine collagen IV matrix produced in PFHR-9 cell culture.

(B) High-resolution mass spectrum depicting the multiple oxidation states of tryptic peptides containing the sulfilimine (S=N) crosslink
(C) Extracted ion current (XIC) based quantitation of S=N crosslinked peptides from D_1 and D_2. Full data appears in Figure S1.
(D) Diagram showing the crosslinking status of observed NC1 banding in SDS-PAGE, where D_1 is singly crosslinked and D_2 is doubly crosslinked with a resultant higher electrophoretic mobility.

A

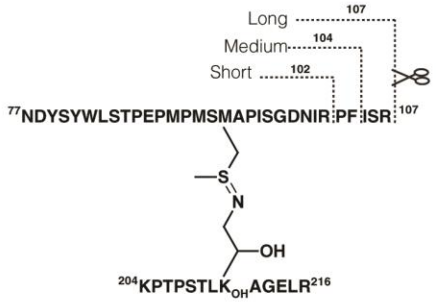

B

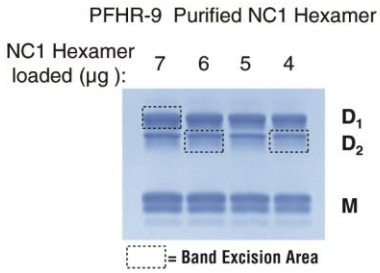

C

Met Peptide	Base Parent	z	Base Theoretical Mass	1 S=O Parent	z	1 S=O Theoretical Mass	1 S=O D_1 (Top)	1 S=O D_2 (Bottom)	2 S=O Parent	z	2 S=O Theoretical Mass	2 S=O D_1 (Top)	2 S=O D_2 (Bottom)
Short NDY…NIR 2971.3190	4382.1021	4+	1096.5334	4398.0970	4+	1100.5322	87283	115329	4414.0919	4+	1104.5309	411139	702317
		5+	877.4283		5+	880.6273	853832	855943		5+	883.8263	2529217	4139830
		6+	731.3583		6+	734.0241	151593	158656		6+	736.6899	558480	793900
		7+	627.0209		7+	629.3059	ND	ND		7+	631.5909	ND	ND
Medium NDY…NIRPF 3215.4402	4626.2233	4+	1157.5637	4642.2182	4+	1161.5625	ND	ND	4658.2131	4+	1165.5612	719095	1600176
		5+	926.2526		5+	929.4515	1372165	2014464		5+	932.6505	4978966	8915072
		6+	772.0451		6+	774.7109	549083	1021684		6+	777.3768	1151406	2085452
		7+	661.8954		7+	664.1804	ND	ND		7+	666.4653	ND	ND
Long NDY…NIRPFISR 3571.6574	4982.4405	4+	1246.6180	4998.4354	4+	1250.6168	ND	ND	5014.4303	4+	1254.6155	720668	1085000
		5+	997.4960		5+	1000.6950	2260070	3304881		5+	1003.8940	7159435	15550206
		6+	831.4147		6+	834.0805	2922292	4298477		6+	836.7463	11342024	22162322
		7+	712.7835		7+	715.0685	358124	566905		7+	717.3535	1917608	3923592

Met Peptide	3 S=O Parent	z	3 S=O Theoretical Mass	3 S=O D_1 (Top)	3 S=O D_2 (Bottom)	4 S=O Parent	z	4 S=O Theoretical Mass	4 S=O D_1 (Top)	4 S=O D_2 (Bottom)
Short NDY…NIR 2971.3190	4430.0868	4+	1108.5296	83837	216585	4446.0817	4+	1112.5283	82050	114277
		5+	887.0253	766616	1485566		5+	890.2242	214145	583989
		6+	739.3557	173814	439713		6+	742.0215	ND	ND
		7+	633.8759	ND	ND		7+	636.1609	ND	ND
Medium NDY…NIRPF 3215.4402	4674.208	4+	1169.5599	234819	605066	4690.2029	4+	1173.5586	ND	ND
		5+	935.8495	1502869	3456663		5+	939.0485	616753	980348
		6+	780.0426	359072	818349		6+	782.7084	199948	331917
		7+	668.7503	ND	ND		7+	671.0353	ND	ND
Long NDY…NIRPFISR 3571.6574	5030.4252	4+	1258.6142	224545	641648	5046.4201	4+	1262.6129	50107	231163
		5+	1007.0929	2928706	7266473		5+	1010.2919	1443057	2945549
		6+	839.4121	4268805	9306196		6+	842.0779	1697001	4113842
		7+	719.6385	608572	1298076		7+	721.9235	329516	677461

Hydroxylysine Peptide

KPT...AGELR (1412.7987)

ND= Not detected

D

Oxidation Status	Total S=N Peptide Ion Counts D_1 (Top)	D_2 (Bottom)
1 S=O	8554442	12336344
2 S=O	31488038	60957866
3 S=O	11151655	25534335
4 S=O	4632577	9978546
Sum	55826712	108807092

Ratio S=N peptides

$$\frac{D_2}{D_1} = 1.95$$

E

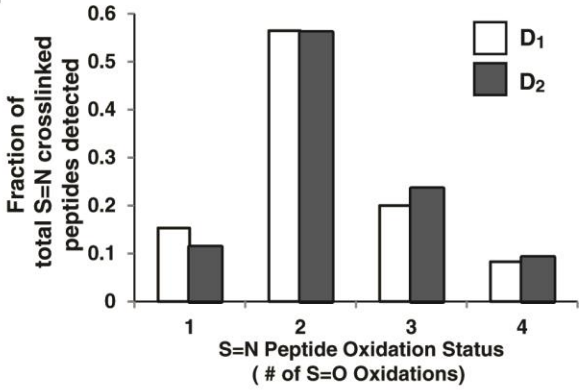

Figure 4. Quantitation of sulfilimine (S=N) crosslinked peptides (associated with Figure 3) (previous page)

(A) Schematic representation of the crosslinked peptide. Dashed lines with scissors indicate the multiple cleavage sites and the resultant peptides.

(B) Coomassie Blue G250 stained gel of PFHR-9 purified NC1 subunits after non-reducing SDS-PAGE. Bands density was quantified using Bio-Rad Image Lab 3.0 (Hercules, CA) and excised to match the total amount of protein obtained from D_1 and D_2.

(C) Results table from mass spectrometric analysis of S=N cross-linked peptides, displaying the observed and predicted permutations of cleavage patterns, oxidation states, and charges. Theoretical mass refers to the calculated mass of the crosslink-containing ion after accounting for charge state and number of S=O within the ion. Data is grouped according to the number of observed S=O within the ion and presented for both D_1 and D_2 bands. Ion counts were obtained from the Extracted Ion Chromatogram (XIC) and compared after correction for total ion counts observed over the entire elution of all tryptic peptides. ND= none detected. S=O denotes methionine sulfoxide.

(D) Summary table of the number of observed ions containing the S=N crosslink within the D_1 and D_2 bands.

(E) Graph of the proportional contribution of each oxidation state to the total observed S=N peptides by mass spectrometry. Gray bars denote D_2 and white denote D_1. Because of the largely stochastic nature of S=O formation through sample processing, little difference should be expected, and was not observed.

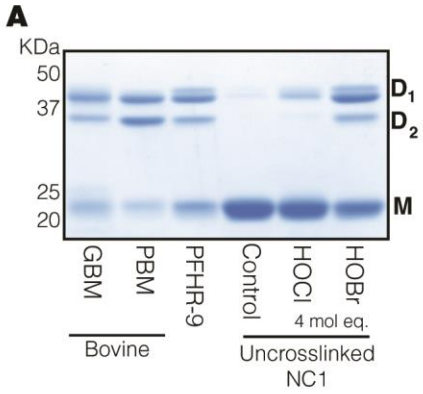

B

Basement Membrane Source			S=N Bonds / Hexamer
GBM			2.48
PBM			3.45
Control PFHR-9			2.08
Uncross-linked NC1 Hexamer	Untreated		0.16
	10.7 mol eq.	HOCl	1.35
		HOBr	3.89

Figure 5. HOBr reproduces physiologic levels of S=N crosslinking within the NC1 Hexamer (Associated with Figure 3)

(A) SDS-PAGE comparison of NC1 banding patterns from bovine placental basement membrane (PBM) and glomerular basement membrane (GBM), PFHR-9 murine cell-culture model of matrix, PFHR-9 cells grown in the presence of phloroglucinol (PHG) (50μM), and PHG-derived NC1 hexamer (1.7 μmol) treated with 4 mol equivalents of HOBr or HOCl relative to the amount of Met^{93} residues.

(B) Table comparing S=N crosslinking per hexamer based on treatment and tissue source.

robustly catalyzed crosslink formation at 10 μM while Cl^- remained inactive until 100 mM (Figure 6B).

While these data pointed to a strong preference for Br^- over Cl^- in crosslink formation, we considered whether contaminating Br^- in our Cl^- solutions might confound the results. Indeed, we measured Br^- content at 5.91 μM/100 mM KCl (ICP-MS)(Table S1), making the apparent Cl^- activity difficult to distinguish from that of contaminating Br^-. To address this, we produced Br-free NaCl and KCl (<11.4 nM Br^-) (Figure 6C, Figure 7, Table 1). Significantly, Br-free Cl^- did not support crosslink formation when tested with either 100 mM purified KCl (Figure 6D). Crosslink formation was restored upon addition of 5 μM Br^-.

For validation, we tested the efficiency of crosslink formation in PFHR-9 cells grown in Br-free conditions using media verified as Br-free by Neutron Activation Analysis (NAA) (<2.5 μM Br^-) (Table 4). In Br-free and Br-added culture conditions, there was no appreciable difference in cell proliferation, cell viability, or collagen IV production. Importantly, Br-Free media did not support formation of sulfilimine crosslinks in the collagen IV matrix, while the addition of 100 μM Br^- rescued physiologic levels of crosslinks (Figure 6E). This establishes that Br^- is required for sulfilimine formation, implying a key role for the ion in collagen IV scaffold assembly within tissues.

Peroxidasin catalyzes sulfilimine crosslink formation via Br^-

Recombinant human peroxidasin and NC1 hexamer were purified under Br-free conditions to enable rigorous interrogation of the oxidation dynamics of Br^-. For comparison, we also prepared other mammalian peroxidases (myeloperoxidase [MPO]

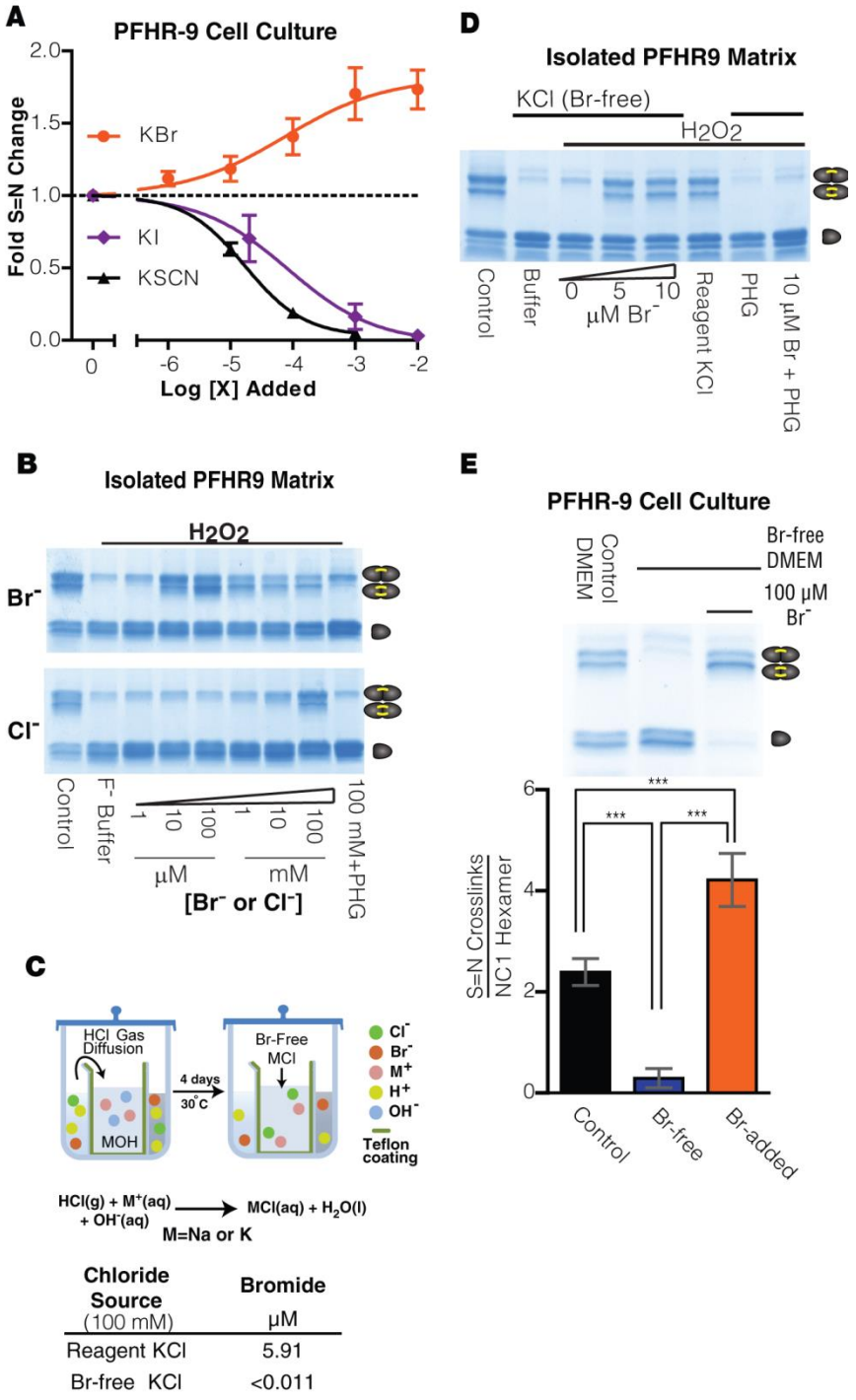

Chloride Source (100 mM)	Bromide µM
Reagent KCl	5.91
Br-free KCl	<0.011

Figure 6 Bromide is the required cofactor for sulfilimine crosslink formation
(A) The effect of halide ions on sulfilimine crosslink formation is examined in PFHR-9 matrix. Inhibition values were calculated from non-linear curve fitting: KI (IC_{50}= 84µM 95%CI[30-241µM]), KSCN (IC_{50}=17µM 95%CI[3-24µM]). Contrasting with these effects, exogenous potassium bromide (KBr) enhanced the reaction. Points represent

mean ± S.D. (n=3). (Original cell culture experiments performed by C. Cummings, all subsequent analysis, curve fitting, and equation derivation performed solely by me)
(B) Uncrosslinked PFHR9 matrix was crosslinked *in vitro* in the presence of KCl and KBr. Reacted for 1 hr. at 37^{o} C with 1 mM H_2O_2. 100 mM KF used as ionic strength control. Collagenase digest analyzed by SDS-PAGE and Coosmassie staining. (Performed by C. Cummings)
(C) Schematic of Br-free Cl- salt purification apparatus and setup. Resulting salt was analyzed by ICP-MS for bromide content. Further analysis of salt reagents appears in Table 1 and an additional diagram of the purification apparatus appears in Figure 7
(D) Crosslink formation in PFHR-9 matrix with Br-free KCl. Reaction buffer contained 10 mM phosphate buffer (pH 7.4), 100 mM Br-free or reagent grade KCl, and 1 mM H_2O_2 and 200 µM PHG where appropriate. Displayed SDS-PAGE gels were stained with Coomassie blue. (Performed by C. Cummings)
(E) Sulfilimine (S=N) crosslink formation in PFHR-9 cell-culture tested under Br-free conditions. Culture conditions and media formulations are presented in detail in the supplementary methods. NC1 hexamers were isolated via collagenase treatment and analyzed by SDS-PAGE. The amount of crosslinks per hexamer is graphed as the mean±95% C.I. (n=3). All sample groups had equal variance, one-way ANOVA was performed ($p<0.001$) and differences between groups was tested using Tukeys post-hoc analysis (***$p<0.001$)

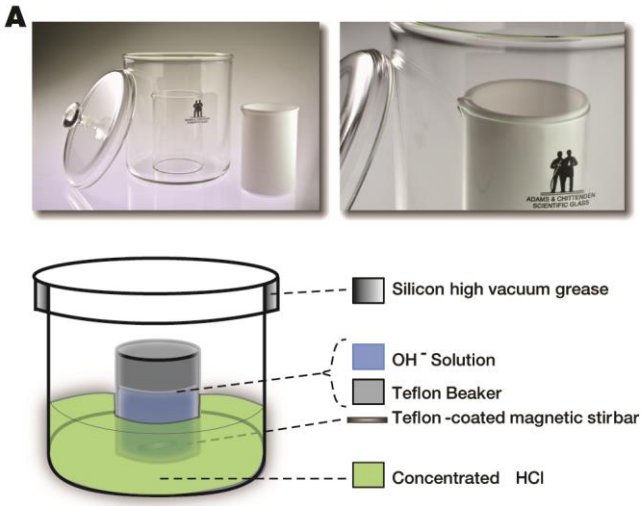

Figure 7. Purification apparatus and setup for the purification of Br-Free Chloride Salts and (associated with Figure 6)
A specialized chamber was designed and constructed for the reaction of concentrated HCl with concentrated aqueous hydroxide solutions within a sealed environment. The chamber was manufactured by Adams and Chittenden Scientific Glass (Berkeley, CA). Pictures and diagram of reaction chamber with inner Teflon beaker. Pictures show how the Teflon beaker is positioned inside a holder within reaction chamber. Diagram reveals how the chamber and key reaction solutions were assembled. Pictures courtesy of Adams and Chittenden.

and eosinophil peroxidase [EPO]) under Br-free conditions. Generally, peroxidases use peroxide to oxidize a halide ion to the corresponding hypohalous acid (HOX, X=Cl or Br). After normalization of peroxidase activity of all enzyme preparations (Bozeman et al., 1990), we found peroxidasin to be much more effective in forming crosslinks than MPO or EPO under identical conditions, especially regarding D_2 (two crosslinks) formation (Figure 8A). Crosslink formation by peroxidasin exceeded EPO despite normalized enzyme activity, indicating that hypohalous production is not the only contributing factor for the reaction. This suggests the potential of a putative binding event between peroxidasin and the hexamer where nascent HOBr molecules are directed towards Met^{93}. Considering that the *in vivo* reaction occurs within basement membranes, a peroxidasin-NC1 complex may limit non-specific oxidation of the surrounding matrix.

We sought to characterize the responsiveness of peroxidasin and MPO to Br^- levels. Both enzymes generated only a small amount of crosslinks per hexamer in Br-free saline. Under these conditions, HOCl is the only hypohalous product of either enzyme. The addition of 100 μM Br^- significantly enhanced crosslink formation by peroxidasin, as did increased H_2O_2 levels, (Figure 8B), suggesting that the *in vivo* enzymatic mechanism is responsive to both Br^- and oxidant concentrations. When Br^- was titrated into the system, D_1 formed prior to D_2 indicating a sequential crosslinking mechanism (Figure 8C), wherein D1 has one and D_2 has two sulfilimine crosslinks. Thus, the relative amount of D_2 represents a key index of crosslinks within the overall NC1 hexamer, and is a notable feature of tissue-isolated collagen IV (Figure 5; (Langeveld et al., 1988)). *In vitro*, we find that crosslink formation by either a Br-H_2O_2-

peroxidasin system or the direct HOBr application produces D_2 to a similar degree as observed in tissues (Figure 5).

To address the effect of physiologic Br^- levels, we calculated the EC_{50} for Br^- in this system to be 4.5 μM (95% CI 3.8-5.2 μM) in the presence of 140 mM Cl^- (Figure 8D). Using MPO as a baseline for the efficacy of Cl-based oxidants, these data indicate a >50,000-fold efficacy difference for Br^- over Cl^- as a cofactor in the peroxidasin-catalyzed formation of crosslinks, demonstrating a strong selectivity for Br^-. Bromide has a normal range of 10-100 μM in serum (van Leeuwen and Sangster, 1987), and within these levels peroxidasin formed cross-links at more than 90% of the available sites but was markedly less effective below this range, potentially indicating an optimal Br^- level for *in vivo* sulfilimine formation.

Modelling thiocyanate effects on peroxidasin mediated sulfilimine crosslinking in smokers

The observation of an optimal Br concentration coupled with the observation that SCN^- potently inhibited sulfilimine formation in cell culture, suggests that an increase of thiocyanate levels in humans may have pathologic relevance. It is well known that smoking results in elevated levels of SCN^- (Pattison et al., 2012). Considering other peroxidases such as myeloperoxidase (MPO), SCN^- competes with Cl^- within the enzyme active site to form hypothiocyanous acid (HOSCN). With this general peroxidase trend in mind, we hypothesized that SCN^- was competing with Br^- for oxidation by peroxidasin. We thus analyzed the data reported in Figure 6A, providing an estimate of IC_{50} using sulfilimine (S=N) content as a functional assay for HOBr production; Figure 8D, providing a crude estimation of a K_m for Br^- as a substrate for

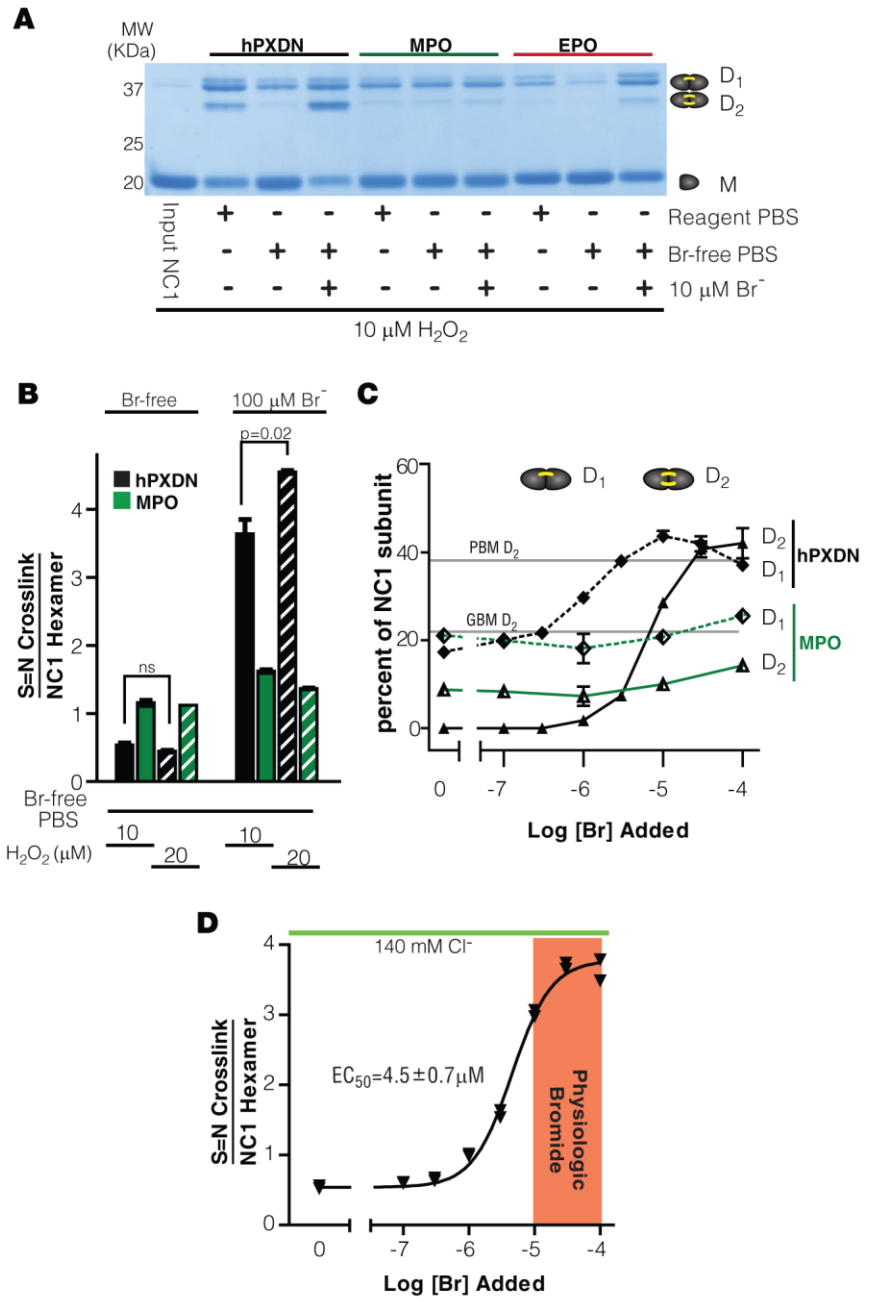

Figure 8. Peroxidasin uses physiologic Br^- levels to form sulfilimine crosslinks (A-D) Mammalian peroxidases are compared for ability to crosslink collagen IV NC1 domains in Br-free 1x PBS, (recombinant human peroxidasin (hPXDN), myeloperoxidase (MPO), eosinophilperoxidase (EPO).Uncrosslinked NC1 domains were isolated from PHG-treated PFHR-9 cultures. All peroxidase activity of the enzymes was nominalized by TMB assay prior to assay (Bozeman et al., 1990). Reactions proceeded for 10 minutes at 37° C after initiation by the addition of H_2O_2 and quenched with 5 mM PHG, 0.2 mg/ml bovine catalase, and 10 mM methionine. Gel representative of 3 experiments.

(**A)** Coomassie stained gel of enzymatic crosslink formation under reagent grade and Br-free conditions.
(B) Quantitative analysis of crosslinks formed per NC1 hexamer by MPO and hPXDN under Br-free and Br-added (100 μM) conditions. Data shown as mean ± 1 S.D. n=2. Student's T-Test was performed (n=2) due to equal variance between groups.
(C) Effect of bromide titration on the proportion of D_1 (1 crosslink) and D_2 (2 crosslinks) NC1 populations following reaction with MPO and hPXDN. For reference, the proportions of D_2 found in PBM and GBM are denoted on the graph. Data shown as mean ± 1 S.D. (n=2).
(**D)** Crosslinking efficacy of peroxidasin measured as crosslink formed per hexamer upon Br^- titration. EC_{50} value ± 95% C.I. (n=2).

peroxidasin, again with S=N bond formation as a functional assay; and our Neutron Activation Analysis (NAA) of the Br content of normal media (Table 4). These accumulated data points were sufficient to estimate the K_i for SCN^- under the conditions tested in the PFHR-9 cells culture experiment in Figure 6A. We thus used a modified Cheng-Prusoff relationship and the parameters above to estimate K_i:

Parameter	Concentration μM(95% CI)
IC_{50} for SCN^- in culture	17(3-24)
K_m for Br^- by hPXDN	4.5(3.8-5.2)
[Br] in culture media	12.5(12.4-12.6)

Adapted Cheng-Prusoff Equation

$$K_{i_{SCN}} = \frac{IC_{50_{SCN}}}{1 + \frac{[Br^-]}{K_{m_{Br^-}}}}$$

The estimated K_i for SCN^- is 4.5 μM (95% CI 0.8-6.4 μM). We interpret the inhibition of peroxidasin activity in our functional S=N bond formation assay to mean that SCN^- is competing with Br^- for oxidation at peroxidasin's active site, though other modes of activity cannot be excluded. It is known that HOSCN, which has been observed as an oxidation product of SCN^- via peroxidasin (Li et al., 2012), will not oxidize methionine (Peskin et al., 2009), implicating a competitive inhibition picture for this system whereby thiocyanate is being oxidized and thus 'inhibits' S=N bond formation by outcompeting Br^- within the enzyme active site, and therefore precluding HOBr production.

To estimate the potential impact of smoking on sulfilimine formation, we evaluated the presumed impact that normal serum thiocyante concentration (33 μM), and serum thiocyante concentration from a 1 pack/day smoker (134 μM) (Tsuge et al., 2000) might have on the ability of peroxidasin to cross-link the collagen IV scaffold.

Using the classic Michaelis-Menten equation modified for a competitive inhibitor, and using cross-link formation (S=N) as a surrogate for HOBr production (and therefore Br- oxidation velocity) by peroxidasin, we obtained the following equation:

$$v_{S=N} = \frac{v_{max_{S=N}}[Br]}{K_m\left(1 + \frac{[SCN^-]}{K_{i_{SCN}}}\right) + [Br]}$$

By using $v_{max(S=N)}$ obtained PFHR-9 cell culture and hPXDN oxidation of hexamer of 4.5 S=N bonds/hexamer as the maximal possible crosslink, the K_m for Br discussed above, the estimated $K_{i(SCN)}$ from above, and an average human serum concentration of Br (67 μM) (Olszowy et al., 1998), we were able to calculate the potential effect of SCN^- on maximal physiologic S=N bond formation by peroxidasin. Based on the physiologically observed ranges for Br^- and SCN^- available, Figure 9 demonstrates the interaction of their concentration on maximally possible S=N crosslinking. As a finite example, the crosslinking effect of a one pack-per-day smoker with normal serum Br^- compared to a normal nonsmoker appear below, highlighting the effective halving of maximal potential crosslink:

Physiologic State (serum SCN^- conc. in μM)	Maximum S=N bond formation/Hexamer
Normal (33 μM)	2.9
1 pack/day smoker (134 μM)	1.4

The serum levels of both Br and SCN are heavily influenced by diet and environment, demonstrated in part by the dose dependent elevation on serum SCN^- in response to smoking. These calculated values represent a reasonable estimate of the effect of smoking on cross-link formation in collagen IV scaffolds where the Br^- and SCN^- levels are comparable to the assumptions presented here.

Discussion

The identification of bromide as the required cofactor for peroxidasin mediated sulfilimine crosslinking coupled with the delineation and quantitation of sulfilimine content from tissues forms the foundation for understanding sulfilimine biochemistry within the collagen IV scaffold. Prior to this work, peroxidasin function and therefore sulfilimine content was understood in mainly qualitative terms for both the terminal oxidant that the enzyme generated (more HOBr than HOCl was made)(Bhave et al., 2012) and sulfilimine content (more dimer in the placental basement membrane than in the lens capsule) (Langeveld et al., 1988; Weber et al., 1984). The demonstration that Br^- is quantitatively required to recapitulate physiologically observed degrees of crosslinking in a purified enzyme system (Figure 8), more complex isolated matrix environment(Figure 6D), and ultimately in a cell culture model of basement membrane deposition (Figure 6E) strongly suggests that Br will have an essential biologic function through its role as cofactor for peroxidasin in the formation of the sulfilimine bond.

The ability to precisely and quantitatively assess sulfilimine crosslink content within the NC1 domain was an important technical advance which facilitated many of the subsequent experimental advances in sulfilimine biochemistry in this work. Demonstration that D_2, the dimeric NC1 band with higher electrophoretic mobility by

SDS-PAGE, possessed essentially twice the sulfilimine crosslinked present in D_1 magnified many postulated in S=N content differences previously thought to be relatively minor. For example, PBM and GBM only differ in total dimer content by ~8.5%, but differ in S=N content by nearly 30% (Figure 5), meaning there is on average one additional crosslink per hexamer, a previously underappreciated difference in the collagen IV matrix between these tissues. This observation is interesting in the context of overall collagen IV crosslinking within a network (Figure 1). All collagen IV molecules share NC1 and 7S domains, but the α112 network which composes the placenta has 10 potential inter-protomer disulfide bonds (3.5 S=N/Hexamer), while the α345 network of the glomerulus has 27 possible inter-protomer disulfides (2.5 S=N/Hexamer) (Figure 5) (Gunwar et al., 1998). The fact that the more heavily disulfide crosslinked network has less sulfilimine content could potentially reflect differing mechanical responsibilities for the S=N crosslink within these different networks and tissues, and therefore differential responses to perturbed peroxidasin function.

Peroxidasin crosslinking of the NC1 hexamer to tissue relevant levels in the span of physiologically observed Br ranges, coupled with the requirement of Br to achieve those levels of crosslink, was only discernable because of the development of Br-free salts and buffers. The 5.91 μM Br contamination in 100mM KCl was sufficient to have masked these findings because of the 4.5 μM apparent Km of peroxidasin for Br in sulfilimine crosslinking even in the presence of 140 mM NaCl (Figure 8). Considering the robust selectivity for Br^- over Cl^-, the nearly identical 4.5 μM K_i for SCN^- has the potential to effectively compete with Br^- for oxidation at physiologically observed concentrations. Because competitive inhibition of Br^- oxidation by SCN^- would be

functionally similar to insufficient Br^- concentrations to efficiently crosslink the collagen IV scaffold, even in the presence of normal serum Br levels, excess SCN^- could mimic a Br-deficit from the perspective of the tissue (Figure 6). Ergo, in active smokers with elevated SCN^- levels (130 μM, 1 pack per day) (Tsuge et al., 2000), reinforcement newly synthesized collagen IV scaffolds with sulfilimine crosslinks may be reduced by almost half (Figure 9).

The >50,000-fold efficacy difference for Br^- over Cl^- as a cofactor in the peroxidasin-catalyzed crosslinking likely has two components, namely the enzyme selectively oxidizing Br over Cl and the intrinsically different response of the NC1 domain to HOBr compared to HOCl for sulfilimine formation(Figure 5) (Bhave et al., 2012). Since peroxidasin has been tightly conserved along the same evolutionary timescales that collagen IV and the sulfilimine bond have existed (Fidler et al., 2014; Soudi et al., 2012), it is plausible that peroxidasin's enzymatic preference for Br as a cofactor has been driven at least in part by the preference of the NC1 domain for HOBr as the apparent oxidant of choice for sulfilimine formation. While appealing, the NC1 driven 'selection' of HOBr an oxidant is an unexplained phenomena within the context of unique crosslink in biology.

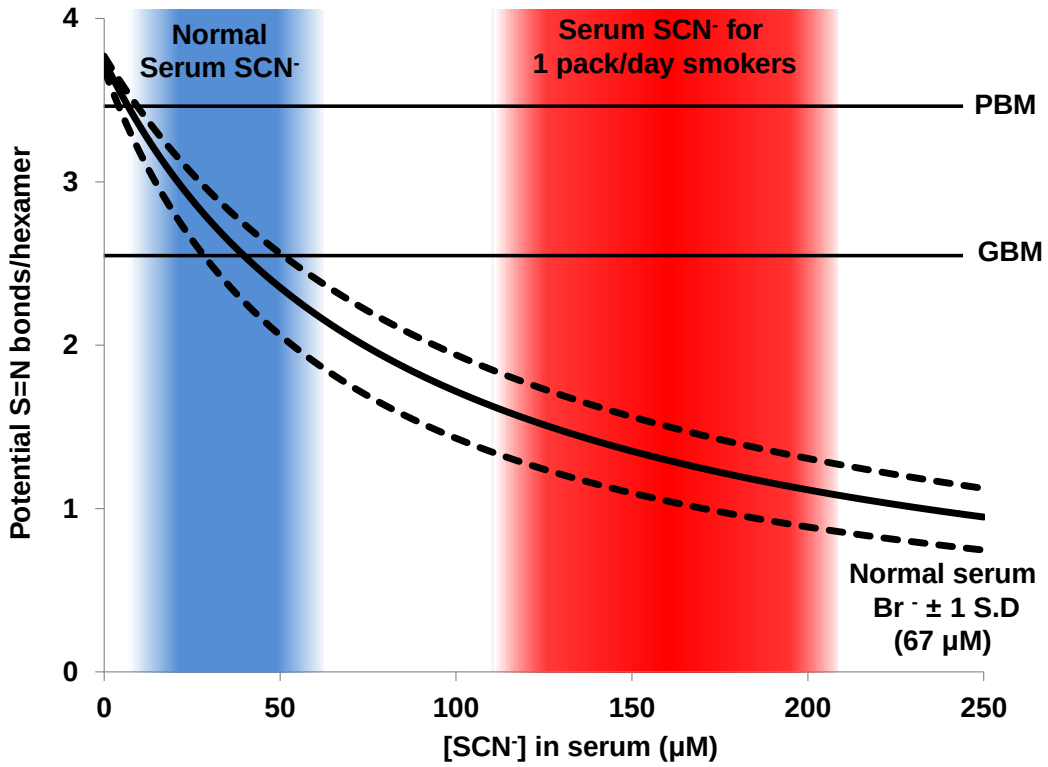

Figure 9. Model of the interaction between serum Br and SCN^- on sulfilimine crosslinking in normal individuals and smokers
Modeling of S=N crosslinking in the presence of normal plasma Br and varying concentrations of SCN^-, with the area's for normal serum (blue) SCN^- (range represents mean± 1 S.D), as well as serum SCN^- from smokers (highlighted in red).

Chapter IV

The chemical basis for selection of Br^- over Cl^- as the cofactor in peroxidasin mediated NC1 sulfilimine crosslink formation

These data appear as part of McCall, A.S.*, Cummings, C.F.*, Bhave, G.*, Vanacore, R., Page-McCaw, A., and Hudson, B.G. (2014). Bromine is an essential trace element for assembly of collagen IV scaffolds in tissue development and architecture. *Cell 157*, 1380-1392. *Co-first authors. I generated all data and models in this chapter.

Abstract

The observations that HOBr is the optimal sulfilimine (S=N) crosslink forming oxidant for collagen IV coupled with the strong enzymatic selectivity for the production of HOBr by peroxidasin elevates the question of why Br is the cofactor of choice for this biologically unique crosslinking reaction. Based on the well-established cyclization of methionine, we were able to construct a model for sulfilimine crosslink formation within the NC1 hexamer and the dead-end oxidation product of methionine sulfoxide (S=O) through a common halosulfonim intermediate (HSI) at the Methionine-93 (Met^{93}) sulfur. This model, combined with the mass spectrometric conformation of sulfoxide formation in the case of unproductive oxidation, enabled the direct thermodynamic comparison of Cl and Br as potential cofactors within the NC1 domain as a whole. Br preferred S=N to S=O formation by approximately 1 kcal/mol more than Cl. This analysis further revealed the unexpected result that one S=N crosslink potentiates the formation of the second within the NC1 domain. The relative selectivity for Br as a cofactor is therefore governed by the orbital controlled selectivity of the $S\text{-}Br^+$ intermediate preferentially reacting with the conjugate amine on the lysine to form a sulfilimine crosslink, as opposed to bulk water to form a sulfoxide. This reactivity pattern represents the chemical foundation for the role of Br as the cofactor for sulfilimine formation and thus as an essential trace element.

Introduction

The discovery of the sulfilimine crosslink within collagen IV represented the first new covalent bond identified in a native protein in least two decades (Vanacore et al., 2009). While novel biologically, sulfilimine chemistry *per se* was a long mature field with significant kinetic and mechanistic data (Gilchrist and Moody, 1977). Despite the wealth of data on sulfilimine synthesis, the application of this anhydrous chemistry to the formation of a sulfilimine bond in a biomacromolecule, in an aqueous environment, is a major methodologic challenge. Mechanistic detail, however, is necessary to understand the reasons why HOBr is the preferred terminal oxidant generated by peroxidasin and required for the physiologically observed levels of sulfilimine crosslink in collagen IV.

As cofactors, peroxidasin oxidizes Br^- and Cl^- to produce their hypohalous acids (HOBr and HOCl, respectively), which in turn mediate the oxidation of methionine-93(Met^{93}) to form sulfilimine crosslinks (Bhave et al., 2012). HOBr is superior to HOCl for crosslinking efficiency. The synthesis of dehydromethionine, a cyclic sulfilimine product, provided a mechanistic framework to investigate the chemical basis for the selectivity of Br over Cl. In that framework, a methionine halosulfonium intermediate (**HSI**) reacts with an amine forming a sulfilimine bond, or water, forming a sulfoxide. (Figure 10A) (Armesto et al., 2000; Peskin et al., 2009; Young and Hsieh, 1978). We hypothesized that sulfilimine formation in collagen IV proceeds through an HSI at Met^{93} and that selectivity resides with a bromosulfonium intermediate which predominately reacts with the ϵ-NH_2 of Hyl^{211} to form the crosslink, whereas the chlorosulfonium intermediate predominantly reacts with water to form methionine sulfoxide, precluding crosslink formation.

Results

Chemical oxidations and sulfoxide formation

In vitro, HOBr effectively promoted sulfilimine formation in a dose dependent manner while HOCl poorly formed NC1 crosslinks (Figure 10B). We used mass spectrometry to determine the oxidation state of Met^{93} within HOCl-reacted monomers and found increased amounts of methionine sulfoxide (**Figure 11**). To test whether methionine sulfoxide is indeed a "dead end" with respect to crosslink formation, uncrosslinked NC1 hexamers were reacted with increasing concentrations of HOCl, and subsequently treated with HOBr. Crosslink formation by HOBr was inhibited by the pre-treatment in a dose dependent manner until it resembled treatment with HOCl alone (Figure 10C). Thus, Met^{93} is indeed successfully targeted by HOBr and HOCl, but the latter oxidant creates an uncrosslinkable product, namely methionine sulfoxide. To verify this, we generated methionine sulfoxide within uncrosslinked hexamers via prolonged (>12 hours) treatment with high concentrations of H_2O_2 (Levine et al., 1996). Expectedly, crosslink formation by HOBr was inhibited in a dose-dependent manner (Figure 11G) providing strong orthogonal validation for methionine sulfoxide as a dead-end for crosslinking in the NC1 domain .

Model for S=N Bond Formation within the NC1 Hexamer and Thermodynamic Calculations

We constructed a model of sulfilimine (S=N) cross-link formation within the NC1 hexamer (Figure 10A), based on the chemical precedent delineated for an intramolecular sulfilimine bond between the amino and thioether groups of free methionine to produce dehydromethionine (Peskin et al., 2009), a cyclic product that is chemically similar to the sulfilimine bond in collagen IV. Both HOBr and HOCl rapidly oxidize the methionine sulfur to form a presumed halosulfonium intermediate(S-X, where X=Cl or Br) (**HSI**) (Armesto et al., 2000; Gensch and Higuchi, 1967; Pattison and Davies, 2004). In dehydromethionine, two competing products are observed: an intramolecular S=N bond, or methionine sulfoxide through reaction of the HSI with bulk water. We found that the *in vitro* reaction with hypohalous acids yields either sulfilimine (S=N) or sulfoxide (S=O) products at Met^{93} (Figure 11A-F). These observations supported the model that oxidation of methionine-93 (Met^{93}) by either hypohalous reagent, HOCl or HOBr, yields a halo-sulfonium intermediate (**HSI**). This intermediate then has a dichotomous choice between forming a sulfoxide (S=O) via hydrolysis or alternatively reacting with the amine group on hydroxylysine (Hyl^{211}) to produce the S=N crosslink. Since NC1 dimers may possess up to two S=N cross-links, the NC1 domain may exist in three distinct forms with respect to cross-linking status (Figure 3D). In practice, SDS-PAGE and densitometric analysis of dissociated NC1 hexamers provided a means of measuring uncross-linked, singly cross-linked, and doubly cross-linked NC1 populations, where the dimer band with higher electrophoretic mobility (D_2) contains 2 S=N cross-links, while D_1 contains only 1 S=N cross-link (Figure 4). Monomeric NC1 bands lack any sulfilimine cross-links.

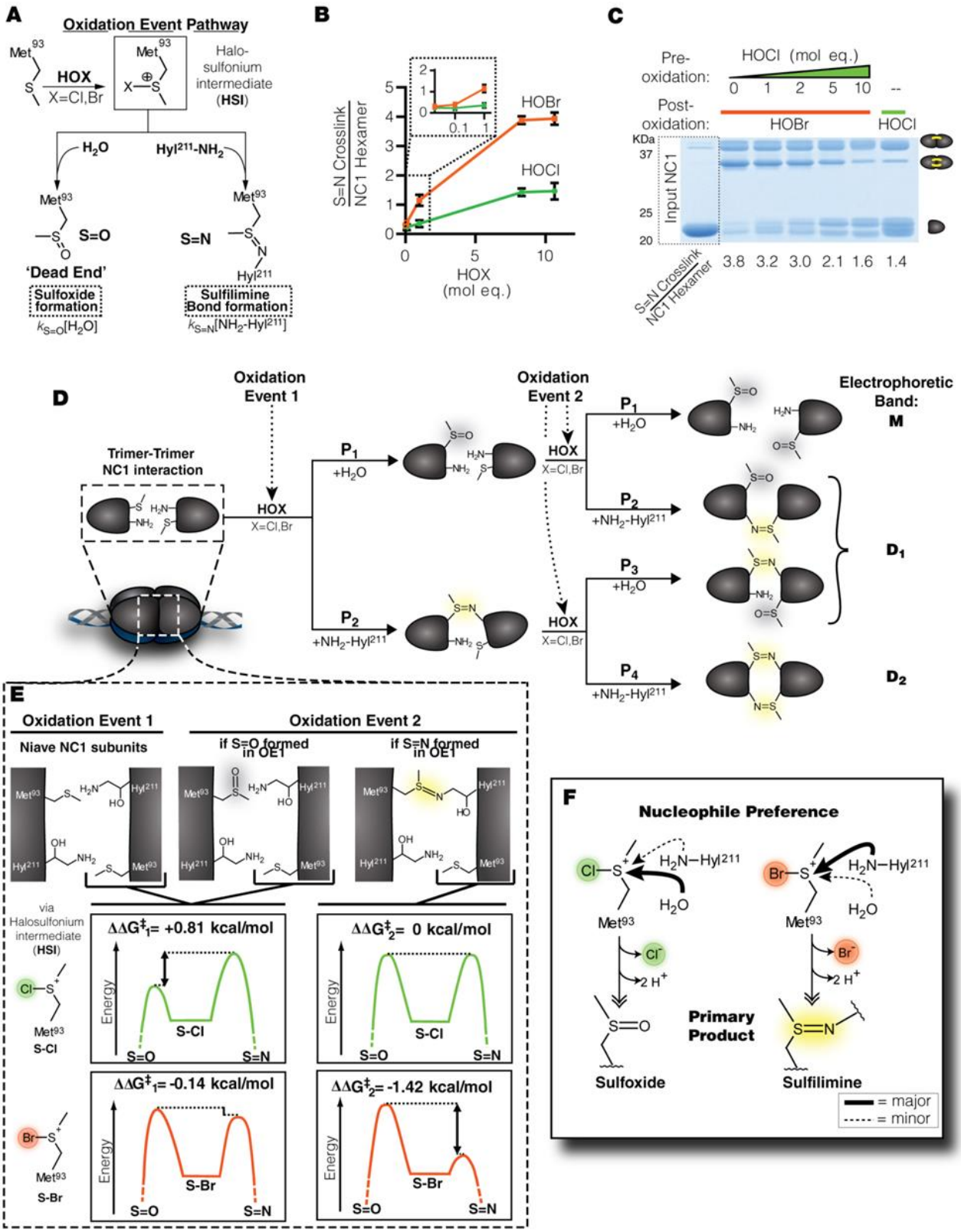
A
Oxidation Event Pathway
HOX
X=Cl,Br
Halo-sulfonium intermediate (HSI)
H2O
Hyl211-NH2
S=O
'Dead End'
Sulfoxide formation
kS=O[H2O]
S=N
Sulfilimine Bond formation
kS=N[NH2-Hyl211]
B
S=N Crosslink / NC1 Hexamer
HOBr
HOCl
HOX (mol eq.)
C
Pre-oxidation:
HOCl (mol eq.)
0 1 2 5 10 --
Post-oxidation:
HOBr
HOCl
KDa
37
25
20
Input NC1
S=N Crosslink NC1 Hexamer
3.8 3.2 3.0 2.1 1.6 1.4
D
Oxidation Event 1
Oxidation Event 2
Trimer-Trimer NC1 interaction
HOX
X=Cl,Br
P1 +H2O
P2 +NH2-Hyl211
P3 +H2O
P4 +NH2-Hyl211
Electrophoretic Band:
M
D1
D2
E
Oxidation Event 1
Oxidation Event 2
Niave NC1 subunits
if S=O formed in OE1
if S=N formed in OE1
via Halosulfonium intermediate (HSI)
S-Cl
S-Br
ΔΔG‡1= +0.81 kcal/mol
ΔΔG‡2= 0 kcal/mol
ΔΔG‡1= -0.14 kcal/mol
ΔΔG‡2= -1.42 kcal/mol
Energy
S=O
S=N
F
Nucleophile Preference
Primary Product
Sulfoxide
Sulfilimine
= major
= minor

Figure 10. Chemical mechanism of sulfilimine (S=N) formation within the NC1 hexamer

Previous Page

(A) Working model of the oxidative formation of either sulfilimine crosslinks or methionine sulfoxide. $k_{S=O}$ and $k_{S=N}$ refer to rate constants in the formation of sulfoxides and sulfilimines, respectively.

(B) Uncrosslinked NC1 hexamers (5 μM) were reacted with hypohalous acids for 5 minutes at 37˚ C and the products analyzed by SDS-PAGE. Values represent mean ± 95%CI. (n=3).

(C) Uncrosslinked NC1 hexamer (1.3 μM) was reacted with indicated amounts of HOCl for 1 minute at 37˚ C in Br-free 1x PBS, followed by subsequent treatment with of 8 mol eq. HOBr (or HOCl as a control) and reacted for an additional minute at 37˚ C. Reactions were quenched with 20 mM methionine. Gel is representative of two experiments.

(D) The sequential model for D_1 and D_2 formation within the NC1 hexamer following complete stoichiometric oxidation of Met^{93}. P_1-P_4 indicate the proportional probabilities of forming the observed products. Calculations are presented in Extended Experimental Methods.

(E) Free energy landscape for S=N formation within the NC1 hexamer based on the model outlined in panel D and Figure 10.

(F) Outline of overall chemical pathway governing the intrinsic chemical reactivity of S-Br and S-Cl at Met^{93}.

Therefore, if complete stoichiometric oxidation of each Met^{93} in the NC1 hexamer occurs, the probability of forming either S=N or S=O can be calculated for Met^{93} because analysis of D_2, D_1, and residual monomer reveal the product ratios of S=N and S=O for each Met^{93} in the system. To be certain of complete oxidation at Met^{93}, we performed a series of oxidations to determine the molar excess of HOX required for stoichiometric complete oxidation. Above 8-fold mole equivalents (mol. eq.) of HOX per Met^{93}, no increase in crosslink formation from either HOCl or HOBr was observed (Figure 10B), and further tested up to 12.8 mol. eq., indicating complete oxidation had been achieved. We therefore elected to use 10.7 mol equivalents (83.3 μM) of HOX /Met^{93} to oxidize 1.3 μM NC1 Hexamer (7.8 μM potential S=N) to aid the accuracy of the calculations by enabling a mass conservation of >90% of the input NC1 subunit for the experiment to model the cross-linking mechanism. After oxidation and quenching with 20 mM methionine, the oxidized NC1 hexamer was subjected to SDS-PAGE and Coomassie blue staining (Figure 12A).

Following the complete oxidation of Met^{93} residues within NC1 hexamers, the probability of forming either a S=N cross-link or S=O at Met^{93} can be calculated through a product ratio analysis of D_2, D_1, and uncross-linked monomers. For simplicity, we initially assumed that each Met^{93} behaved independently and had equal probably of successfully forming cross-link. Notably, we were unable to fit the experimental data to a model where each Met^{93} reacts independently within the hexamer (Table 5). We therefore considered the potential for the outcome of the first cross-linking event to impact the second event. Accordingly, we modified the model to account for two sequential oxidation events, denoted as Oxidation Event 1 (OE1) and 2 (OE2), where

A

Short form Methionine Peptide
^{77}NDYSYWLSTPEPMPMSMAPISGDNIR^{102}

	Parent	Z	Theoretical Mass	XIC Counts: Monomer (Band 1)	XIC Counts: HOCl Monomer (Band 7)	Ratio HOCl/Control
Base	2971.3190	+2	1486.6673	273357	0	
Elution:61.52 min		+3	991.4475	1579131	0	0.00
		+4	743.8376	ND	ND	
1 S=O	2987.3139	+2	1494.6648	519265	251223	
Elution:58.13 min		+3	996.7791	2002214	1699244	0.77
		+4	747.8363	ND	ND	
2 S=O	3003.3088	+2	1502.6622	951189	1294181	
Elution:55.65 min		+3	1002.1107	4222750	3931713	1.01
		+4	751.8350	ND	ND	
3 S=O	3019.3037	+2	1510.6597	1680098	2808840	
Elution: 53.73 min		+3	1007.4424	3979188	19980707	4.03
		+4	755.8337	ND	ND	
4 S=O	3035.2986	+2	1518.6571	154407	315687	
Elution: 54.43 min		+3	1012.7740	674508	2506403	3.40
		+4	759.8325	ND	ND	

C

Long form Methionine Peptide
^{77}NDYSYWLSTPEPMPMSMAPISGDNIRPFISR^{107}

	Parent	Z	Theoretical Mass	XIC Counts: Monomer (Band 1)	XIC Counts: HOCl Monomer (Band 7)	Ratio HOCl/Control
Base	3571.6574	+2	1786.8365	54867	3395.748	
Elution: 62.64 min		+3	1191.5603	20625212	764619.9	0.04
		+4	893.9222	7722040	262376.3	
1 S=O	3587.6523	+2	1794.8340	123350	0	
Elution: 59.84 min		+3	1196.8919	32941292	9785283	0.30
		+4	897.9209	11773834	3713557	
2 S=O	3603.6472	+2	1802.8314	511724	23467.67	
Elution: 57.94 min		+3	1202.2235	66802291	19566249	0.30
		+4	901.9196	31478298	9673289	
3 S=O	3619.6421	+2	1810.8289	591494	467828.2	
Elution: 56.34 min		+3	1207.5552	51917630	90173831	1.73
		+4	905.9183	26118769	45244445	
4 S=O	3635.6370	+2	1818.8263	85961	49.0656	
Elution: 57.04 min		+3	1212.8868	11063931	1025874	0.42
		+4	909.9171	5448686	5969433	

B

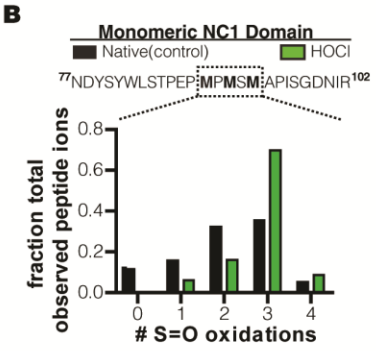

D

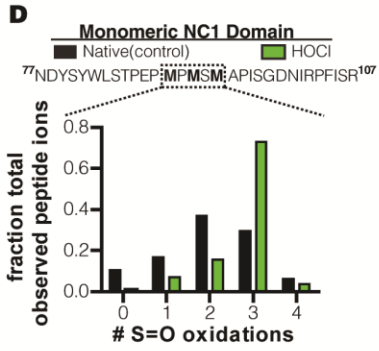

E

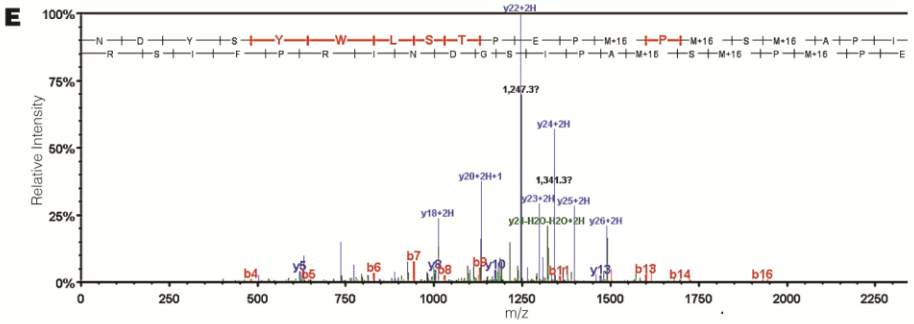

F

# of Met Oxidations	Met89 oxidation	Met91 Oxidation	Met93 Oxidation	Peptide Sequence	Theoretical mass	observed error(±ppm)	Ratio HOCl/Control
3	1	1	1	(R)NDYSYWLSTPEP**M(ox)**P**M(ox)**S**M(ox)**APISGDNIRPFISR(C)	3619.6421	6.4	**3.20**
3	1	1	1	(R)NDYSYWLSTPEP**M(ox)**P**M(ox)**S**M(ox)**APISGDNIR(P)	3019.3037	4.4	**2.62**
2		1	1	(R)NDYSYWLSTPEPMP**M(ox)**S**M(ox)**APISGDNIR(P)	3003.3088	4.5	**2.28**
2		1	1	(R)NDYSYWLSTPEPMP**M(ox)**S**M(ox)**APISGDNIRPFISR(C)	3603.6472	5.4	**1.24**
2	1		1	(R)NDYSYWLSTPEP**M(ox)**PMS**M(ox)**APISGDNIRPFISR(C)	3603.6472	5.2	**0.28**
1			1	(R)NDYSYWLSTPEPMPMS**M(ox)**APISGDNIRPFISR(C)	3587.6523	6.6	**1.44**
1		1		(R)NDYSYWLSTPEPMP**M(ox)**SMAPISGDNIRPFISR(C)	3587.6523	5.6	**0.58**
1	1			(R)NDYSYWLSTPEP**M(ox)**PMSMAPISGDNIRPFISR(C)	3587.6523	5.7	**0.00**
0				(R)NDYSYWLSTPEPMPMSMAPISGDNIR(P)	2971.3190	4.8	**0.00**

G

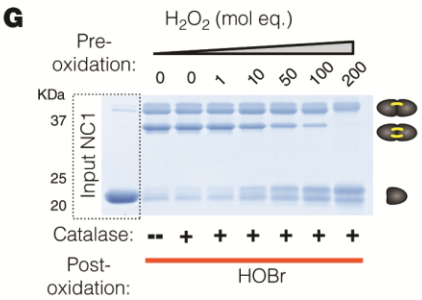

Figure 11. Met93-sulfoxide is formed as a result of HOCl oxidation and is a 'dead-end' for sulfilimine crosslink formation in the NC1 (Associated with Figure 10)

Previous Page

(A-F) Analysis of residual monomeric NC1 subunit after complete stoichiometric oxidation with HOCl. Samples analyzed by high-resolution mass spectrometry after SDS-PAGE and in-gel trypsin digest.

(A) Table showing the ions counts for the observed methionine oxidation states for residues 77-102 of the α1 NC1 domain. Ion abundance was quantified from the Extracted Ion Chromatogram (XIC) after correcting for total protein content. Ratios of XIC counts between HOCl-treated and untreated (control) monomers are provided in the rightmost table column. Stochastic methionine oxidation accounts for the observation of S=O in the untreated control sample (Chen and Cook, 2007).

(B) Graph of the relative abundance of observed methionine oxidation states for residues 77-102 quantified in panel (A).

(C) Quantification of oxidation states for residues 77-107 of the α1 NC1 domain, analyzed identically to the data presented in (A).

(D) Graph of the relative abundance of observed methionine oxidation states for residues 77-107 quantified in panel (C).

(E) Representative MS^3 analysis of residues 77-107 after HOCl oxidation, showing the detection of site-specific Met oxidations at methionine-89, -91, and -93.

(F) Analysis of site specific methionine oxidation from HOCl treated monomer, showing that Met^{93} occurs predominantly as a sulfoxide, consistent with sulfoxide formation at Met^{93} being a 'dead-end' and specifically present in residual monomeric NC1 subunits after stoichiometric oxidation

(G) SDS-PAGE analysis with coomassie blue staining, showing the influence of H_2O_2 on the efficiency of HOBr-induced NC1 crosslinking. Purified uncrosslinked NC1 hexamer (1.3 μM) (7.8 μM potential S=N crosslink) was subjected to pre-oxidation by increasing doses of super-physiologic H_2O_2. After 12 hours, catalase (0.2 mg/ml) was used to hydrolyze the remaining H_2O_2 and the samples were oxidized with freshly prepared HOBr (8 mol eq. per potential S=N bond). Crosslinking by HOBr was inhibited in a dose dependent fashion by pre-oxidation with H_2O_2, a reagent which is super-physiologic quantities is known to cause sulfoxide formation in exposed methionine residues (Levine et al., 1996).

Table 5. Analysis of a two-equal and independent crosslinking event model
Test of the accuracy of a two equal and independent crosslinking even model, where the predicted D_2 content equals $(1-\sqrt{(\text{fraction monomer})})^2$ and is compared to the experimentally observed values upon complete stoichiometric oxidation.

Oxidant Source	Fraction Experimentally Observed Monomer (±95%CI)	Predicted D_2 Content	Fraction of Experimentally observed D_2 (±95%CI)	% Error
HOCl	0.62 (±0.03)	0.045	0.11(±0.03)	**55.7%**
HOBr	0.20 (±0.02)	0.311	0.51(±0.02)	**38.7%**

the outcome of OE2 is determined in part by the outcome of OE1 (Figure 10D, Figure 12B).

By applying this refined model to the observed SDS-PAGE NC1 banding patterns, the proportional pathway contributions were defined (Figure 12C). The fractional representation of each band (D_2, D_1, and Monomer) of the total NC1 subunits represents the product of the probability distributions between generating either a S=N or S=O during Oxidation Events (OE) 1 and 2 (Figure 12C). For example, residual monomer will only exist if both oxidation events resulted in a sulfoxide(S=O). Since OE1 was unproductive with respect to forming an S=N bond, there is no *a priori* reason to believe the Met^{93} oxidized in OE2 would have a different S=N vs. S=O probability relationship since the rest of the protein would presumably be otherwise unchanged. Therefore, the fraction of residual monomer represent the probability of forming a sulfoxide from the same event twice [fraction monomer=$(P_1)^2$].

The proportions (P_1-P_4) were then calculated based on the table in Figure 12C. Data is represented as the mean±95% CI of 3 experiments. Errors for P_1 and P_4 are shown because those terms were calculated directly from the densiometrically derived fractional band data, while P_2 and P_3 were derived by subtraction (eg. P_2=1-P_1) and therefore share the same experimental error as P_1 and P_4 respectively. These data demonstrated that the potential for cross-link formation during OE2 is influenced by whether a S=N or S=O was formed during OE1.

Based on these data, and the model detailed in Figure 12B, we then could calculate a thermodynamic difference in transition state energy between two competing

pathways through analysis of the distribution between S=N and S=O products. Based on the dichotomous choice of the **HSI (**shown here as S-X**)**, equation (1) represents the rate of its disappearance along the two pathways with the rate of sulfoxide ($k_{S=O}$) and sulfilimine ($k_{S=N}$) formation and the respective H_2O and NH_2-R (where R=Hyl[211]) concentrations.

$$\frac{d[S-X]}{dt} = -k_{S=O}[H_2O] - k_{S=N}[NH2-R] \quad (1)$$

The thermodynamic difference in transition state energy along the competing sulfilimine (S=N) and sulfoxide (S=O) pathways can be calculated via equation (2) from the distribution of the reaction products:

$$\frac{[S=N]}{[S=O]} = e^{\frac{-\Delta\Delta G^{\ddagger}}{RT}} \quad (2)$$

The free energy difference in transition state energy for OE1 ($\Delta\Delta G_1^{\ddagger}$) and OE2 ($\Delta\Delta G_2^{\ddagger}$) can then be calculated by equations (3) and (4) respectively:

$$\Delta\Delta G_1^{\ddagger} = -RT\ln\left(\frac{P_2}{P_1}\right) \quad (3)$$

$$\Delta\Delta G_2^{\ddagger} = -RT\ln\left(\frac{P_4}{P_3}\right) \quad (4)$$

These data are represented numerically and graphically in Figure 10E.

Initial Sulfilimine formation potentiates a second crosslink through changing the apparent amine concentration

The inability of two independent crosslinking events to adequately model the observed product ratios indicates that the crosslinking events not independent (Table 5), but rather sulfilimine formation during the first event enhances the potential of forming a sulfilimine in the second event. This conclusion is bolstered strongly by the similar increase in crosslinking efficiency for the second crosslink in both Cl and Br mediated reactions. To rigorously address this, we noted that an explanation for this phenomena could likely be found within the derived rate law for the halosulfonium intermediate (HSI) (equation (1)). While our current methodology prevented the determination of the absolute numerical values for either $k_{S=O}$ or $k_{S=N}$, it is reasonable to assume that the constants are equal for both oxidation events since the reaction mechanisms for both are similar. This rationale then suggests that the change in product distribution between OE1 and OE2 should come from a change in the effective local concentration of water (to form S=O) or the Hyl^{211} amine moiety from the conjugate Hyl^{211} (to form S=N). Water acts as the bulk solvent for the biologic reaction as well as our *in vitro* experiments, providing an abundance of reactant for sulfoxide formation. While the hydration status of the intermediate may indeed be different for HOBr- versus

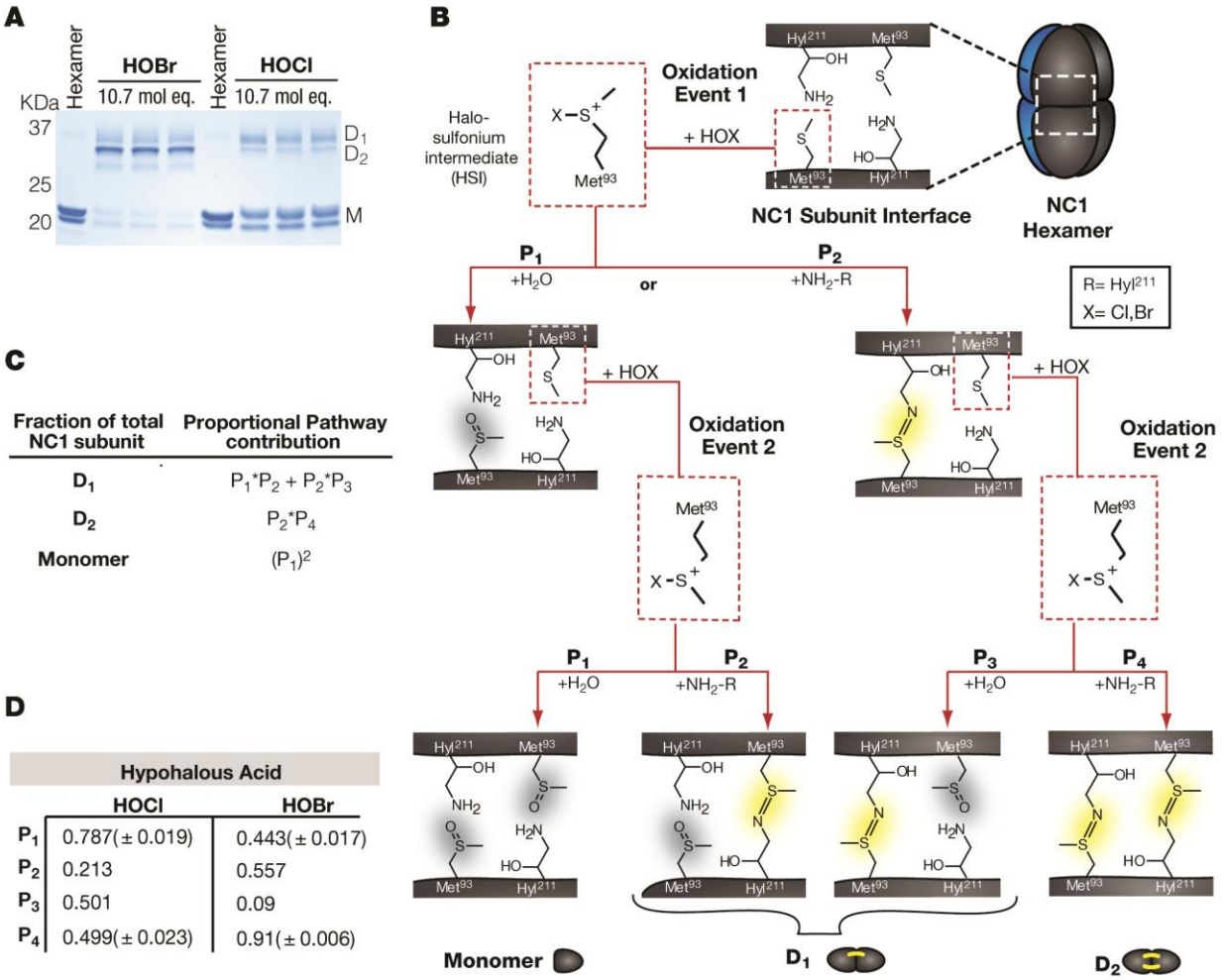

Fraction of total NC1 subunit	Proportional Pathway contribution
D_1	$P_1{*}P_2 + P_2{*}P_3$
D_2	$P_2{*}P_4$
Monomer	$(P_1)^2$

Hypohalous Acid		
	HOCl	HOBr
P_1	0.787(± 0.019)	0.443(± 0.017)
P_2	0.213	0.557
P_3	0.501	0.09
P_4	0.499(± 0.023)	0.91(± 0.006)

Figure 12. Analysis of S=N formation via a halo-sulfonium intermediate. (Associated with Figure 10)

(A) SDS-PAGE analysis with coomassie blue staining, showing the stoichiometric oxidation of the NC1 hexamer by HOBr and HOCl. 10.7 mol equivalents of HOX /Met^{93} was used to oxidize 1.3 µM NC1 Hexamer. Concentrations of up to 100 µM (12.8 mol eq HOX/Met^{93}) were tested with no change in S=N formation from either HOCl or HOBr indicating complete oxidation had been achieved. To aid the accuracy of the calculations, a mass conservation of >90% input NC1 subunit was maintained. Band fractions were calculated based on densiometric analysis.

(B) Diagram of the working model of S=N formation from a halo-sulfonium intermediate (HSI) generated through hypohalous acid oxidation of methionine-93 (Met^{93}). The model accounts for the occurrence of two oxidation events during the complete oxidation of NC1 dimers.

(C) Table detailing the relationship between the observed electrophoretic NC1 banding and the contributing probabilities along the reaction pathways. As predicted by the working model in (B), D_2, D_1, and Monomer bands represent the product of the probability distributions of forming S=N versus S=O during both oxidation events.

(D) Results table presenting the proportional product distribution within NC1 subunits treated with either HOCl or HOBr, as calculated from data presented in (A) Data is represented as the mean±95% CI of 3 experiments. Errors for P_1 and P_4 are shown because those terms were calculated directly from the densiometrically derived fractional band data, while P_2 and P_3 were derived by subtraction (eg. $P_2=1-P_1$) and therefore share the same experimental error.

HOCl-based reactions, the observed increase in S=N formation between P_2 and P_4 suggests that this is not a dominant factor. Furthermore, we consider it unlikely that the introduction of a sulfilimine cross-link in the hexamer causes a meaningful change in the hydration of the **HSI**, though this possibility cannot be formally excluded**.** It seems more likely that the introduction of an S=N cross-link during OE1 could influence the conformation of the NC1:NC1 interface such that an increase in the apparent local concentration of amine ([NH_2-Hyl^{211}]) would occur. Given the ability of cross-links in other proteins to substantially influence conformational dynamics, we favored the interpretation of the change in product proportions between OE1 and OE2 to be attributable to an increase in amine concentration within the vicinity of the halosulfonium intermediate.

This hypothesis would predict that there should be a similar increase in apparent change in local amine concentration following cross-link formation during OE1 via either HOBr or HOCl (Figure 12B). This change will manifest mathematically in the change in the ratio of OE1 and OE2, shown in equation (5):

$$\frac{\frac{k_{S=N}[NH_2 - Hyl^{211}]_{OE2}}{k_{S=O}[H_2O]}}{\frac{k_{S=N}[NH_2 - Hyl^{211}]_{OE1}}{k_{S=O}[H_2O]}} = \frac{\frac{P_4}{P_3}}{\frac{P_2}{P_1}} \qquad (5)$$

After cancellation of the sulfoxide formation terms, this simplifies to:

$$\frac{k_{S=N}[NH_2 - Hyl^{211}]_{OE2}}{k_{S=N}[NH_2 - Hyl^{211}]_{OE1}} = \frac{P_4 * P_1}{P_2 * P_3} \quad (6)$$

From equation 6, the apparent change in local amine concentration can be determined. Since $k_{S=N}$ is constant, the change should reflect the change in local amine concentration ($[NH_2\text{-}Hyl^{211}]_{app}$). Data for Cl and Br is in the following table:

Halide (as HOX)	Fold change in $[NH_2\text{-}Hyl^{211}]_{app}$ between OE2 and OE1 (mean± 95%CI)
Cl	2.7±0.1
Br	7.0±0.6

The similar magnitude of these values can be interpreted to mean that the introduction of one cross-link increases the spatial proximity of the reacting Met^{93} and Hyl^{211} side chains. This calculation assumes a constant water shell surrounding the **HSI**, however it is possible that the S-Cl intermediate is differently solvated than the S-Br, which could also influence this analysis. Taken together, the change in $[NH_2\text{-}Hyl^{211}]_{app}$ following cross-link formation by either HOBr or HOCl indicates that the conformational dynamics within the hexamer are likely modified by the introduction of a sulfilimine (S=N) cross-link resulting in the observed increase in cross-linking efficacy in OE2.

Discussion

Through the examination of the relative free energy difference in the transition states for the competing sulfilimine and sulfoxide reaction pathways (Figure 10E; and Figure 12B-D)(Seeman, 1983), we found that the presence of one sulfilimine crosslink lowered the energy barrier in forming a second crosslink (Figure 10E). Comparing the effects of HOBr versus HOCl within this model, the bromosulfonium (**S-Br**) intermediate encountered a lower energetic barrier to sulfilimine formation for both oxidative events. Conversely, the chlorosulfonium (**S-Cl**) intermediate faced an unfavorable barrier to sulfilimine formation relative to methionine sulfoxide (Figure 10E, Figure 12D).

The fundamental difference in crosslinking efficacy between Br and Cl in collagen IV is best explained in terms of the chemical behavior of the intermediates, which display similar overall reactivity but markedly different selectivity due to a combination of electronegativity of the halide substituent and molecular orbitals characteristics of the **HSI**. Experimental and *in silico* studies indicate that **S-Cl** species have highly polar transition states and participate in charge-controlled reactions which preferentially select for 'harder' nucleophiles (such as H_2O relative to NH_2-R), while **S-Br** species participate in orbital-controlled reactions that select for 'softer' nucleophiles (here understood as NH_2-R relative to H_2O) and generate smaller partial charges (Chmutova et al., 1999; Klopman, 1968; Pearson, 1968). We conclude that HOBr oxidation of Met^{93} yields an **S-Br** intermediate that selects for amine nucleophiles in an orbital-controlled reaction, while the charge controlled reactivity of chlorosulfonium intermediates favors hydrolysis (Figure 10F). Taken together, sulfilimine formation is thermodynamically favorable via the selectivity of an **S-Br** intermediate. This property of the **S-Br** intermediate is likely a

foundational component of Br essentiality and a potential pressure on the evolutionary development of peroxidasin's profound Br selectivity and subsequent production of HOBr as a terminal oxidant.

Chapter V

Bromide is essential for Drosophila development and normal basement membrane ultrastructure

These data appear as part of McCall, A.S.*, Cummings, C.F.*, Bhave, G.*, Vanacore, R., Page-McCaw, A., and Hudson, B.G. (2014). Bromine is an essential trace element for assembly of collagen IV scaffolds in tissue development and architecture. *Cell 157*, 1380-1392. *Co-first authors. I generated all data in this chapter with special technical assistance for election microscopy by J. Williams in the VUMC Cell Imaging Shared Resource.

Abstract

With data demonstrating the chemical necessity for Br-catalyzed sulfilimine formation and peroxidasin's preferential Br oxidation, in vivo evidence for the peroxidasin-Br-collagen IV axis is required to understand sulfilimine based basement membrane stabilization in tissues. To test the role of Br is tissues, we developed a Br-free Drosophila Melanogaster culture system. Br-deficiency (demonstrated by Neutron Activation Analysis of larval Br content) significantly reduced development and survival, while re-introduction of Br rescued these effects, indicating that Br is essential for development. Sulfilimine content in the Br-free flies was substantially reduced with the simultaneous observation of defects in the intestinal basement collagen IV scaffold. Ultrastructural analysis of the intestinal basement membrane quantitatively demonstrated that Br-deficiency phenocopies the absence of peroxidasin, providing the first concrete ultrastructural evidence that sulfilimine crosslinking modulates basement membrane structure. To show that Br is uniquely acting through peroxidasin *in vivo*, we used the collagen IV molecular corset of drosophila embryos and the 'gain-of-function' phenotype we observed with superphysiologic bromide. Through either pharmacologic or RNAi based inhibition of peroxidasin we were able to ameliorate the Br-induced gain of function. These data collectively demonstrate in vivo that Br acts through peroxidasin to crosslink collagen IV and stabilize basement membranes.

Introduction

The evolutionary conservation of collagen IV and the sulfilimine bond across all animal phyla supports a foundational role for this crosslinking process in basement membrane structure (Fidler et al., 2014). With biochemical evidence for a Br requirement to recapitulate physiologically observed levels of sulfilimine crosslinking , an in vivo assessment of this role for Br is required to effectively test the functional linkage between the Br-peroxidasin-collagen IV triad and basement membrane structure in tissues. The *in vivo* demonstration of an exclusive role for Br in this process is made more significant because to date, there have been no biologically essential functions attributed to Br (Nielsen, 1998).

The choice of model organism for the exploration of the biological role of bromine is complicated by technical requirements for dietary elimination of Br coupled with adequate experimental flexibility for manipulation of collagen IV and peroxidasin. Genetic manipulation of peroxidasin has been previously evaluated in nematodes, flies, and zebrafish (Bhave et al., 2012; Fidler et al., 2014; Gotenstein et al., 2010). In flies and nematodes there was intestinal morphology changes and cuticle detachment observed respectively. The already observed peroxidasin phenotypes are important in flies and nemotodes because as model species, these are the only two which can be reared on axenic (chemically defined) diets (Piper et al., 2014; Samuel et al., 2014). With the ubiquitous presence of Br in plant and animal tissue (van Leeuwen and Sangster, 1987), it necessitates a choice of model organisms with defined diets or those which can be reared on complex nutrient sources derived only from single celled

organisms (bacteria and yeast), since these would not be expected to require Br for growth because they lack basement membranes. Thus, the agar and bacterial media of *C. Elegans* or the agar and yeast based media of *Drosophila* represent ideal candidate organisms. Because of well characterized peroxidasin and collagen IV phenotypes in *Drosophila* (Bhave et al., 2012; Haigo and Bilder, 2011), we elected to develop a Br-free *drosophila* culture system to evaluate the *in vivo* role of Br in sulfilimine crosslinking, basement membrane structure, and organismal development.

Results

Bromide is essential for Drosophila development

Based on the chemical requirement for Br^- in collagen IV sulfilimine bond formation, we hypothesized that Br^- is essential for stabilizing tissues. Because standard Drosophila media contains ~15 µM Br^-, we prepared a custom diet (Table 6) in which final dietary Br^- was undetectable by NAA (Table 7). To address the impact of Br^- deficiency over multiple generations, we raised flies on Br-free media, and compared their development to cohorts raised on either similar media with Br^- supplementation or standard media (Figure 13A). Initial maternal Br^- contribution in embryos was 24.3 µM on the standard diet (Table 7). After moving embryos to the indicated media, Generation 1 larvae grown on Br-free conditions exhibited developmental delay (Figure 13B), yet development rates were similar between Br-added and standard media. Adult Generation 1 flies that survived were maintained on the same diet for 14 days to continue Br^- depletion, and progeny Generation 2 larvae showed significantly reduced survival in Br-free versus standard; the phenotype was rescued in Br-added diet (Figure 13C). Thus, Br^- is essential for development in *Drosophila*.

Seeking to accelerate Br-depletion, we fed flies a Br-free diet containing elevated NaCl levels to reduce Br^- half-life *in vivo* via halide flux seen in mammals (Pavelka et al., 2005). Female *Drosophila* were placed on a Br^- depleting (Br-free$^{DEP)}$ diet with or without supplemental 100 μM Br^- prior to egg deposition, and the dietary conditions were maintained throughout progeny development. Initially, the Br-free^{DEP} egg cohort had a significantly reduced hatching percentage relative to Br-free^{DEP}+100μM Br^- (Figure 13D), suggesting that Br is required for successful embryogenesis. Nearly all hatched larvae died prior to eclosion under Br-free^{DEP} conditions, while 100 μM Br^- rescued development to adulthood (Figure 13E). NAA analysis confirmed lower Br^- levels in third instar larvae (3.4 vs. 23.6 μM for controls) in Br-free^{DEP} conditions (Figure 13F).

Br-deficiency decreases sulfilimine content

In Br-free^{DEP} conditions, we assessed the impact of Br-deficiency on crosslink formation *in vivo*. We used *vkg^{454}-GFP* flies in which the single collagen IV α2 gene locus contains a GFP insertion near the 7S domain. We grew these *vkg^{454}-GFP* flies on Br-free^{DEP}, Br-free^{DEP}+100μM Br^- and standard diets and biochemically assayed sulfilimine-bond content via immunoblot. We found grossly reduced sulfilimine-bond content in the Br-free^{DEP} cohort, which was rescued with Br^- supplementation (Figure 13F, *Figure 15*A). Thus, Br^- promotes sulfilimine formation *in vivo*.

Tissue Defects with Br Deficiency

Peroxidasin (Pxn) mutants have reduced amounts of collagen IV sulfilimine crosslinks and consequent perturbation of midgut basement membranes, as shown previously (*Pxn^{f07229}*, Bhave et al, 2012). Predicting that Br-depletion would phenocopy

the *Pxn* mutant, we compared the midgut from Br-free^{DEP} larvae to two independent mutants of *Pxn* (*Pxn*^{MI01492} and *Pxn*^{f07229}). While normal scaffold architecture was seen on standard diet (Figure 13G), Br-free^{DEP} conditions displayed gross disruptions to the overall collagen IV scaffold in (Figure 13H, red arrows), and splitting by longitudinal section (Figure 13H, asterisk). Both phenotypes were rescued in Br-free^{DEP} + 100μM Br^- media (Figure 13I). Significantly, similar disruptions were seen in the *Pxn* mutants using an anti-NC1 antibody (Figure 13J-M). The *Pxn*^{f07229} phenotype appeared more severe than the *Pxn*^{MI01492}, and the *Pxn*^{MI01492}/*Pxn*^{f07229} transheterozygote demonstrated an intermediate phenotype. These data indicate similarities between Br-deficiency and the loss of peroxidasin.

We used transmission electron microscopy (TEM) to compare the basement membrane ultrastructure in Br-depleted larvae with *Pxn* mutant larvae. Larvae raised on standard diet exhibited normal enterocyte and basement membrane structure (Shanbhag, and Tripathi, 2009) (Figure 13N). In Br-free^{DEP} larvae, the basement membrane was irregular, thickened, occasionally diffuse, and wavy in various sections (Figure 13O). Strikingly, both *Pxn* mutants exhibited irregular and thickened basement membrane similar to the Br-free^{DEP} cohort (Figure 13Q-R). Moreover, Br-free^{DEP} conditions and *Pxn* mutants displayed circular muscles protruding into and deforming the epithelium, (*Figure 15*C,E,F), mirroring the perturbed actin staining in circular muscles observed in Br-free^{DEP} and *Pxn* mutant alleles (Figure 13H,K,M). All sections from the Br-free^{DEP}+100μM Br^- and standard diet cohorts displayed normal basement membrane and circular muscle morphologies (Figure 13N,P; *Figure 15*B,D). We quantified the basement membrane morphologic changes observed by TEM, finding

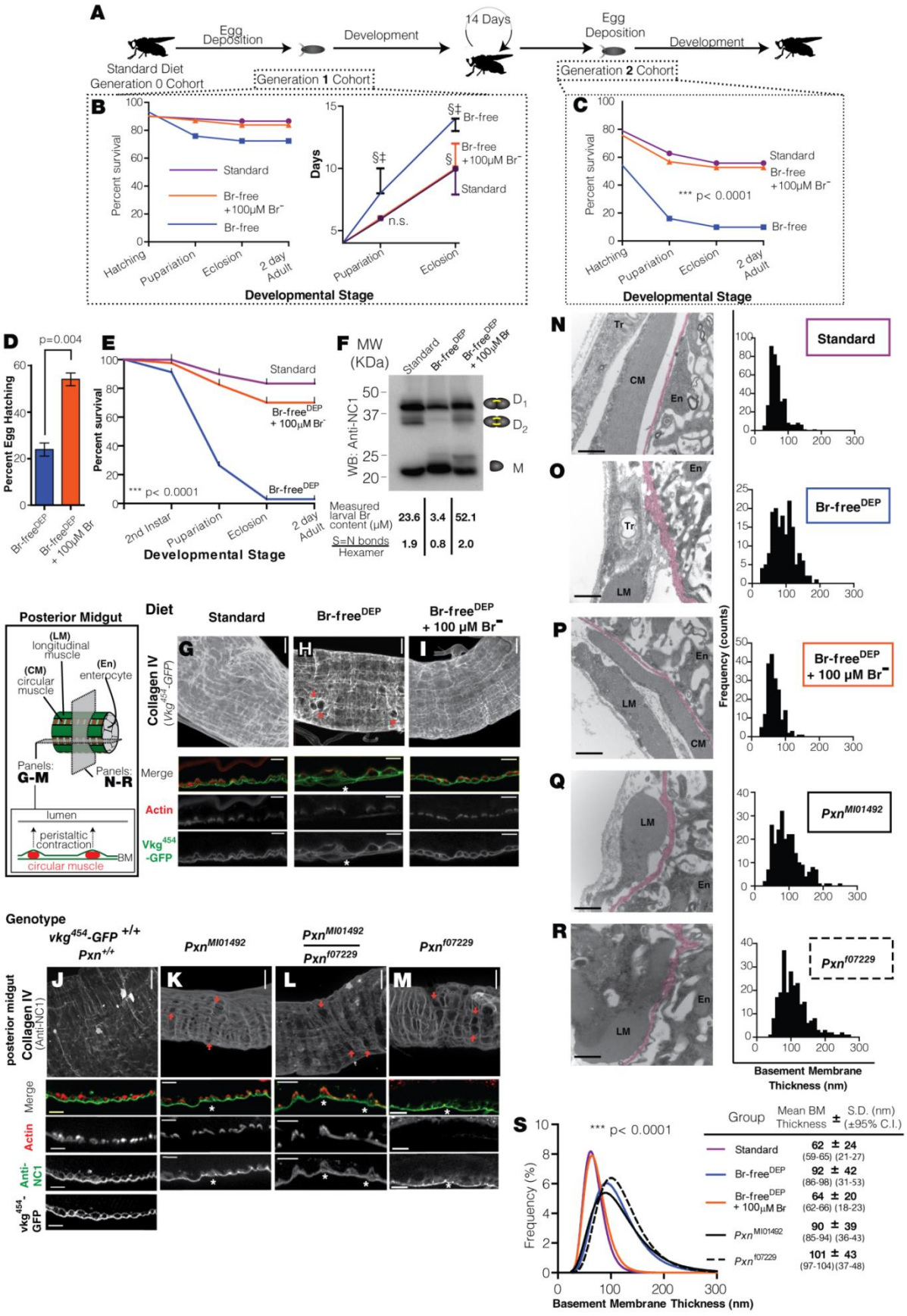
A
Egg Deposition
Development
14 Days
Egg Deposition
Development
Standard Diet
Generation 0 Cohort
Generation 1 Cohort
Generation 2 Cohort
B
Percent survival
Standard
Br-free +100μM Br⁻
Br-free
Hatching
Pupariation
Eclosion
2 day Adult
Developmental Stage
Days
§‡
§
n.s.
Br-free
Br-free +100μM Br⁻
Standard
C
*** p< 0.0001
D
p=0.004
Percent Egg Hatching
Br-free^DEP
Br-free^DEP + 100μM Br
E
Standard
Br-free^DEP + 100μM Br⁻
Br-free^DEP
*** p< 0.0001
2nd Instar
F
MW (KDa)
WB: Anti-NC1
D1
D2
M
Measured larval Br content (μM)
23.6
3.4
52.1
S=N bonds Hexamer
1.9
0.8
2.0
Posterior Midgut
(LM) longitudinal muscle
(CM) circular muscle
(En) enterocyte
Panels: G-M
Panels: N-R
lumen
peristaltic contraction
BM
circular muscle
Diet
Standard
Br-free^DEP
Br-free^DEP + 100 μM Br⁻
Collagen IV (Vkg^454-GFP)
Merge
Actin
Vkg^454 -GFP
N
O
P
Q
R
Tr
CM
En
LM
Standard
Br-free^DEP
Br-free^DEP + 100 μM Br⁻
Pxn^MI01492
Pxn^f07229
Frequency (counts)
Basement Membrane Thickness (nm)
Genotype
vkg^454-GFP +/+ Pxn^+/+
Pxn^MI01492
Pxn^MI01492 / Pxn^f07229
Pxn^f07229
posterior midgut
Collagen IV (Anti-NC1)
Merge
Actin
Anti-NC1
vkg^454-GFP
S
*** p< 0.0001
Frequency (%)
Basement Membrane Thickness (nm)
Group
Mean BM Thickness ± S.D. (nm) (±95% C.I.)
Standard 62 ± 24 (59-65) (21-27)
Br-free^DEP 92 ± 42 (86-98) (31-53)
Br-free^DEP + 100μM Br 64 ± 20 (62-66) (18-23)
Pxn^MI01492 90 ± 39 (85-94) (36-43)
Pxn^f07229 101 ± 43 (97-104) (37-48)

Figure 13. Bromide is essential for development and basement membrane architecture in Drosophila. (Previous page)

(A) Generational Br-depletion scheme

(B) Generation 1 survival and time-to-development curves for w^{1118} flies on the standard diet vs experimental diets. Embryos from mothers fed a standard diet were placed on the indicated diet, and progeny were scored every 24 hours. The Br-free+ 100μM Br^- diet supported the same timing of development as the standard diet, whereas the Br-free diet caused a significant delay ($p<0.001$ compared to both standard diet and Br-free +100μM Br^-) prior to pupariation (8 days) and eclosion (14 days). Data plotted as the group median ± interquartile range. N=30 for each group. 2 way ANOVA test showed a significant difference for pupariation and eclosion ($p<0.001$) §=different from standard, ‡=different from Br-free +100μM Br^-.

(C) Generation 2 developmental survival on experimental diets. n>40 for each cohort. Tested by Log-Rank test.

(D) Percentage of eggs (mean +/- 95% C.I.) completing embryogenesis from mothers reared on Br-free^{DEP} or Br-free^{DEP}+100μM Br^- diets for 5 days. In the Br-free^{DEP} experimental group, mothers were fed Br-free synthetic diet containing 80 mM total NaCl (Br-free^{DEP}) for 3 days prior to egg collection. The Br-free^{DEP}+100μM Br^- was treated in the same manner except that 100 μM NaBr was added to all food components of the Br-free^{DEP} synthetic diet. Hatching rate differences were observed for eggs collected 3-7 days after maternal diet implementation. n=300 eggs. Analyzed by the Mann-Whitney U test.

(E) Survival curve for w^{1118} flies under Standard, Br-free^{DEP}, and Br-free^{DEP}+100μM Br^- dietary conditions. The survival difference between groups was highly significant (log rank test, n>40 for each group).

(F) Western blot of isolated NC1 domain from larvae treated as in (E), probed with an anti-Drosophila NC1 polyclonal antibody (Extended Experimental Methods). Associated larval Br-content was measured by EINAA (additional data in Table S2). Bonds/hexamer were calculated from the Western blot.

(G-I) Representative images of *vkg^{454}-GFP homozygous* larvae reared under the conditions tested in (E) demonstrating holes in the BM (basement membrane) (indicated by orange arrows) in the distal posterior midgut of Br-free^{DEP} larvae. Optical sections of mid-lateral gut plane visualizing the circular muscles in cross-section (f-actin stained with phalloidin) surrounded by a collagen IV (vkg^{454}-GFP) scaffold and the gut epithelial BM. Gut lumen is oriented at the top of the image, anterior-posterior axis is horizontal. *= BM defect. Whole gut images, scale bar = 20 μ, mid-lateral plane optical sections, scale bar = 10 μ.

(J-M) Representative images of posterior midgut of 4 day old larvae with indicated peroxidasin genotype on standard food. Collagen IV anti-NC1 staining on non-permeablized samples, demonstrating similar BM staining as Vkg^{454}-GFP (J). F-actin was stained with phalliodin. No muscle actin staining is visible in (M) due to muscle death, directly visualized by EM in (R). *= BM defect. Whole gut images, scale bar = 20 μ, mid-lateral plane optical sections, scale bar = 10 μ.

(N-R) Electron micrographs of circular sections through the posterior midgut, focusing on the BM (magenta psuedocolor) beneath the enterocyte (En) near a longitudinal muscle belly (LM). Trachioles (Tr) are occasionally visualized. Standard diet control (N) has thin normal BM. BMs are thickened and irregular in Br-free^{DEP} (O), *Pxn^{MI01492}*(Q), and *Pxn^{f07229}*(R); BM is similar to control in Br-free^{DEP}+100μM Br^- (P). BMs from 15 independent sections for each group were evaluated for thickness and the histograms plotted. Scale bar = 0.5 μ.

(S) Distribution curves and parameters from fitted distributions of each experimental group. Optimal Box-Cox transformations were performed for normality and the transformed distributions were fitted. The curves to fit the data were significantly different by the F test. Pairwise comparison revealed no significant difference between standard and Br-free^{DEP}+100μM Br^- while both curves differed significantly from Br-free^{DEP}, *Pxn^{MI01492}*, and *Pxn^{f07229}*. Bootstrapping was performed to obtain the 95% C.I.s for the mean and S.D. for each group, revealing that the variance in BM thickness in Br-free^{DEP}, *Pxn^{MI01492}*, and *Pxn^{f07229}*is substantially higher. (See also Figure 15)

similar basement membrane thickness in the standard and Br-free^{DEP}+100μM Br^- diets but significantly thicker basement membranes in Br-free^{DEP} and both *Pxn* mutants (Figure 13S, *Figure 15*G).

Br-Peroxidasin-Collagen IV interaction in the 'molecular corset'

Br-free^{DEP} conditions phenocopy the genetic loss of *Pxn*, so we hypothesized that Br^- and *Pxn* interact *in vivo* to strengthen collagen IV scaffolds. It has been reported that collagen IV acts during *Drosophila* oogenesis as a "molecular corset" to control egg shape, restricting circumferential expansion so that egg growth promotes elongation along the anterior-posterior axis (Figure 14A) (Haigo and Bilder, 2011). In eggs from mothers fed varying concentrations of Br^-, we found a dose-dependent relationship between Br^- and aspect ratio (Figure 14B), evident after ~ four days, a time course consistent with Br^- having a long biologic half-life. Interestingly, the aspect ratio of eggs on the Br-added diet (100 μM Br^-) exceeded the ratio for eggs on standard diet (NAA measured 15μM Br^-, Table S2)(Figure 14B) suggesting that elevated Br^- promotes additional sulfilimine formation to enhance tensile strength in the collagen IV molecular corset.

We used this elongated egg aspect ratio to probe whether Br^- and Pxn act via a common mechanism in strengthening collagen IV. We asked if Pxn is required for the elongation phenotype via two methods. First, we used an irreversible inhibitor, phloroglucinol, to inhibit peroxidasin activity, and we observed a dose-dependent suppression in egg aspect ratio in the presence of elevated Br^- (Figure 14C). Second, to confirm the specificity of this interaction, we used two separate ubiquitously driven temperature sensitive conditional RNAi constructs (*TubGal4Gal80^{TS}>UAS::Pxn^{RNAi})* to

knock-down peroxidasin in adult females in the presence of 100 μM Br^-. In both RNAi experiments, aspect ratio was significantly decreased relative to controls after 3-4 days of *Pxn* knockdown (transition to permissive temperature) (Figure 14D-E, *Figure 15*) while controls displayed normal augmentation of aspect ratio under identical conditions. Thus Pxn is required for the Br-induced elongation phenotype. To address the alternative hypothesis that Br^- levels modulate collagen IV deposition, we examined Vkg-GFP immunofluorescence in eggs from mothers raised on Br-free^{DEP} media. Like the Br-deficient diet, the Br-free^{DEP} media reduced egg aspect ratio (Figure 14F), but collagen IV content appeared similar to controls (Figure 14G) after one week of maternal exposure to Br-free^{DEP} diet, suggesting that the egg aspect-ratio phenotypes are caused by structural deficiencies within the scaffold.

Discussion

Through the development of novel Br-free *Drosophila* culture techniques, we were able to demonstrate that Br is an essential element for *Drosophila* development, acting specifically through peroxidasin to form sulfilimine crosslinks within collagen IV to stabilize basement membrane. By measuring Br levels in the Br-free experimental larval cohorts by NAA, we found that Br-deficiency (3.4 μM Br in Br-free^{DEP} animals vs 23.6 μM Br in control animals)(Figure 13F) corresponds with decreased survival and sulfilimine crosslinking, thus confirming the *in vitro* biochemistry suggesting that Br should be required *in vivo* for physiologic sulfilimine formation. The ability to restore survival to control levels and rescue sulfilimine crosslinking by only the re-addition of Br to the culture media indicates this effect is specific for Br (Figure 13A-C,E). These findings cumulatively represent the first evidence of an essential role for Br in biology.

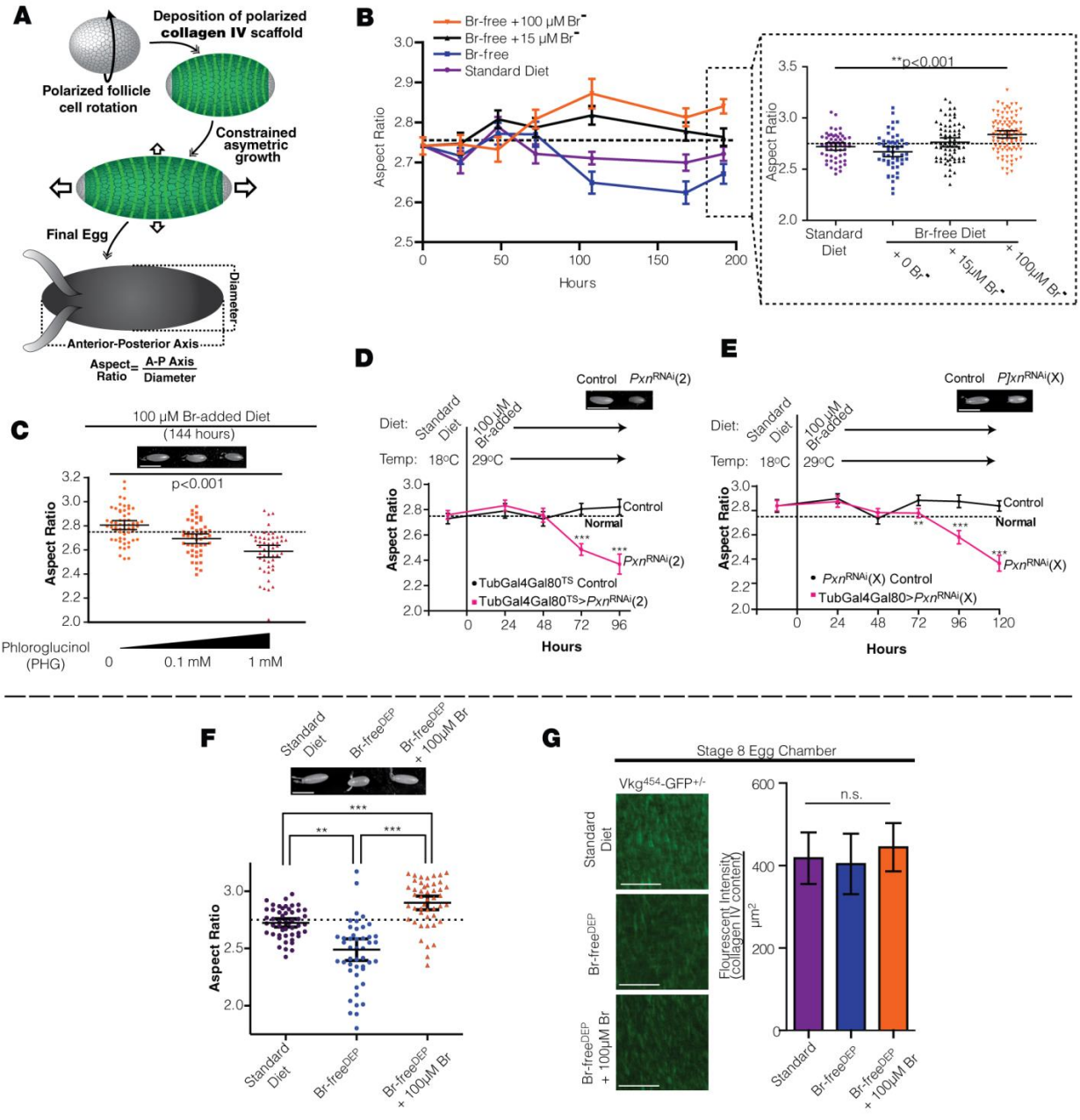

Figure 14. Br⁻ and peroxidasin interact in vivo to strengthen collagen IV scaffolds.
(A) Schematic overview of polarized collagen IV scaffolds (molecular corset, green) which determines aspect ratio in *Drosophila* eggs.
(B) Br⁻ concentration effect on egg aspect ratio, in single age-matched cohort of w^{1118} flies, over time. Vertical axis represents mean aspect ratio (±S.E.M). At 192 hours (inset), egg aspect ratio had increased proportionally to Br⁻ concentration, with similar aspect ratios in 15 µM added NaBr and standard diet (measured as 15 µM Br⁻ by NAA). Inset plotted as mean±95% C.I. and significance calculated with the Kruskall-Wallis test. Dotted line indicates egg aspect ratio reported by (Haigo and Bilder, 2011).

(C) An irreversible peroxidasin inhibitor, PHG, causes a dose-dependent reduction in the exaggerated egg elongation caused by excess dietary (100µM) Br^-. PHG was administered in the food. All wild-type (w^{1118}) mothers were from the same cohort and reared identically, then divided into sub-cohorts for exposure to the indicated experimental diet. Significance among the conditions calculated using the Kruskal-Wallis test. Data plotted as mean±95% C.I. (*image*; scale bar = 500 µm). Dotted line indicates reported value for egg aspect ratio (Haigo and Bilder, 2011). All groups also differed significantly when compared individually using Dunn's multiple Comparison testing ($p<0.05$).
(D-E) Pxn is required for Br-induced egg elongation. Two independent temperature-inducible RNAi constructs targeting *Pxn* were expressed in adult females fed 100 µM added Br^-. Aspect ratios from maternally expressed Pxn^{RNAi} were significantly different than sibling-matched controls after induction for 72 hours (29° C) by Mann-Whitney U test. *$p<0.05$, ***$p<0.001$. Data plotted as mean as mean±95% C.I., (inset image scale bar = 500 µm). Dotted line indicates reported value for egg aspect ratio (Haigo and Bilder, 2011).
(F) Egg aspect ratio on standard diet and synthetic Br-free^{DEP} and Br-free^{DEP} + 100µM Br^-diets. Eggs were collected after mothers were fed indicated diet for 7 days. Differences in egg aspect ratio were observed in eggs collected after 5-7 days of experimental diets. Representative pictures of eggs are shown (scale bar = 500 µm). Aspect ratio plotted as mean +/- 95% C.I. (*graph*; Mann Whitney U Test **$p<0.01$ ***$p<0.001$). Dotted line indicates reported value for egg aspect ratio (Haigo and Bilder, 2011).
(G) Collagen IV density appears normal in eggs from Br-depleted mothers. BM of stage 8 egg chambers from mothers expressing Vkg-GFP and fed the indicated diet (confocal images). For quantitation, fluorescence intensities of z-stack projections were summed in areas where the whole thickness of the BM had been observed, and normalized to the observational area. n=9 for each group, There was no difference in the medians between the groups by the Kruskal-Wallis test. Data plotted as mean ±95% C.I.., (*image*; scale bar = 20 µm). (See also Figure 15)

The functional demonstrations that Br is acting through peroxidasin to crosslink the basement specifically pinpoints the Br-peroxidasin-collagen IV axis as essential for development in *Drosophila.* Br-deficient embryos failed to complete development at the same rate as controls (Figure 13D), suggesting that an appropriately sulfilimine crosslinked collagen IV scaffold is necessary for embryogenesis. While there are many potential explanations for this observation, one intriguing possibility is the disruption of BMP-based embryonic patterning gradients which rely on collagen IV (Wang et al., 2008). By exploiting the 'gain-of-function' phenotype associated with the collagen IV molecular corset surrounding embryos, we were able to show that either pharmacologic inhibition or RNAi of peroxidasin could ameliorate the increased aspect ratio phenotype (Figure 14). These data show that Br is exerting its biologic effect through the enzymatic activity of peroxidasin. Collagen IV has been appreciated as a key determinate of tissue morphology in flies (Pastor-Pareja and Xu, 2011), but the direct demonstration of peroxidasin and Br^-modulating tissue-level functionality for collagen IV highlights the degree to which crosslinking is crucial for normal collagen IV biology.

While peroxidasin had been shown previously to be important for intestinal collagen IV integrity on a whole tissue level, there had thus far been no direct investigation on the role of the sulfilimine crosslink in basement membrane ultrastructure. By interrogating the intestinal basement membrane by TEM and manipulating sulfilimine content through Br-deficiency and hypomorphic peroxidasin expression, we were able to demonstrate in two independent ways that sulfilimine crosslinking directly influences basement membrane consolidation and morphology on the ultrastructural level (Figure 13 and Figure 15). Adequate sulfilimine crosslinking seems to influence both the consolidation

(in terms of overall thickness) and homogeneity (in terms of differences in the standard deviation of thickness) of the intestinal basement membrane (Figure 13S and Figure 15G). These ultrastructural changes are reminiscent of the changes observed in human basement membranes with mutations in either the α1 chain (associated with HANAC [Hereditary angiopathy with nephropathy, aneurysms, and muscle cramps] or any of the α3, α 4, or α5 chains (associated with Alports syndrome)(Alamowitch et al., 2009; Cangiotti et al., 1996; Lees et al., 1998). While mutations in the collagen IV molecule themselves likely have more significant network disruption, the very analogous ultrastructural changes in terms of thickening and irregularity by altering sulfilimine crosslinking suggests this crosslink confers substantial stability within the collagen IV network and basement membrane as a whole.

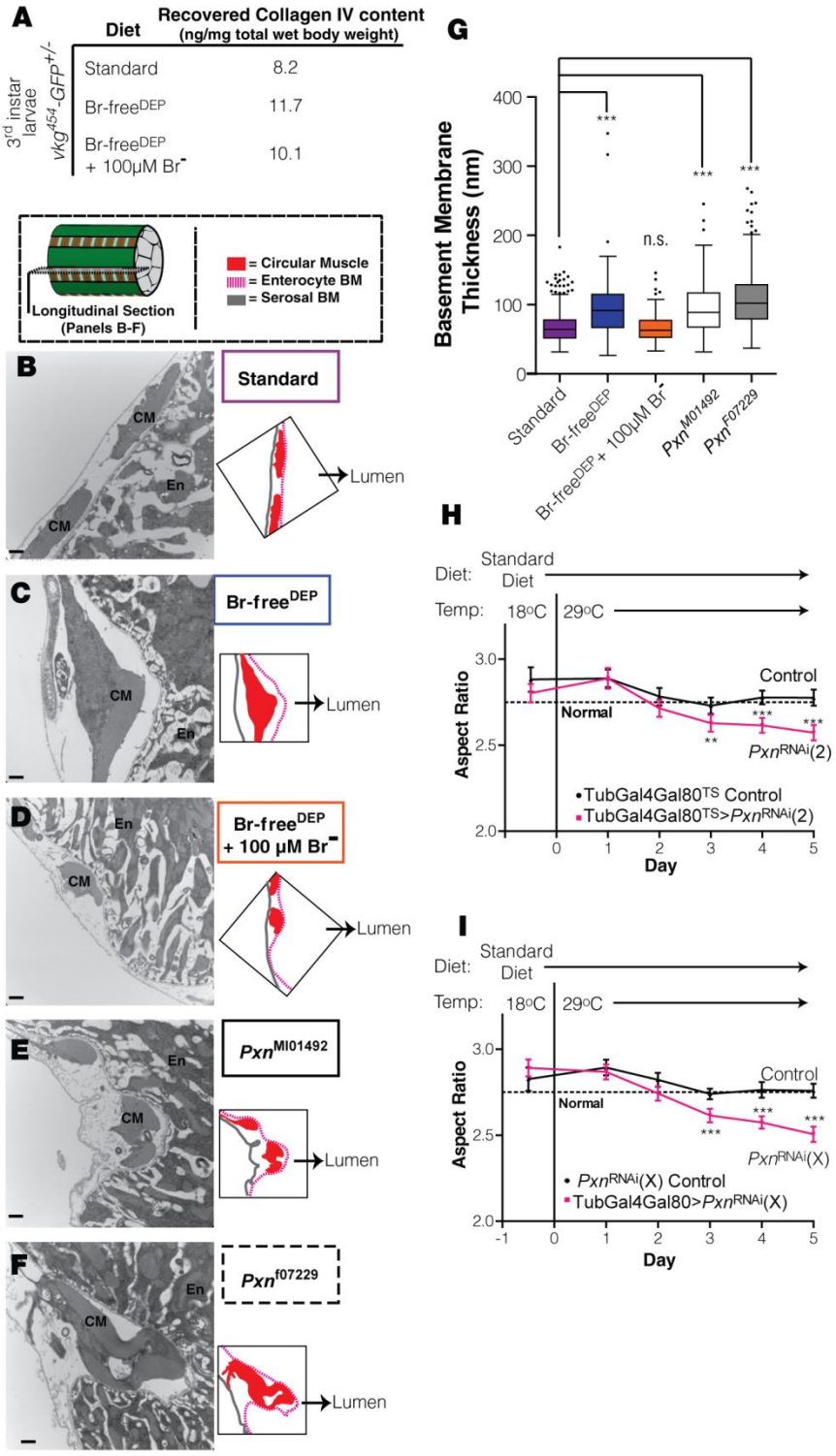

Figure 15: Legend next page.

Figure 15: Phenotypic and genetic analysis of the role of Br^- and Pxn in Drosophila (Associated with Figure 13 and Figure 14)

(A) Quantitation of total recovered collagen IV yield per wet starting weight of 3rd instar larvae from the indicated experimental condition. GFP liberation after collagenase digestion used to determine molar quantities and present in initial sample.

(B-F) Electron micrographs of longtitudinal section of posterior midgut demonstrating the deformation of the circular muscle toward the lumen, the direction of applied force during peristalsis in Br-free^{DEP}, *Pxn*^{MI01492}, and *Pxn*^{f07229}; while Standard and Br-rescued diets appear normal with little deformation.. (B-D) *vkg*^{454}*-GFP*$^{+/+}$ larvae fed the indicated diet (E-F) *Pxn*$^{MI01492\ +/+}$ or *Pxn*$^{f07229\ +/+}$ fed a standard diet, aged 4 days. Panels are additional phenotypic analysis of the conditions and hypomorphic alleles that are represented in Fig 5. Scale Bar = 0.5μm. En= Enterocyte, CM= Circular Muscle.

(G) Basement membrane thickness(Tukey's Box and Whisker plot) demonstrating the differences in median of unfitted data between experimental conditions.There is a highly signifigant overall difference in the goups ($p<0.0001$ by the Kruskal-Wallis Test) and differences between individual groups and the Standard diet control are displayed (Mann-Whitney U test, ***$p<0.001$). Importantly, there is no difference between the Standard and the Br-rescued diet.

(H-I) Egg aspect ratio depression by Pxn^{RNAi} from two independent RNAi alleles on flies fed the standard diet. Control flies for each group importantly maintained a similar aspect ratio to the literature value (Haigo and Bilder, 2011) while both RNAi lines sifgnifigantly dropped below controls (Mann-Whitney U test, **$p<0.001$, ***$p<0.0001$). Data plotted as mean±95% C.I. for each time point assessed

Table 6. Fly Vitamin and Mineral Additive Mixture

Component	Sigma Catalog No.	Formula Weight	1x Concentration (mg/L)	1x Concentration (μM)
Essential Salt Additives				
Ca-Lactate	L4388	218.22	50	229.1
$Fe(NO_3)_2 \cdot H_2O$	254223	404.0	20	49.5
$ZnSO_4 \cdot H_2O$	307491	179.47	20	111.4
$MnSO_4$	M7634	169.02	20	118.3
$CuSO_4$	451657	159.61	5	31.3
Vitamins				
Thiamine Nitrate	CDS000474	327.36	2	6.1
Riboflavin	R4500	376.36	10	26.6
Niacinamide	PHR1033	122.12	12	98.3
D-calcium pantothenate	P5155	238.27	16	67.2
Pyridoxine (neutral)	P5669	169.18	2.5	14.8
Folic Acid	F8758	441.4	3	6.8
Biotin	B4639	244.31	0.2	0.8
Choline Citrate	C2004	295.29	120	406.4

Table 7. Neutron Activation Analysis of Fly Diet Components and *Drosophila* tissues

Sample	Bromide		
	ppm	µM	Method
Biologic Samples (Eggs, larvae, Adults)			
Baseline Values for w^{1118} flies: Standard Diet			
Adults (male and female)	5.258	65.7	EINAA
Eggs	1.950	24.4	EINAA
3rd instar larvae	1.889	23.6	EINAA
14 day Exposure Adults			
W^{1118} Standard Diet	5.407	67.6	EINAA
W^{1118} Br-free	1.762	22.0	EINAA
W^{1118} Br-free + 15 µM NaBr	2.952	36.9	EINAA
W^{1118} Br-free + 100 µM NaBr	20.695	258.7	EINAA
Br-Depleting Conditions (See Figure 13F)			
$Br\text{-}free^{DEP}$ Larvae	0.271	3.4	EINAA
$Br\text{-}free^{DEP}$ + 100 µM NaBr Larvae	4.172	52.1	EINAA
$Br\text{-}free^{DEP}$ Adults	1.877	23.4	EINAA
$Br\text{-}free^{DEP}$ + 100 µM NaBr Adults	3.686	46.0	EINAA

CHAPTER VI

Novel Anti-Peroxidasin antibodies in preclinical and clinical Goodpasture's disease

These data are assembled as part of the following planned manuscript: McCall, A.S., Bhave, G., Pedchencko, V., Fogo, A.B., Little, D.J., Baker, T.P., Olson, S.W., and Hudson, B.G. Novel Anti-Peroxidasin Antibodies Are Part of the Autoimmune Milieu in Preclinical and Clinical Goodpasture's Disease (in preparation).

Abstract

Goodpasture's disease (GP) is a devastating rapidly progressive glomerulonephritis with or without pulmonary hemorrhage. Goodpasture's disease is characterized by autoantibodies directed against the NC1 domains of the α3 and α5 chains of collagen IV in the glomerular and alveolar basement membranes. There is also a strong epidemiologic coincidence of Anti-myeloperoxidase (MPO) positivity with GP diagnosis which has unclear influence on disease course or outcome. The normally cross-linked collagen IV scaffold forms through the action of the heme peroxidase Peroxidasin via its HOBr production to from a sulfilimine (S=N) crosslink in the NC1 domain, however loss of the S=N crosslink changes recognition of the NC1 domain by GP antibodies. Herein, we demonstrate the presence of anti-peroxidasin autoantibodies in GP patient sera, both before and at the time of clinical presentation. Unexpectedly, the anti-peroxidasin specific antibodies cross-react with coated, but not native MPO, accounting for a subset of the dual-positive patients. Overall circulating cytokine analysis of samples preceding disease revealed significant time dependent elevations in T_H17 cytokines and a differential VEGF response in patients providing important context for the elevated focal peroxidasin staining in crescentic glomeruli of GP patients. Importantly, purified anti-peroxidasin antibodies inhibited HOBr production, suggesting a possible contribution of these antibodies in GP pathogenesis within this subset of anti-peroxidasin positive patients.

Introduction

Goodpasture's (GP) disease is a devastating autoimmune condition characterized by a rapidly progressive glomerulonephritis (RPGN), and pulmonary hemorrhage and Anti-Glomerular Basement Membrane (Anti-GBM) antibodies directed principally against the α3 chain of type IV collagen. Patients who present clinically with GP require immediate plasmapheresis and strong immunosuppressive treatment. Even with these efforts, the most severe presentations requiring hemodialysis have only 60% patient survival and approximately 90% will require lifetime dialysis. (Levy et al., 2001). Despite the disease being rare (about 1 per 1 million per year), its study has revealed much of what is known about collagen IV networks in the glomerular basement membrane (GBM) (Hudson, 2004; Hudson et al., 2003) For the last 30 years, the definitive finding in Goodpasture's disease has been an autoantibody targeted at the Non-Collagenous 1(NC1) domain of the α3 and α5 chains of type IV collagen found in the glomerulus (Pedchenko et al., 2010). Normally, NC1 hexamers of basement membrane collagen IV, and the α345 network in the kidney, are cross-linked by the sulfilimine (S=N) bond. The S=N bond prevents the GP autoantibody (anti-α3 and/or anti-α5 NC1 domains) recognition and grants immune privilege, as well as resistance to proteolysis *in vitro*. (Vanacore et al., 2009; Vanacore et al., 2011; Vanacore et al., 2008) Peroxidasin was recently identified as the enzyme responsible for the formation of the S=N crosslink. (Bhave et al., 2012) *In vivo*, peroxidasin generates HOBr which then chemically forms the S=N crosslink. (McCall et al., 2014). Because the S=N bond influences autoantibody recognition of α3/5(IV) NC1 domains, the etiology of Goodpasture's disease may then involve the disruption of peroxidasin's normal cross-linking function.

While GP is defined by the presence of α3(IV) autoantibodies, one notable epidemiologic feature is co-incidence of Anti-MPO antibodies in GP patients. These 'double positive' patients account for 10-38% of GP cases. (Hellmark et al., 1997; Levy et al., 2004b). While differences in clinical outcomes and NC1 domain autoantibody specificity have been suggested between these two groups, no clear trend has emerged (Hellmark et al., 1997; Levy et al., 2004b; Yang et al., 2007b). Intriguingly, a unique pre-diagnosis study of GP patients, up to 80% of GP cases were found to have Anti-MPO antibody recognition preceding active disease at some point (Olson et al., 2011). Peroxidasin shares 48% sequence identity with myeloperoxidase through the peroxidase domain, with peroxidasin as the oldest evolutionary peroxidase (Soudi et al., 2012). This degree of sequence identity makes potential epitope overlap an appreciable possibility. The concurrence of Anti-MPO antibodies before and at the time of GP diagnosis, coupled with the degree sequence similarity with Peroxidasin, suggest the potential for autoantibodies recognizing peroxidasin to exist within the GP population, particularly within the 'double positive' group.

Herein, we tested two independent GP cohorts, one uniquely preceding diagnosis, for recognition of peroxidasin as an autoantigen. By ELISA and competition binding, anti-peroxidasin antibodies were identified both before and during active disease in GP patients. These antibodies are distinct from Anti-MPO antibodies and account for sizable proportion of ELISA based 'Anti-MPO' positivity in this patient group. Because of the unique pre-diagnosis GP cohort, we were also able to observe a T_H17 polarized cytokine environment with unique VEGF response in pre-diagnosis patients. With peroxidasin likely to respond to VEGF, we stained crescentic glomeruli of GP patients

and indeed found elevated focal peroxidasin levels. Finally, we were able to show that anti-peroxidasin autoantibodies functionally inhibit HOBr production. Collectively, these data demonstrate that peroxidasin is a novel autoantigen in a subset of GP patients with multiple potential contributions to disease pathogenesis.

Results

Anti-Peroxidasin Antibodies in Pre-Clinical and Clinical Goodpasture's Disease

We initiated our investigation of potential peroxidasin immunoreactivity with GP patients by screening a cohort of GP sera and plasmapheresis fluid collected during the hospital course of the patients by Enzyme Linked Immunosorbant Assay (ELISA)(n=24 patients and 7 healthy controls used to determine threshold values)[Figure 16A-B]. Amongst this cohort, 46% (11/24 patients) demonstrated peroxidasin positivity, compared to 33% (8/24 patients) Anti-MPO, and 100% (24/24) reactive strongly with recombinant α3 derived from mammalian cell lines as the positive control. Importantly for this assay, only the trimeric, fully heme loaded form of recombinant human peroxidasin was used as the coated antigen. In all control samples thus far analyzed, none have been grossly reactive to peroxidasin. These results demonstrate that there is IgG recognizing peroxidasin as an antigen as the time of clinical GP presentation.

To assess if there is a pre-diagnostic role for peroxidasin antigenicity, we obtained serial samples from the Department of Defense Serum Repository (DoDSR) from individuals who would eventually have GP coupled with an age, sex, race, and time-of-draw matched control samples. The six patients included in this cohort all had four pre-diagnostic serum samples with three matched control individuals (18 total controls).

Unfortunately, no samples at the time of admission are available for these cases. A demographic overview and sample draw timing schematic (Figure 16C) detail this cohort and sample accrual timing within the DoDSR in relation to diagnosis. For preliminary analysis, the highest value for each tested antigen was taken for each patient and control. Excitingly, within this extracted set, 3/6 patients recognized peroxidasin with at least one positive sample and had generally elevated values compared to controls (p=0.0183) (Figure 16D). To more comprehensively analyze this data longitudinally, we included all control samples to recalculate thresholds for peroxidasin, MPO, and α3 (Figure 17 and Figure 18). Two patients (4X and 6X) demonstrated obviously elevated PXDN immunoreactivity over the timeframe represented (5.6 to 1.6 and 6.6 to 1.6 years pre-diagnosis respectively) (Figure 17). Similar to the other pre-diagnostic GP cohort (Olson et al., 2011) where 87% of patients had at least one positive pre-diagnostic Anti-MPO positive sample, this cohort had 3/6 patients with elevated Anti-MPO reactivity (p=0.007) (Figure 16D) with 4/6 patients demonstrating positivity in the more comprehensive longitudinal analysis(Figure 17) . Anti-α3 antibodies were also generally elevated in patients above controls (p= 0.0148) (Figure 16D), and were ‘positive’ in 4/6 patients longitudinally when compared to the time-of-accrual matched samples, with two patients (2X and 3X) demonstrating a sharp increase in reactivity in the most disease-proximate samples (Figure 18). Intriguingly, the strongly peroxidasin-positive patients also demonstrated some of the highest pre-diagnostic anti-α3 reactivity which was maintained over their observed pre-clinical

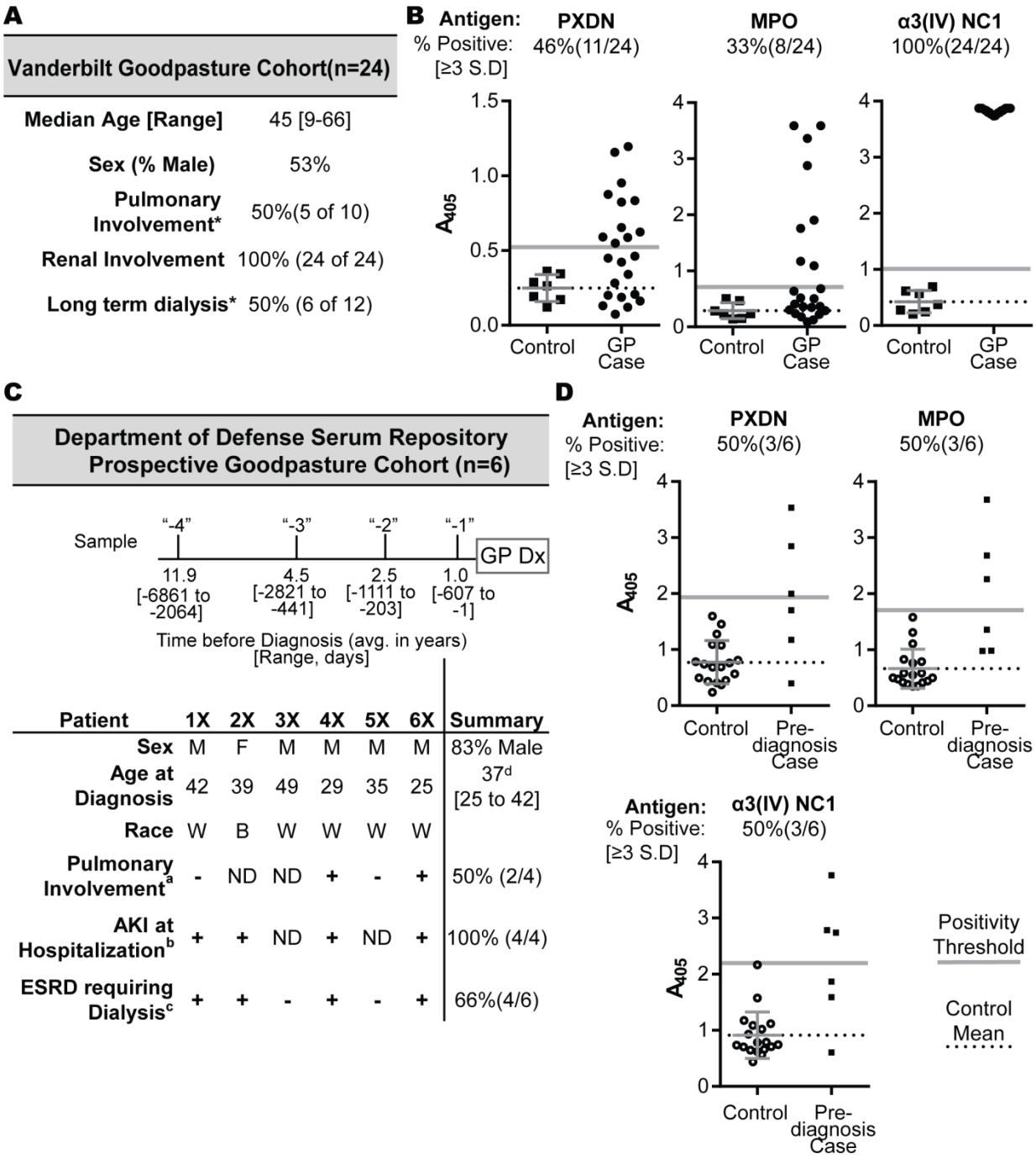

Figure 16: Antibodies recognizing peroxidasin are present in Goodpasture's disease patients before and at the time of diagnosis.

(A) Demographic and limited clinical information of the Vanderbilt Anti-GBM cohort. * Pulmonary involvement and final dialysis requirements based on medical records of inpatient and outpatient course where available.

(B) ELISA data for specified native recombinant antigens from 1:100 dilutions of either serum or early plasmapheresis fluid at the time of presentation. Positivity threshold was determined from the control mean (n=7) plus 3 standard deviations for each antigen.

Controls plotted with mean±S.D. Dotted reference line represents control mean for the specified antigen, and grey line represents positivity threshold.
(C) Demographic information and sample draw timing for the prospective Goodpasture's disease cohort from the DoDSR. Race (W=white, B=Black), ND=No relevant data. Disease involvement based on ICD9 codes associated with inpatient and outpatient visits following the index hospitalization where available [a] Pulmonary involvement (pulmonary hemorrhage) derived from ICD9 786.3. [b] Acute kidney injury based on ICD9 584.9. [c] End Stage Renal Disease requiring dialysis ICD9 585.6 from subsequent outpatient visits used to identify ongoing dialysis. If ICD9 585.3 (Stage III CKD), the patient was deemed to not need dialysis. [d] Median age and range
(D): ELISA data for specified native recombinant antigens from 1:100 dilutions for each individual serum sample, maximal values from each patient and control are plotted, regardless of time-of-draw. Each patient's specific time-course appears in Figure 17 and Figure 18 with positivity thresholds derived from all control samples. Controls plotted with mean±S.D. Dotted reference line represents control mean for the specified antigen, and grey line represents positivity threshold.

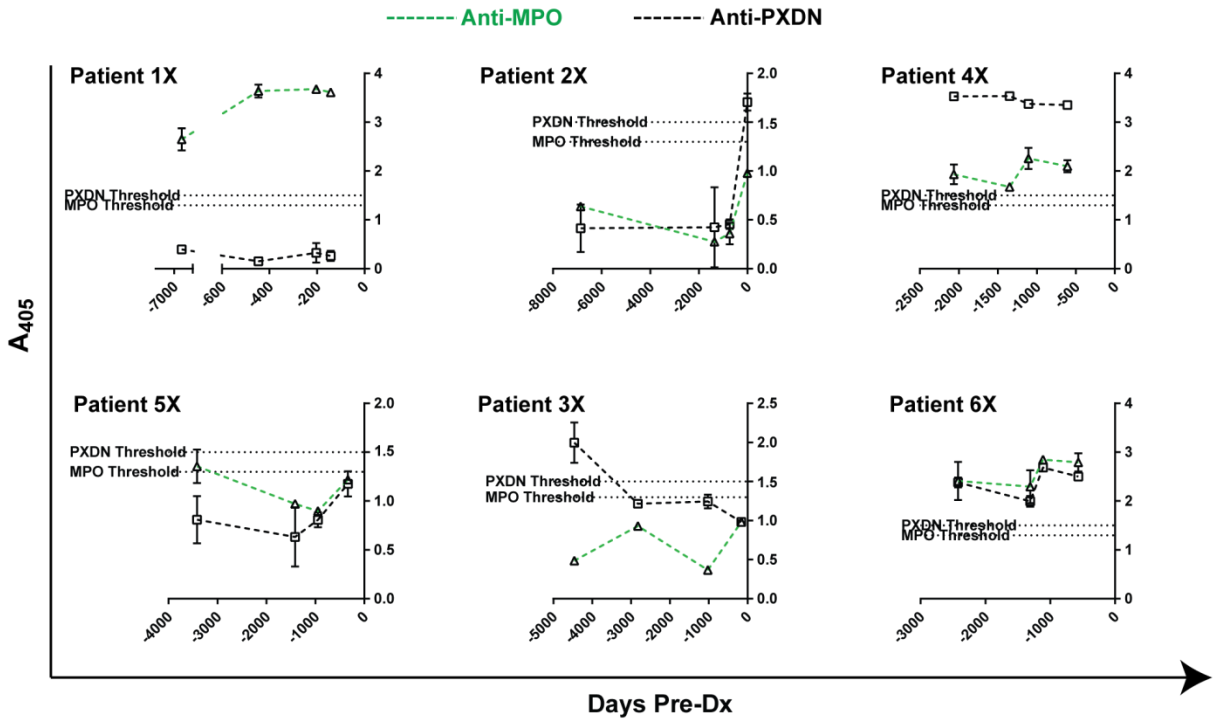

Figure 17: Time resolved Anti-peroxidasin and Anti-MPO antibodies in pre-diagnosis GP patients by ELISA from the DoDSR.
Positivity thresholds defined as control mean (n=18) + 3 S.D derived from all control samples at all time points.

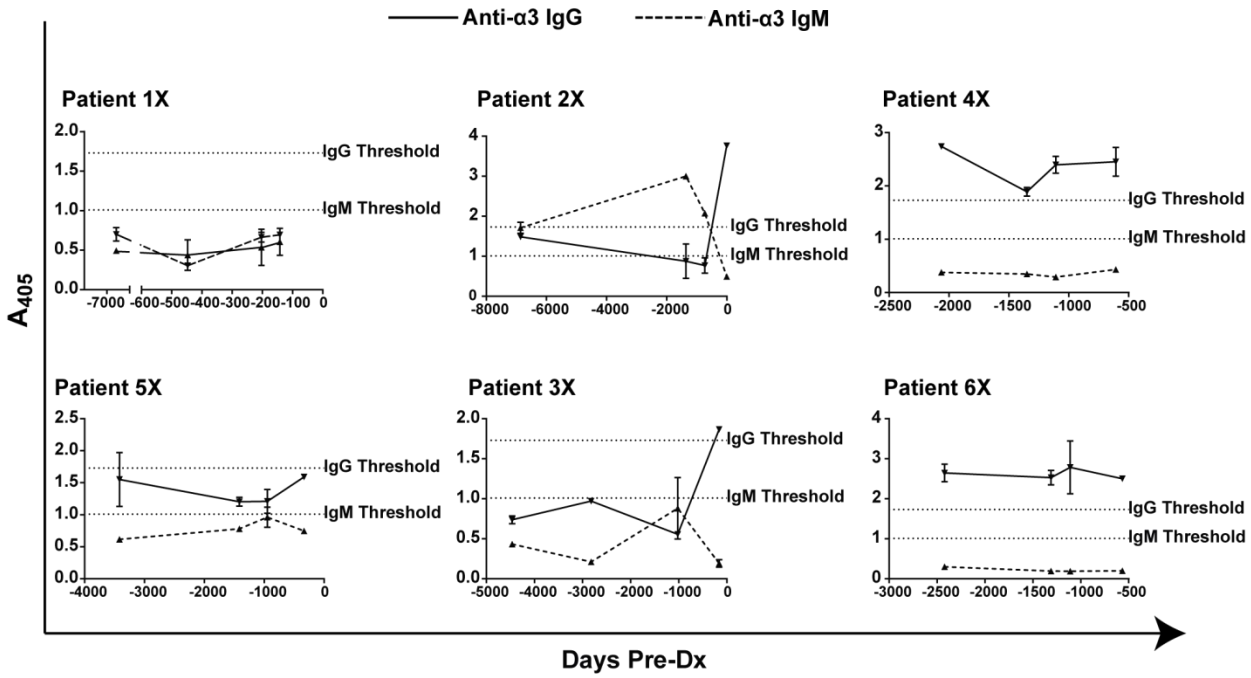

Figure 18: Anti-α3 IgG and IgM levels in pre-diagnosis GP patients from the DoDSR by ELISA.

Positivity thresholds defined as control mean (n=18) + 3 S.D. derived from all control samples at all time points

course. Because these are pre-diagnosis samples, we also tested for the presence of IgM recognizing these antigens as part of a potentially detecting an evolving autoimmune response. There was a trend of elevated anti-α3 IgM at approximately 1000 days pre-diagnosis in 3/6 patients (Figure 18). There was no elevation in IgM recognizing peroxidasin above control values in any case, and only Anti-MPO IgM in one patient (1X) who also demonstrated strong Anti-MPO IgG (data not shown). Unfortunately, because of the heterogeneity of sample timing between patients, it is difficult to make strong conclusion about the temporality of any of these antibody responses related to GP clinical disease onset. However, when combined with data from the Vanderbilt cohort, this second independent and uniquely prospective GP cohort corroborates IgG recognition of peroxidasin in GP patients, validating peroxidasin as an autoantigen in this population both before and at the time of active disease.

Anti-Peroxidasin Antibody Specificity

While these data are the first evidence of peroxidasin as an autoantigen, the co-incidence of peroxidasin and MPO recognition in almost all cases obliges the determination of antibody specificity between these two related antigens. One initial observation made was that peroxidasin and MPO, when coated at the same molarity for ELISA, produced different qualitative groups (Figure 19A) where either 1) there is similar peroxidasin and MPO immunoreactivity or 2) peroxidasin negative but highly MPO positive. We used competition binding in a 2x2 combinatorial way with MPO and peroxidasin to dissect these groups with representative patients from both cohorts. Patients who demonstrated peroxidasin reactivity could have both the peroxidasin and MPO reactivity competed away by peroxidasin in a dose dependent manner (Figure

19B), while soluble MPO only modestly competed away either peroxidasin or MPO reactivity in this group. This result indicates that antibodies in this group are specific to peroxidasin, and cross-reacting only with coated, not native, MPO. The non-equivalence of coated and soluble MPO for recognition within this group is consistent with conformation changes upon direct coating of antigens directly to hydrophobic surfaces (Butler et al., 1993). In the other group, patients that demonstrated no serologic reactivity to peroxidasin but robust reactivity to MPO could have MPO reactivity competed away by soluble MPO, but not peroxidasin (Figure 19C), indicating that, indeed, these are Anti-MPO specific antibodies in these patients. These results show that peroxidasin specific antibodies are part of the autoimmune milieu in a subset of GP patients and further, that these anti-peroxidasin positive patients would be mischaracterized as Anti-MPO positive under standard clinical lab conditions(Csernok, 2013; Holle et al., 2012), while their reactivity pattern is in fact consistent with anti-peroxidasin specific autoantibodies .

Cytokines in Pre-Clinical Goodpasture's Disease Patients

In addition to the autoantibody milieu before disease onset, the prospective DoDSR cohort in this study offered the ability to probe the cytokine environment surrounding those autoantibodies in this preclinical snapshot. The circulating cytokine profile, while not reflective of tissue or germinal center cytokines guiding specific autoantibody development, has been used previously to understand autoimmune bias in multiple conditions (Radstake et al., 2009). A 29-plex cytokine panel was performed on each time point for the cases and matched controls (Figure 20A). As mentioned previously, the limited number of patients and heterogeneity of sample timing between them

complicates analysis; however, several significant differences appeared (Table 8), and some in a time dependent manner. Previous animal models of Anti-GBM have implicated IL-23 specifically for pathogenesis (Ooi et al., 2009), indeed, these pre-diagnosis individuals demonstrated significant elevation in both IL-1a and IL-12p40 (part of IL-23), but not IL-12p70 (IL-12) (Figure 20B-C). IL-1α and IL-23 are known to synergize to promote IL-17 production and ultimately T_H17 polarization (Sutton et al., 2006), a key factor in the formation of crescentic glomerulonephritis in ANCA vasculitis (Velden et al., 2012). While we did not observe clear systemic elevation in IL-17 in pre-diagnosis patients, we did find a significantly different VEGF correlation with IL-17 levels in patients vs. controls (Figure 20D). The differential elevation of VEGF in response to elevated IL-17 levels in patients suggests possible modulation of VEGF levels as a key downstream regulator of IL-17 function and systemic spill-over of a locally involved T_H17 driven process (Pickens et al., 2010; Ryu et al., 2006). The relationship between VEGF and downstream glomerular crescent formation during injury is complex, but is VEGF clearly important to both podocyte integrity and response to vascular and glomerular injury (Hohenstein et al., 2010; Masuda et al., 2001; Nitta et al., 1999). The prominent expression of peroxidasin in the vasculature (Shi et al., 2011) and its emerging role in angiogenesis ((Bell et al., 2001; Liu et al., 2010) (both VEGF responsive events), coupled with its up-regulation in a murine kidney injury model (Peterfi et al., 2009), suggests that peroxidasin might be elevated as part of crescentic GN and provide additional ways in which anti-peroxidasin antibodies might contribute to the GP disease process.

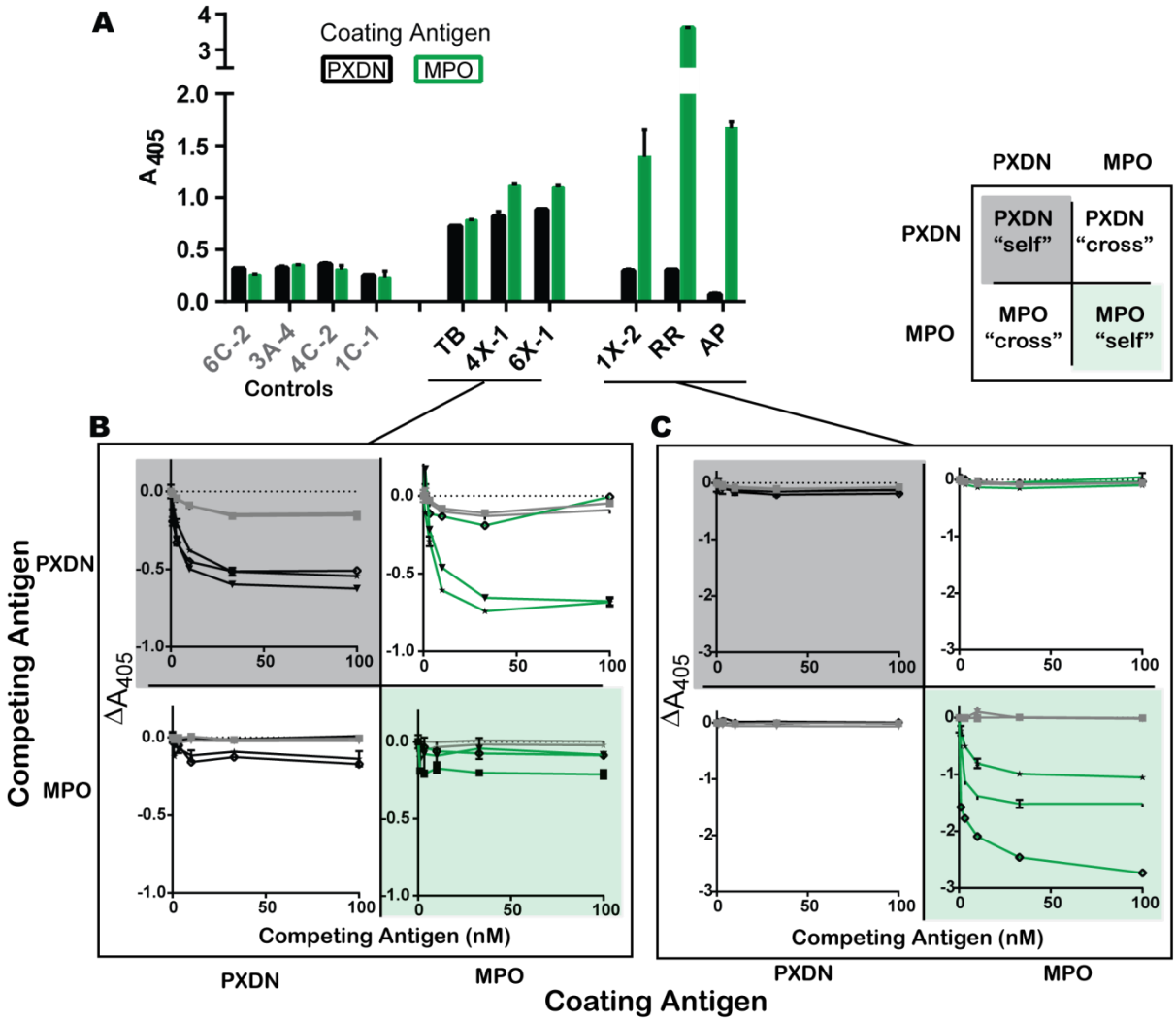

Figure 19: The subset of patients recognizing peroxidasin has anti-peroxidasin specific antibodies.

Peroxidasin positive, MPO positive and matched controls were tested for antigen specificity using competition ELISA. Antigens were coated (2.8 nM) and native, soluble peroxidasin or MPO were pre-incubated with 1:500 dilutions of patient sera for 12 hours at 4^{O}C before exposure to coated antigens.

(A) Binding to coated antigens in the absence of any competing protein.

(B) Peroxidasin postive patients have peroxasin and MPO recognition inhibited by peroxidasin, but not MPO, indicating the presence of peroxidasin specific antibodies.

(C) MPO-only postive patients have MPO binding which is uneffected by soluable peroxidasin, but completely inhibitable by soluable MPO, indicating these antibodies are MPO specific.

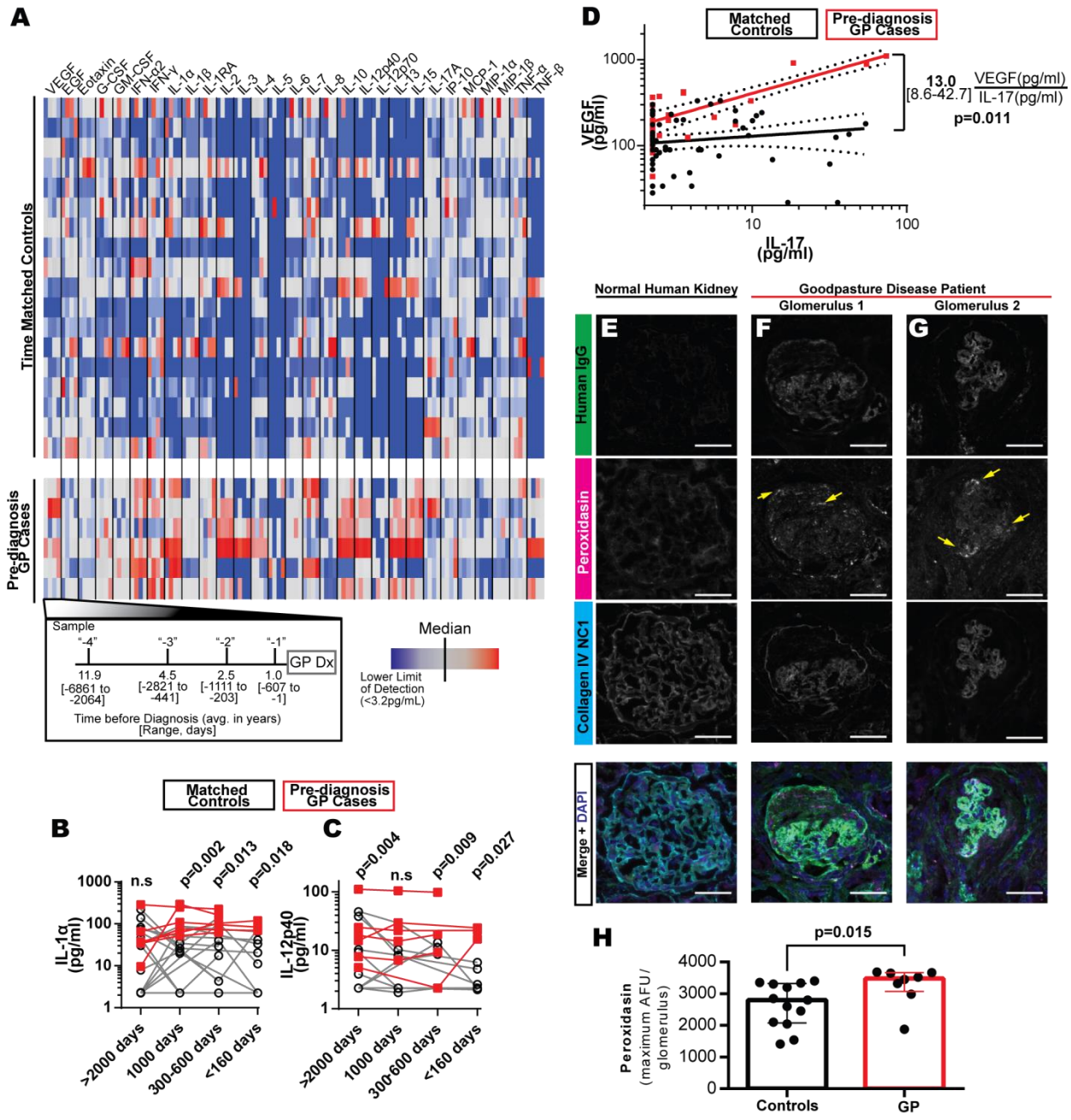

Figure 20: GP patients have T_H17 cytokines before diagnosis and elevated focal peroxidasin levels in crescentic glomeruli.

(A) Heatmap of cytokine levels for patients and matched controls (3n for each case). Color levels are set individually for each cytokine.

(B) IL-1α levels graphed over time for individual patients and controls demonstrating a significant increase approaching diagnosis.

(C). IL-12p40 (a surrogate for IL-23 levels) demonstrates significant elevations in pre-diagnosis patient compared to controls at multiple time points.

(D) Significantly different correlation between IL-17 and VEGF in pre-diagnosis patients vs. controls **(**assessed via interaction within a general liner model**)** suggesting a different systemic response to IL-17 in patients compared to controls, despite overall levels of either chemokine not significantly differing in univariate analysis. (Pre-diagnosis cases and controls were fit and plotted with 95% confidence intervals for demonstration, difference in slopes [95% confidence interval] taken from 1000 bootstrapped samples) Dashed lines represent 95% C.I for fitted slope.

E-G are frozen sections of either normal kidney or GP patient biopsy at time of presentation.(scale bar= 50 µm, all sections stained with the identical primary and secondary antibody mixtures simultaneously, and imaged on the same day with identical exposure settings to enable comparison).

(E) Normal Kidney, showing peroxidasin staining (magenta, anti-human peroxidasin) primarily adjacent to the basement membrane (cyan, JK2 anti-collagen IV NC1 antibody), with overall relatively low levels of peroxidasin in mature, healthy kidney.

(F-G) Representative images of crescentic glomeruli in a Goodpasture's disease biopsy demonstrating prominent linear GBM staining (green, patient deposited IgG) as well as increased peroxidasin (magenta, anti-human peroxidasin) staining in crescentic glomeruli. The patient was p-ANCA positive, however the anti-peroxidasin status of this patient is unknown.

(H) Quantification of maximum peroxidasin levels in glomeruli from normal and crescentic glomeruli in Goodpasture's patients demonstrating a significant increase in maximum focal peroxidasin levels within GP crescentic glomeruli (Mann-Whitney U test)(Error bars represent mean and interquartile ranges).

Table 8: Pre-diagnosis Cytokine differences in pre-diagnosis GP patients vs matched controls.

Differences in cytokine values from the DoDSR pre-diagnosis GP cohort. Significant differences were based on a bonferroni-adjusted threshold of p<0.0017. Significant associations are bolded.

Cytokine	Control vs. Case difference (pg/ml)	95% C.I. for difference	p value (Mann-Whitney U)
VEGF	-188.6	-309. to -68.0	.0122
EGF	61.1	-12.6 to 134.8	.6407
Eotaxin	144.4	-25.4 to 314.1	.1615
G-CSF	-34.7	-60.1 to -9.17	.0163
GM-CSF	-5.9	-19.0 to 7.3	.0462
IFN-α2	-26.0	-40.5 to -11.5	.0242
IFN-γ	-3.2	-5.60 to -0.72	.0449
IL-1α	**-93.9**	**-132 to -55.3**	**.0014**
IL-1β	4.2	-15.4 to 23.89	.0324
IL-1RA	-20.9	-49.6 to 7.938	.0232
IL-2	**-14.4**	**-20.1 to -8.54**	**.0016**
IL-3	-3.4	-6.37 to -0.45	.0646
IL-4	-42.5	-106. to 21.92	.3502
IL-5	-1.3	-2.88 to 0.226	.0646
IL-6	4.5	-115. to 124.9	.0059
IL-7	-8.9	-15.1 to -2.56	.1813
IL-8	-17.2	-156. to 122.1	.3861
IL-10	-38.2	-50.8 to -25.4	.0025
IL-12p40	**-23.7**	**-38.2 to -9.25**	**.0002**
IL-12p70	1.3	-2.12 to 4.762	.0226
IL-13	**-25.7**	**-35.0 to -16.2**	**.0005**
IL-15	-15.2	-23.4 to -6.88	.0137
IL-17A	-2.7	-10.4 to 5.027	.3165
IP-10	-54.1	-218. to 110.5	.4634
MCP-1	21.9	-241. to 284.8	.3861
MIP-1α	18.8	-35.6 to 73.21	.7369
MIP-1β	11.2	-37.0 to 59.40	.3173
TNF-α	-1.2	-9.09 to 6.647	.5050
TNF-β	-12.8	-23.4 to -2.28	.0021

We therefore sought to determine if peroxidasin is differentially present in crescents derived from GP patient biopsies. Immunofluorescence of crescentic glomeruli of GP patient biopsies demonstrated morphologically different peroxidasin staining from control glomeruli, with prominent punctate staining (Figure 20E-G). With no corresponding serum for the individuals from which these biopsies were taken, it is not possible to determine the peroxidasin status of these patients, making any co-localization of IgG and peroxidasin uninterpretable. Regardless, there is significantly more intense focal peroxidasin localization in crescentic glomeruli in GP patients (Figure 20H).

Peroxidasin Inhibition by Anti-Peroxidasin Antibodies

With knowledge of anti-peroxidasin antibodies before and at the time of GP disease, framed by elevated peroxidasin levels within crescentic glomeruli, the obvious question is if anti-peroxidasin antibodies have any functional inhibition of peroxidasin activity. This is a central question to the characterization of this novel autoantibody since insufficient peroxidasin function has direct effects on basement membrane architecture (McCall et al., 2014), an essential component of efficient wound and tissue regeneration in response to injury(Thorning and Vracko, 1977; Vracko, 1974). Peroxidasin mediated HOBr production is essential for sulfilimine bond formation within the NC1 hexamer, thus we tested if the purified IgG from Anti-peroxidasin positive patients could inhibit HOBr production by peroxidasin *in vitro.* Using a fluorogenic reporter of hypohalous acid production (Aminophenyl fluorescein) (Flemmig et al., 2012), there was a significant 70.3% reduction in apparent rate of oxidant production by peroxidasin in the presence of Anti-peroxidasin antibodies (mean difference $4.85x10^{-3}$ $AFU*sec^{-1}$ [95% CI

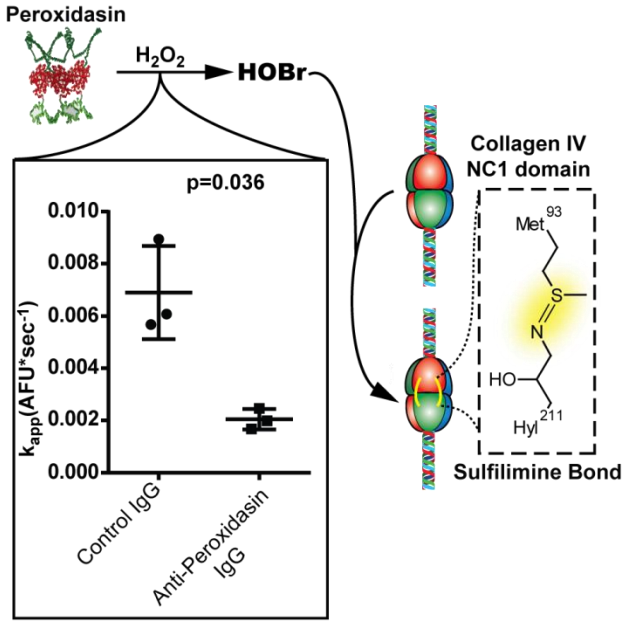

Figure 21: Peroxidasin is inhibitable by patient anti-peroxidasin antibodies *in vitro*.

APF (aminophenyl fluorescein) based peroxidase activity assay (500 pM peroxidasin, 218 µM whole patient IgG (437.5-fold mol excess), 100µM NaBr, 140mM NaCl, 10µM APF) with initial rates measured after the addition of 7.5 µM H_2O_2 in the presence of purified IgG from anti-peroxidasin positive patients or matched controls demonstrating significant inhibition of activity by anti-peroxidasin antibodies (Student's t-test used, variances found to not significantly differ).

9.02 $x10^{-3}$ to 0.6 $x10^{-3}$]) derived from three separate patients compared to matched controls (Figure 21). The ability of anti-peroxidasin antibodies to inhibit the enzymatic activity of peroxidasin offers the additional possibility that these antibodies could play a feed-forward role in crescent formation by inhibiting appropriate re-establishment of basement membrane following the initial insult.

Discussion

This work has demonstrated peroxidasin to be a novel autoantigen within a subset of GP patients. Through examination of a unique cohort composed of serial pre-disease samples from GP patients, Anti-peroxidasin antibodies co-exist with modest anti-α3 antibodies before the onset of fulminate disease, indicating that inhibitory anti-peroxidasin antibodies might be part of the GP pathogenesis in this subset of patients based on the importance of appropriate sulfilimine crosslinking of the collagen IV NC1 domain to prevent pathogenic anti-α3 antibodies from binding. (Pedchenko et al., 2010; Vanacore et al., 2011; Vanacore et al., 2008). However, GP rarity also suggests the requirement for multiple hits including genetic (Ooi et al., 2013) and environmental factors (Hudson et al., 2003), so the presence of anti-peroxidasin antibodies in a subset of patients might simply represent an additional hit. The T_H17 polarized cytokine environment, essential to GP pathogenesis in animal models (Ooi et al., 2009), and concomitant systemic elevation in VEGF specific to pre-diagnosis GP cases, enables another avenue of peroxidasin involvement. The likely response of peroxidasin levels to angiogenic stimulation via VEGF enables the elevated levels of peroxidasin within the crescentic glomeruli to potentially feed-forward the renal insult as an additional primary

antigen possibly contributing to loss of renal function in the anti-peroxidasin positive GP subset. With multiple potential nodes of peroxidasin and anti-peroxidasin autoantibody involvement for some GP patients, additional cases are necessary to determine which, if any, of these hypotheses are valid.

Broadly, the finding that Anti-peroxidasin antibodies cross-reacted with coated MPO highlights the need to further investigate patients currently described as ‘double positive’ (anti-MPO and anti-α3). This cross-reactivity with MPO is notable because ‘Anti-MPO’ antibodies are known to not cross-react with closely related eosinophil peroxidase. (Sullivan et al., 1994) Thus, re-evaluation of the clinical differences and presentation within this subset of GP patient is warranted based on peroxidasin positivity since there has been conflicting outcomes data for both renal and overall survival (Hellmark et al., 1997; Levy et al., 2004b; Lionaki et al., 2007; Rutgers et al., 2005; Yang et al., 2007b). Indeed, it was notable that both patients with strong anti-peroxidasin positivity pre-diagnosis both went on to develop pulmonary hemorrhage and require dialysis, whereas the one strictly anti-MPO patient did not. The small size of the prospective cohort and limited clinical data on the active disease cohort emphasize the need of a larger cohort accompanied by a complete clinical picture to discern any clinical and molecular differences associated with anti-peroxidasin antibodies. Because anti-peroxidasin antibodies can appear on current laboratory serologic testing as ‘Anti-MPO’ positive, exploration of the scope of anti-peroxidasin antibodies within other conditions such as microscopic polyangiitis (MPA) which have known Anti-MPO associations could also be assessed. If inhibitory anti-peroxidasin antibodies are involved it might yield insight into

the pathogenesis of these conditions where robust vascular collagen IV plays an important role in tissue homeostasis and function.

Chapter VII

Conclusions and Future Directions

Essential function of Bromide-Peroxidasin-collagen IV axis in the basement membranes of Animals

We provide evidence that bromine is essential in animals, satisfying the principal requirements for elemental essentiality: 1) Element deficiency leads to physiologic dysfunction, 2) Repletion of the element reverses dysfunction, and 3) Biochemical explanation of the physiologic function (Mertz, 1981). Br-deficient *Drosophila* display altered basement membrane and tissue morphology, aberrant embryogenesis, larval mid-gut defects, and lethality, while Br^- repletion restored normal development. Mechanistically, the assembly of crosslinked collagen IV scaffolds requires Br^-.

Sulfilimine- crosslinked collagen IV scaffolds are central to the form and function of basement membranes in animals (Bhave et al., 2012; Fidler et al., 2014). Our data indicate that the crosslink stabilizes nascent collagen IV scaffolds, effectively modulating scaffold assembly and basement membrane thickness. Since sulfilimine formation involves the concerted activity of collagen IV, Br^-, peroxidasin, and oxidant, we view each as being critical for basement membrane assembly and tissue development (Figure 22A-B).

Mechanistic and Chemical Role of Bromide in Sulfilimine Formation

The requirement for Br^- during sulfilimine formation derives from the selectivity of the bromosulfonium reaction intermediate. The chemical character of bromine uniquely creates an energetically favorable reaction between the **S-Br** intermediate and Hyl[211]. The **S-Br** molecular orbital structure facilitates selective reactivity with an amine nucleophile to form the crosslink, contrasting with the highly polar **S-Cl** intermediate that preferentially forms a sulfoxide via charge-controlled reaction with water (Figure 22C). Peroxidasin harnesses this HOBr-based selectivity during crosslinking while apparently avoiding oxidative damage to the broader basement membrane.

Bromine Essentiality and Physiology

Bromine, existing almost entirely as bromide *in vivo*, is present in the human body in levels around 3 mmol/75 kg (240 mg total in a normal human), placing its content between other known essential trace elements such as Copper (Cu) and Iron (Fe)(Frieden, 1985). Essential trace elements, by their very definition, are present in the body in very low concentrations yet have profound effects on biologic processes. Because of Bromine's relative abundance in both the oceans and human tissue, Frieden hypothesized that "Bromine is probably the most likely remaining nonmetal to qualify as an essential element" (Frieden, 1985).

The biochemical and biologic function of bromide can be better understood when examined by the criteria also established by Mertz (Mertz, 1981) for assessing the basis

for essential trace element action which involves three additional key areas of emphasis: amplification, specificity, and homeostatic regulation.

Amplification*:* It is recognized for all essential trace elements yet identified that there is a need to interact with an enzyme or act as a part of a hormone to enable the interaction with a larger mass of physiologic substrate. Iodine requires activation and incorporation into thyroid hormones T_3 and T_4 (Frieden, 1981), and Cu incorporation into metalloenzymes (Uauy et al., 1998) both expand the effect of these elements beyond their stoichiometric presence *in vivo*. The activation of Br^- by peroxidasin enables the crosslinking of many potential collagen IV molecules through its electrophilic catalysis of sulfilimine crosslink formation.

Specificity: The niche of the essential element must be absolutely specific, and a deficiency only rectified by that element alone and not another, even chemically related element. Our data shows specificity at multiple levels within peroxidasin-collagen IV axis. Enzymatically, peroxidasin is unable to form physiologic levels of S=N crosslink with any other halide than bromide. The finding that there is an energetic preference by Met^{93} for a S-Br **HSI** in S=N bond formation within the NC1 domain provides clear rationale why Cl and Br are not interchangeable for this essential biological function. Finally, the depletion of bromide within *Drosophila* and its ability to rescue the observed phenotypes upon repletion shows its hitherto unappreciated specificity within physiology.

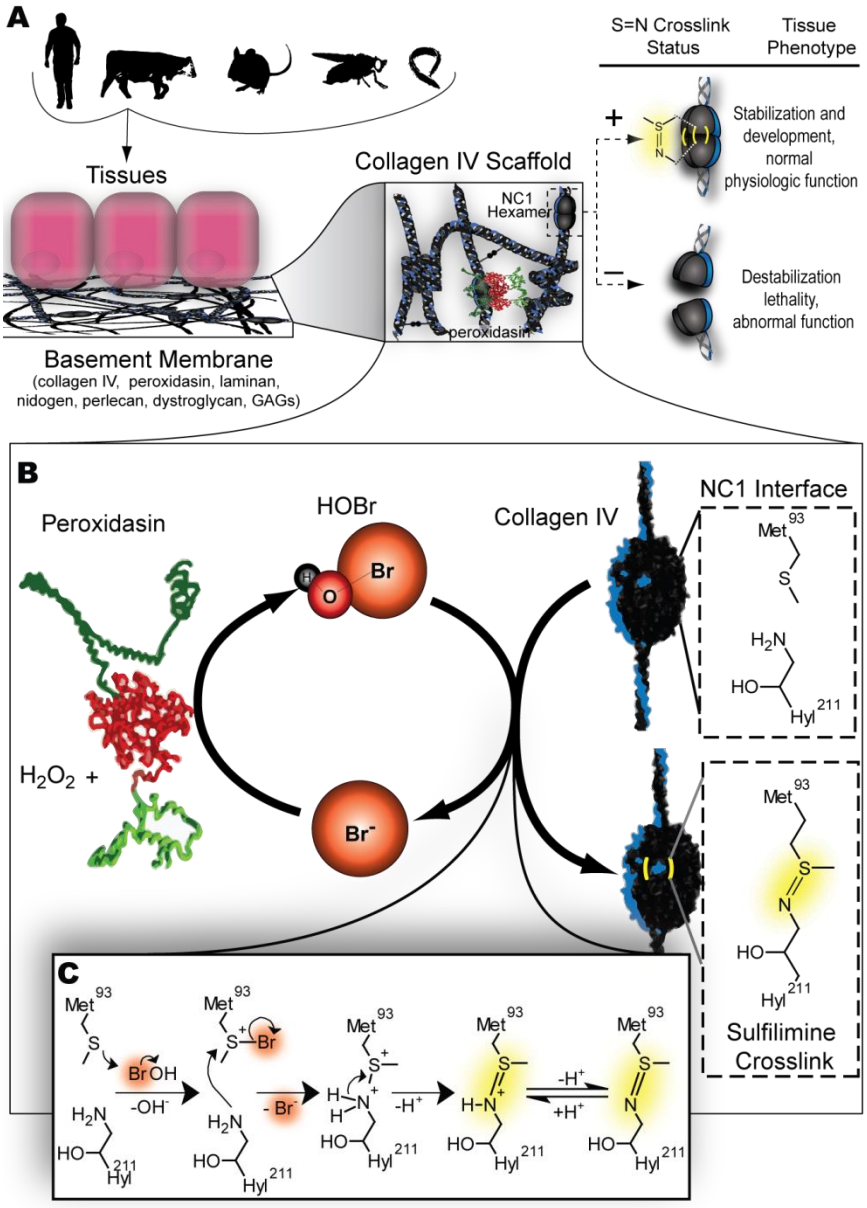

Figure 22. Model of the essentiality of bromine in forming collagen IV sulfilimine crosslinks.

(A) Diagrammatic relationship between collagen IV sulfilimine formation and tissue phenotype.

(B) Schematic representation of role of bromide in oxidative formation of sulfilimine crosslinks.

(C) Proposed chemical mechanism of sulfilimine formation by HOBr.

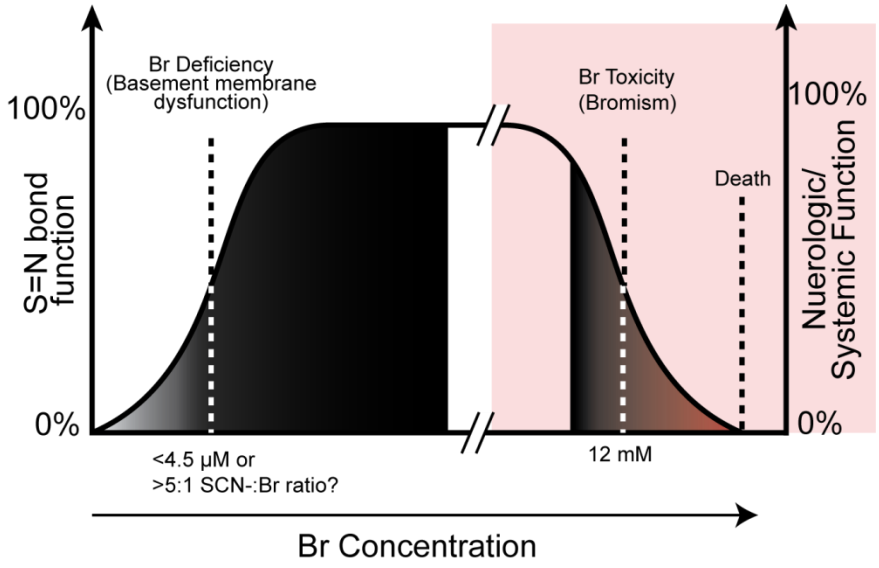

Figure 23. Schematic of Br function at a range of concentrations demonstrating deficient, optimal, and toxic concentration ranges

Based on Bertrand's rule for essential elements. Left axis plots hypothetical sulfilimine crosslink formation, while the right axis plots the red shaded portion of the schematic (>8mM plasma Br^-) by systemic function.

Homeostatic Regulation*:* The element must be maintained at a relatively constant and optimal physiologic concentration across a variety of dietary and environmental conditions. There has been consensus across five decades, multiple methods of measuring serum bromide, and many investigators on several continents that serum bromide in healthy individuals is remarkably consistent around 5.4 mg/L (67.6μM) (Kirk, 1991; Olszowy et al., 1998; van Leeuwen et al., 1987). The Br^- concentrations that support sulfilimine formation in *D. Melanogaster* are congruent within an order of magnitude to those observed in many species (freshwater fish (Woods et al., 1979), flies (Piedade-Guerreiro et al., 1987), rodents (Van Logten et al., 1974), and humans (Olszowy et al., 1998; van Leeuwen et al., 1987)). Bromide is found primarily extracellularly (Barratt and Walser, 1969), and in humans, with plasma Br^- maintained via diet and renal excretion (Trautner and Wieth, 1968b; van Leeuwen et al., 1987; Walser and Rahill, 1966a; Wolf and Eadie, 1950a). Several studies in humans and dogs demonstrate that bromide has preferential tubular reabsorption to chloride (Trautner and Wieth, 1968a; Walser and Rahill, 1966b; Wolf and Eadie, 1950b). Given the tight regulation of physiologic chloride concentrations, these observations offer a plausible mechanism by which serum bromide concentrations are maintained at optimal ratios by linkage to tubular chloride regulation (Trautner and Wieth, 1968a). Drosophila likely conserved Br^- under our experimental conditions, contributing to the substantial time before phenotypes appeared in our generational dietary Br-deficiency model. Lending support to this hypothesis, the only reported instance of bromide deficiency in

humans occurred in patients undergoing hemodialysis (Canavese et al., 2006). One other demonstration of potential Br-deficiency in goats has been suggested to suppress tissue growth and increase lethality (Anke et al., 1990). Conversely, the long medical history of pharmacologic use of bromide to treat neurological and psychiatric issues has demonstrated that the clinical syndrome of 'Bromism' occurs when there is excess bromide present (>12 mM), resulting in neurologic and occasionally dermatologic manifestations (Carney, 1971; van Leeuwen et al., 1987). The observation of a maintained plateau, suboptimal, and toxic ranges for bromide in physiology is consistent with Bertrand's rule for essential nutrients (Mertz, 1981) and likely evidence of homeostatic regulation (Figure 23).

Recent developments since the establishment of Br as an essential trace element

Since the publication of our work in June 2014 (McCall et al., 2014), several studies have appeared addressing Br content in tissues specifically. Excitingly, widely distributed bromide content was observed in all tissue tested with areas of increased focal concentration of bromine in the sub-endothelial space (Ceko et al., 2015a; Ceko et al., 2015b). The authors concluded that the non-uniform distribution of Br is tissue (which they went on to speciate and show is in fact bromide), was evidence of active biologic regulation at the tissue level (Ceko et al., 2015b). In another study, an ischemia-reperfusion model of cardiac injury showed modest differences in infarct volume in animals fed additional NaBr (Iwata et al., 2014). While these data are difficult to interpret, it is encouraging to see Br levels intentionally included in experimental injury models and studied in different tissue contexts.

Clinical Implications of Bromide Deficiency

Bromide deficiency may have implications in human health and disease. Patients receiving total parenteral nutrition (TPN) are reported to have low plasma Br^- levels due to nutritional Br-deficiency (Dahlstrom et al., 1986), and end-stage renal disease patients have enhanced Br^- losses as a consequence of dialysis (Miura et al., 2002; Oe et al., 1981; Wallaeys et al., 1986). Since Br has not been considered an essential trace element, systematic investigations on Br^- replacement have not been pursued in these disease states. Intriguingly, TPN alters intestinal mucosal architecture and function in a manner reminiscent of the mid-gut phenotypes of *Drosophila Pxn* mutants and Br-deficient larvae (Groos et al., 2003). Furthermore, functional Br-deficiency may occur in smokers in spite of normal plasma Br^- levels because of elevated levels of serum SCN^-, which inhibits sulfilimine bond formation. We found SCN^- to be a potent inhibitor of peroxidasin-mediated crosslink formation (Figure 9). Therefore, in some smokers with elevated SCN^- levels (130 μM, 1 pack per day) (Tsuge et al., 2000), reinforcement of collagen IV scaffolds with sulfilimine crosslinks may be substantially reduced. Indeed, smoking has been associated with architectural changes within basement membranes (Asmussen, 1979; Soltani et al., 2012). Finally, since basement membrane assembly involves Br^-, tissue development or remodeling may be vulnerable to Br-deficiency. These findings provide rationale for further investigating the clinical implications of either objective Br-deficiency (such as in dialysis or TPN) or functional Br-deficiency (as in smoking) and the physiologic consequences of mechanically perturbing collagen IV scaffolds.

Future directions in Br-related essential element research

Through the establishment of a specific physiologic requirement for Bromine in the synthesis of a functional collagen IV scaffold, there are important remaining questions which need to be addressed about the tissue- and organism-level function of Br as a nutrient and its influence on basement membrane biosynthesis in normal physiology and disease.

Future experiments need to expand Br-depletion into mammalian systems with stringent biochemical analysis to better understand the role of the Br^{-}peroxidasin-collagen IV triad on basement membrane physiology. Protein level analysis of the collagen IV scaffold's sulfilimine bond status is crucial because mammals, compared to the flies in which Br-essentiality was tested, have other collagen genes on which they can draw for structural reinforcement. Higher mammals, including humans, possess six distinct collagen IV chains, as well as other fibrillary collagens (such as collagen I and III) not found in flies. While sulfilimine conservation throughout the animal kingdom into humans suggest that this covalent crosslink plays an important role, this has never been formally tested *in vivo* in mammals, nor have any compensatory mechanisms for sub-optimally crosslinked basement membranes been recognized. The survival of peroxidasin null mice and humans, despite the profound phenotypes, strongly suggests that compensation for the suboptimal sulfilimine crosslinking is possible, and represents an exciting area for additional research (Khan et al., 2011). Coupled with the analysis of the influence of Br on basement membranes, more stringent analysis of peroxidasin null mice and their basement membrane characteristics could have the experimental power

to dissect the continuum of collagen IV crosslinking and its impact on tissue development and function.

The first major hurdle to any future studies on Br and its basement membrane impact in mammals is the definition of what constitutes Br-deficient phenotype in target organs in terms of cellular and organismal behavior. Clues from a Br-deficiency experiment conducted in goats, despite the lack of measurement of Br levels in any test animal, support the idea of multisystem dysfunction (Anke et al., 1990). Among the interesting findings of a similar study, “disturbances of carbohydrate, lipid and mineral metabolism” as well as “focal proliferative extracapillary glomerulonephritis” were both observed (Zhavoronkov et al., 1996). The observed metabolic changes possibly indicate derangements in intestinal handling of nutrient intake because of enterocyte dysfunction and the proliferative changes in kidney histology are intriguing because of their proliferative similarity to Goodpasture’s disease biopsies. Both findings could represent cellular dysfunction because of inadequate basement membrane properties.

Regardless of the relation of these previous potential Br-deficient findings in goats to the present work, clear obstacles exist to defining the scope and experimental efficacy of Br-depletion techniques in a mammalian (particularly human) system. The obstacles mentioned below are foundational for any clinical application of Br-repletion in either TPN of hemodialysis settings.

1) Reliable Br level testing in a reasonable timeframe to enable testing of patient samples and potentially therapeutic repletion of Br into humans. The work presented here employed Neutron Activation Analysis, which while very sensitive

(typically <10 p.p.b by mass), requires a neutron source from a reactor and typically and is not amenable to a significant number of samples in a short time frame. Other techniques, such as X-Ray fluorescence, will likely be better for the rapid evaluation of Br content in serum, dialysis fluid, TPN preparations, but lack a similar degree of sensitivity as NAA (Srivastava, 2014). The technique ultimately chosen to measure Br content is a major technical issue to be resolved because of the need to analyze complex samples with high sensitivity.

2) Determination of therapeutic endpoints within a potential study of Br-repletion. Because there are a number of ways that Br deficiency could manifest in critically ill patients receiving TPN or in a long term hemodialysis cohort, careful attention to short and long term outcomes is needed. Short term endpoints, such as a gold-standard histologic analysis of intestinal or vascular biopsies, has the potential to cement a role for Br-repletion as a therapy in these treatment groups if clear histologic improvement are noted compared to control subjects. However, clinical endpoints coupled with those histologic analyses would be obviously necessary. Those endpoints could include infection rate (because of improved mucosal integrity in both TPN and hemodialysis patients), weight gain (better intestinal nutrient handling in TPN patients), or changes in hemodynamic parameters (indicative of changed vascular remodeling in hemodialysis patients). Because there are numerous other ways basement membranes direct tissue function, there are many other secondary endpoints which might eventually be considered.

3) Choice of cohort to test therapeutic Br repletion. There are varied populations who receive TPN and hemodialysis treatments. For TPN, patients who had bowel resections who require TPN for sufficient nutrition (Short Bowel Syndrome), critically ill patients who require feeds, or perhaps most intriguingly, the premature babies in the neonatal intensive care unit who rely on TPN for months during rapid growth and development (Morgan et al.). All of these groups could potentially benefit from Br-addition to the TPN mixture; however the actual degree of deficiency would have to be determined in each group. The choice of clinical endpoints also differs for each of these potential cohorts. A TPN trial in a neonatal cohort potentially offers the most rapid path to understanding if Br supplementation is clinically important because of the rapid development of the gut and lung during these times, offering a more acute and potentially informative study (Morgan et al.). Hemodialysis represents a less acute, but far larger population to potentially be studied for Br-deficiency related changes. Because there are likely both acute and chronic effects of Br-deficiency, hemodialysis patients are the optimal population to evaluate long term changes in vasculature remodeling, since this is a key place where Br is suspected to influence the collagen IV scaffold.

Peroxidasin as a novel autoantigen

Through the investigation of Goodpasture's disease (GP), we discovered that peroxidasin is an autoantigen recognized in a subset of these patients. The autoantibodies identified were inhibitory, which has significant potential disease implications in the pathogenesis of GP and other vasculitides. All GP patients have anti-

collagen IV autoantibodies characterized by recognition of epitopes in the α3 and α5 NC1 domains with *in vitro* specificity toward the hexamer without the sulfilimine crosslink (Vanacore et al., 2011; Vanacore et al., 2008). The finding that only a subset of GP patients have anti-peroxidasin antibodies is notable because it could mean either that GP is potentially heterogeneous in its development (if anti-peroxidasin antibodies are part of the pathogenesis), that the methods used in this study were inadequate to detect the presence of anti-peroxidasin antibodies in more patients, or that anti-peroxidasin antibodies are not actively involved in GP disease. Additional patient samples and biopsies from anti-peroxidasin positive GP patients would be required to dissect those competing theories.

The potential mechanistic scenario where anti-peroxidasin antibodies inhibit formation of the sulfilimine crosslink propagating anti-α3 and α5 antibody binding is an exciting hypothesis (Figure 24). Another feasible hypothesis is that through the inhibition of peroxidasin's crosslinking function, the NC1 hexamer is destabilized leading to proteolysis, resulting in self-immunization with auto-antigenic peptide fragments which are ultimately recognized by the pathogenic Goodpasture autoantibodies. Additional studies including antibody purification and passive transfer will be required to demonstrate a causal relationship between these antibodies and Goodpasture's disease.

Additionally, the finding that anti-peroxidasin antibodies, through their recognition of coated MPO, could account for a subset of patients currently considered Anti-MPO positive expands the potential clinical impact of this finding. pANCA (perinuclear Anti-Neutrophil Cytoplasmic Antibody) positive vasculitis which is >90% associated with anti-

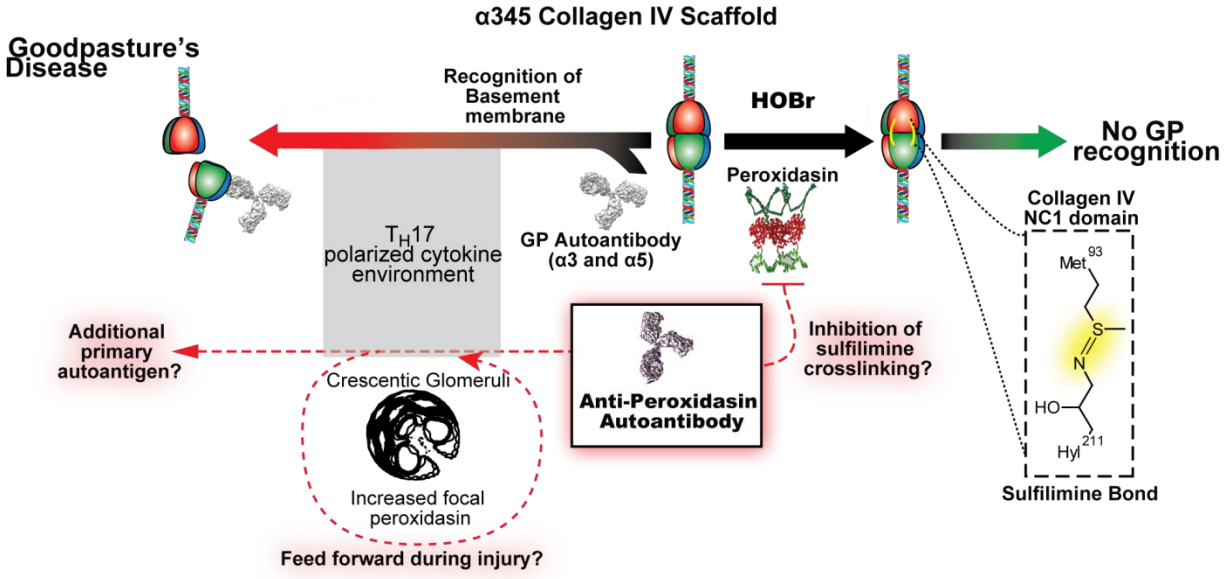

Figure 24 Model of anti-peroxidasin antibodies within the context of Goodpasture's disease pathogenesis

The finding of anti-peroxidasin antibodies before and at the time of Goodpasture's diagnosis raises three potential possibilities for disease involvement highlighted in red: **1)** By inhibiting S=N crosslinking and modifying the a3 epitope **2)** by acting as an additional primary antigen **3)** Coupled with our finding of increased focal peroxidasin in crescentic glomeruli, the antibodies acting to feed-forward the injury in these already injured glomeruli.

MPO antibodies, occurs at roughly 10-times the frequency of Goodpasture's disease (Ntatsaki et al., 2010), significantly increasing the number of patients for which anti-peroxidasin antibodies are possibly relevant. Notably, a recent epitope specific study in patients with anti-MPO positive active vasculitis symptoms identified a cryptic linear epitope of MPO which both correlated well with active disease and could induce experimental vasculitis and nephritis upon passive transfer in mice (Roth et al., 2013). This epitope in MPO (RKIVGAMVQIITY) shares profound identity and very conservative differences with a section of primary sequence in the peroxidase domain of peroxidasin (RKIVGAEIQHITY), suggesting that antibodies against this epitope might also recognize peroxidasin. The prominent vascular expression of peroxidasin (Shi et al., 2011) and our demonstration of elevated focal peroxidasin staining in crescentic glomeruli provide exciting circumstantial clues about a role for peroxidasin in this disease process. Further investigation of pANCA vasculitis and its renal involvement in patient cohorts is required to determine if peroxidasin is indeed an autoantigen for this condition also.

Future Directions for Anti-peroxidasin antibody research

The identification of peroxidasin as an autoantigen in this work suggests three key additional areas of investigation required more fully understand the importance and role of autoantibodies directed specifically at peroxidasin. The current study is confined to two small cohorts of patients. Both from an epidemiologic and reproducibility perspective, additional GP patients need to be tested. As mentioned previously, the potential clinical laboratory reporting overlap between peroxidasin and MPO also necessitates a more nuanced understanding of the autoimmune epitopes found within peroxidasin. Also, this body of works lacks the ability to causally link these

autoantibodies to any portion of disease progression. Thus, the future work on anti-peroxidasin antibodies should expand to these three areas:

1) Is the anti-peroxidasin autoantibody in other patient cohorts, specifically pANCA vasculitis? The MPO overlap in recognition means future evaluation of pANCA vasculitis cohorts and additional GP cohorts are required to understand the prevalence of anti-peroxidasin antibodies and if their presence is potentially relevant in multiple diseases. Ideally, if medical outcomes are linked to the samples in these cohorts, it will facilitate the answers to clinically relevant questions about anti-peroxidasin antibody positivity such as disease severity, correlation with active vasculitic symptoms, renal survival, and association with pulmonary symptoms.

2) What epitope is being recognized by anti-peroxidasin autoantibodies? A major unresolved question is the identity of the epitopes giving rise to the peculiar pattern of antigen recognition between MPO and peroxidasin. Two approaches can be taken to identify the epitopes recognized by patients. Grossly, domain deletion constructs of peroxidasin lacking the LRR, IgG, and vWFc domains could be used to crudely map the major domains responsible for auto-antigenicity (Figure 2B). Another exciting approach could employ constrained cyclic peptide arrays to determine the primary sequence of the main epitopes found in peroxidasin (Mock et al., 2015). The sequence resolution of the autoimmune epitope is important for better assay design as well as potentially allowing for better *in vivo* modelling in the future with epitope specific models of anti-peroxidasin autoimmunity.

3) Are anti-peroxidasin antibodies pathogenic? To answer this question, passive transfer of purified anti-peroxidasin antibodies is the gold-standard. To perform this experiment, peroxidasin knock-out mice would be immunized with purified recombinant peroxidasin, the anti-peroxidasin antibodies purified, and passively transferred to wild-type mice. A similar experiment performed by Lerner, Glasscock and Dixon using purified patient derived antibodies injected into monkeys was a seminal experiment in demonstrating that GP autoantibodies were pathogenic (Lerner et al., 1967). This model is also important to develop because of the need to also investigate anti-peroxidasin antibodies as part of a potential two hit hypothesis. More specifically, experimentally testing if passive transfer of inhibitory anti-peroxidasin antibodies, in the context of different types of physical and immune deposit injuries or inhalational insults, could result in experimental GP disease. If successful, these two-hit experiments would represent biologically and medically relevant insight into GP pathogenesis in patients with anti-peroxidasin antibodies.

Peroxidasin and Disease

As the enzyme responsible for one of the central crosslinking events, which endows collagen IV with its required functionality for basement membranes to fill their biologic niche, peroxidasin has a crucial role in normal physiology and an increasingly appreciated role in disease. The tissue specific duties of the basement membranes during development, tissue homeostasis, and wound healing place a premium on peroxidasin function to enable the collagen IV scaffold to support the demands of those tissues. As additional studies address the physiology of humans who lack peroxidasin (Choi et al., 2015; Khan et al., 2011) and experimental manipulation of peroxidasin null

mice progresses(Lázár et al., 2015), it will be possible to tease apart the specific roles in development and wound healing for which peroxidasin and a sulfilimine-crosslinked collagen IV scaffold are most important. Cumulatively, this work has shown peroxidasin function can be compromised through nutritional deficiency, metabolite accumulation, and autoimmune recognition. The physiologic requirement for Br^- as a cofactor for normal peroxidasin function will be foundational moving forward as the tissue levels sulfilimine crosslink are better understood in the context of development and wound healing.

.

References

Aaij, C., and Borst, P. (1972). The gel electrophoresis of DNA. Biochimica et Biophysica Acta (BBA) - Nucleic Acids and Protein Synthesis *269*, 192-200.

Abrahamson, D.R., John, P.L.S., Stroganova, L., Zelenchuk, A., and Steenhard, B.M. (2013). Laminin and type IV collagen isoform substitutions occur in temporally and spatially distinct patterns in developing kidney glomerular basement membranes. Journal of Histochemistry & Cytochemistry *61*, 706-718.

Alamowitch, S., Plaisier, E., Favrole, P., Prost, C., Chen, Z., Van Agtmael, T., Marro, B., and Ronco, P. (2009). Cerebrovascular disease related to COL4A1 mutations in HANAC syndrome. Neurology *73*, 1873-1882.

Amcheslavsky, A., Jiang, J., and Ip, Y.T. (2009). Tissue Damage-Induced Intestinal Stem Cell Division in Drosophila. Cell Stem Cell *4*, 49-61.

Anke, M., Regius, Á., Groppel, B., and Arnhold, W. (1990). Essentiality of the trace element bromine. Acta Agronomica Hungarica *39*, 297-303.

Armesto, X.L., Canle, L.M., Fernandez, M.I., Garca, M.V., and Santaballa, J.A. (2000). First Steps in the Oxidation of Sulfur-Containing Amino Acids by Hypohalogenation: Very Fast Generation of Intermediate Sulfenyl Halides and Halosulfonium Cations. Tetrahedron *56*, 1103-1109.

Asmussen, I. (1979). Fetal cardiovascular system as influenced by maternal smoking. Clin Cardiol *2*, 246-256.

Barratt, T.M., and Walser, M. (1969). Extracellular fluid in individual tissues and in whole animals: the distribution of radiosulfate and radiobromide. The Journal of Clinical Investigation *48*, 56-66.

Bell, S.E., Mavila, A., Salazar, R., Bayless, K.J., Kanagala, S., Maxwell, S.A., and Davis, G.E. (2001). Differential gene expression during capillary morphogenesis in 3D collagen matrices regulated expression of genes involved in basement membrane matrix assembly, cell cycle progression, cellular differentiation and G-protein signaling. Journal of Cell Science *114*, 2755-2773.

Bhave, G., Cummings, C.F., Vanacore, R.M., Kumagai-Cresse, C., Ero-Tolliver, I.A., Rafi, M., Kang, J.S., Pedchenko, V., Fessler, L.I., Fessler, J.H.*, et al.* (2012). Peroxidasin forms sulfilimine chemical bonds using hypohalous acids in tissue genesis. Nat Chem Biol *8*, 784-790.

Bignon, M., Pichol-Thievend, C., Hardouin, J., Malbouyres, M., Bréchot, N., Nasciutti, L., Barret, A., Teillon, J., Guillon, E., and Etienne, E. (2011). Lysyl oxidase-like protein-2 regulates sprouting angiogenesis and type IV collagen assembly in the endothelial basement membrane. Blood *118*, 3979-3989.

Bissell, M. (1997). The Central Role of Basement Membrane in Functional Differentiation, Apoptosis, and Cancer. In Cell Death in Reproductive Physiology, J. Tilly, J. Strauss, III, and M. Tenniswood, eds. (Springer New York), pp. 125-140.

Borza, D.-B., Bondar, O., Colon, S., Todd, P., Sado, Y., Neilson, E.G., and Hudson, B.G. (2005). Goodpasture Autoantibodies Unmask Cryptic Epitopes by Selectively Dissociating Autoantigen Complexes Lacking Structural Reinforcement: NOVEL MECHANISMS FOR IMMUNE PRIVILEGE AND AUTOIMMUNE PATHOGENESIS. Journal of Biological Chemistry *280*, 27147-27154.

Boudreau, N., Myers, C., and Bissell, M.J. (1995). From laminin to lamin: regulation of tissue-specific gene expression by the ECM. Trends in Cell Biology *5*, 1-4.

Bozeman, P.M., Learn, D.B., and Thomas, E.L. (1990). Assay of the human leukocyte enzymes myeloperoxidase and eosinophil peroxidase. J Immunol Methods *126*, 125-133.

Butler, J.E., Ni, L., Brown, W.R., Joshi, K.S., Chang, J., Rosenberg, B., and Voss Jr, E.W. (1993). The immunochemistry of sandwich elisas—VI. Greater than 90% of monoclonal and 75% of polyclonal anti-fluorescyl capture antibodies (CAbs) are denatured by passive adsorption. Molecular Immunology *30*, 1165-1175.

Canavese, C., De Costanzi, E., Stratta, P., and Sabbioni, E. (2006). A role for bromine deficiency in sleep disturbances of long-term dialysis patients. Am J Kidney Dis *48*, 1018-1019; author reply 1019.

Cangiotti, A., Sessa, A., Meroni, M., Montironi, R., Ragaiolo, M., Mambelli, V., and Cinti, S. (1996). Evolution of glomerular basement membrane lesions in a male patient with Alport syndrome: ultrastructural and morphometric study. Nephrology Dialysis Transplantation *11*, 1829-1834.

Carney, M.W.P. (1971). FIVE CASES OF BROMISM. The Lancet *298*, 523-524.

Ceko, M., Hummitzsch, K., Hatzirodos, N., Rodgers, R., and Harris, H. (2015a). Quantitative elemental analysis of bovine ovarian follicles using X-ray fluorescence imaging. Metallomics *7*, 828-836.

Ceko, M.J., Hummitzsch, K., Hatzirodos, N., Bonner, W., James, S.A., Kirby, J.K., Rodgers, R.J., and Harris, H.H. (2015b). Distribution and speciation of bromine in mammalian tissue and fluids by X-ray fluorescence imaging and X-ray absorption spectroscopy. Metallomics *7*, 756-765.

Chaudhuri, O., Koshy, S.T., Branco da Cunha, C., Shin, J.W., Verbeke, C.S., Allison, K.H., and Mooney, D.J. (2014). Extracellular matrix stiffness and composition jointly regulate the induction of malignant phenotypes in mammary epithelium. Nat Mater *13*, 970-978.

Chen, M., and Cook, K.D. (2007). Oxidation Artifacts in the Electrospray Mass Spectrometry of Aβ Peptide. Analytical Chemistry *79*, 2031-2036.

Chmutova, G., Ziganshina, A.Y., and Movchan, A. (1999). Differences in the Electronic Structure of Sulfenyl Chlorides and Bromides as Possible Reasons for Their Different Reactivities toward Aromatic Compounds. Russian journal of Organic Chemistry *35*, 56-61.

Choi, A., Lao, R., Ling-Fung Tang, P., Wan, E., Mayer, W., Bardakjian, T., Shaw, G.M., Kwok, P.Y., Schneider, A., and Slavotinek, A. (2015). Novel mutations in PXDN cause microphthalmia and anterior segment dysgenesis. Eur J Hum Genet *23*, 337-341.

Clark, A.G., Mackin, K.M., and Foster, M.H. (2011). Genetic elimination of alpha3(IV) collagen fails to rescue anti-collagen B cells. Immunol Lett *141*, 134-139.

Csernok, E. (2013). ANCA testing: the current stage and perspectives. Clinical and Experimental Nephrology *17*, 615-618.

Dahlstrom, K.A., Ament, M.E., Medhin, M.G., and Meurling, S. (1986). Serum trace elements in children receiving long-term parenteral nutrition. Journal of pediatrics *109*, 625-630.

Daley, W.P., and Yamada, K.M. (2013). ECM-modulated cellular dynamics as a driving force for tissue morphogenesis. Curr Opin Genet Dev *23*, 408-414.

Doner, L.W., and Douds, D.D. (1995). Purification of commercial gellan to monovalent cation salts results in acute modification of solution and gel-forming properties. Carbohydrate Research *273*, 225-233.

Eden, E., Geva-Zatorsky, N., Issaeva, I., Cohen, A., Dekel, E., Danon, T., Cohen, L., Mayo, A., and Alon, U. (2011). Proteome half-life dynamics in living human cells. Science *331*, 764-768.

Fairbanks, L.D., and Burch, G.E. (1970). Whole Body Turnover of Chloride in Adults of Drosophila (Drosophilidae) and Megaselia (Phoridae) (Diptera). Annals of the Entomological Society of America *63*, 1628-1631.

Fidler, A.L., Vanacore, R.M., Chetyrkin, S.V., Pedchenko, V.K., Bhave, G., Yin, V.P., Stothers, C.L., Rose, K.L., McDonald, W.H., Clark, T.A.*, et al.* (2014). A unique covalent bond in basement membrane is a primordial innovation for tissue evolution. Proc Natl Acad Sci U S A *111*, 331-336.

Flemmig, J., Zschaler, J., Remmler, J., and Arnhold, J. (2012). The fluorescein-derived dye aminophenyl fluorescein is a suitable tool to detect hypobromous acid (HOBr)-producing activity in eosinophils. J Biol Chem *287*, 27913-27923.

Frieden, E. (1981). Iodine and the thyroid hormones. Trends in biochemical sciences *6*, 50-53.

Frieden, E. (1985). New perspectives on the essential trace elements. Journal of Chemical Education *62*, 917.

Gensch, K.H., and Higuchi, T. (1967). Kinetic investigation of reversible reaction between methionine and iodine. Improved iodometric determination of methionine. Journal of Pharmaceutical Sciences *56*, 177-184.

Gilchrist, T.L., and Moody, C.J. (1977). The chemistry of sulfilimines. Chemical Reviews *77*, 409-435.

Gotenstein, J.R., Swale, R.E., Fukuda, T., Wu, Z., Giurumescu, C.A., Goncharov, A., Jin, Y., and Chisholm, A.D. (2010). The C. elegans peroxidasin PXN-2 is essential for embryonic morphogenesis and inhibits adult axon regeneration. Development *137*, 3603-3613.

Gould, D.B., Phalan, F.C., Breedveld, G.J., van Mil, S.E., Smith, R.S., Schimenti, J.C., Aguglia, U., van der Knaap, M.S., Heutink, P., and John, S.W. (2005). Mutations in Col4a1 cause perinatal cerebral hemorrhage and porencephaly. Science *308*, 1167-1171.

Gould, D.B., Phalan, F.C., van Mil, S.E., Sundberg, J.P., Vahedi, K., Massin, P., Bousser, M.G., Heutink, P., Miner, J.H., Tournier-Lasserve, E*., et al.* (2006). Role of COL4A1 in small-vessel disease and hemorrhagic stroke. N Engl J Med *354*, 1489-1496.

Groffen, A.J., Veerkamp, J.H., Monnens, L.A., and van den Heuvel, L.P. (1999). Recent insights into the structure and functions of heparan sulfate proteoglycans in the human glomerular basement membrane. Nephrology Dialysis Transplantation *14*, 2119-2129.

Groos, S., Reale, E., Hunefeld, G., and Luciano, L. (2003). Changes in epithelial cell turnover and extracellular matrix in human small intestine after TPN. J Surg Res *109*, 74-85.

Gunwar, S., Ballester, F., Noelken, M.E., Sado, Y., Ninomiya, Y., and Hudson, B.G. (1998). Glomerular Basement Membrane: IDENTIFICATION OF A NOVEL DISULFIDE-CROSS-LINKED NETWORK OF α3, α4, AND α5 CHAINS OF TYPE IV COLLAGEN AND ITS IMPLICATIONS FOR THE PATHOGENESIS OF ALPORT SYNDROME. Journal of Biological Chemistry *273*, 8767-8775.

Haigo, S.L., and Bilder, D. (2011). Global tissue revolutions in a morphogenetic movement controlling elongation. Science *331*, 1071-1074.

Hellmark, T., Niles, J.L., Collins, A.B., McCluskey, R.T., and Brunmark, C. (1997). Comparison of anti-GBM antibodies in sera with or without ANCA. J Am Soc Nephrol *8*, 376-385.

Hohenstein, B., Colin, M., Foellmer, C., Amann, K.U., Brekken, R.A., Daniel, C., and Hugo, C.P. (2010). Autocrine VEGF-VEGF-R loop on podocytes during glomerulonephritis in humans. Nephrol Dial Transplant *25*, 3170-3180.

Holle, J.U., Herrmann, K., Gross, W.L., and Csernok, E. (2012). Comparative analysis of different commercial ELISA systems for the detection of anti-neutrophil cytoplasm antibodies in ANCA-associated vasculitides. Clin Exp Rheumatol *30*, S66-69.

Holman, J.D., Ma, Z.Q., and Tabb, D.L. (2012). Identifying Proteomic LC-MS/MS Data Sets with Bumbershoot and IDPicker. Current Protocols in Bioinformatics, 13.17. 11-13.17. 15.

Hudson, B.G. (2004). The molecular basis of Goodpasture and Alport syndromes: beacons for the discovery of the collagen IV family. J Am Soc Nephrol *15*, 2514-2527.

Hudson, B.G., Tryggvason, K., Sundaramoorthy, M., and Neilson, E.G. (2003). Alport's syndrome, Goodpasture's syndrome, and type IV collagen. N Engl J Med *348*, 2543-2556.

Hynes, R.O., and Naba, A. (2012). Overview of the Matrisome—An Inventory of Extracellular Matrix Constituents and Functions. Cold Spring Harbor Perspectives in Biology *4*.

Ilani, T., Alon, A., Grossman, I., Horowitz, B., Kartvelishvily, E., Cohen, S.R., and Fass, D. (2013). A secreted disulfide catalyst controls extracellular matrix composition and function. Science *341*, 74-76.

Iwata, A., Morrison, M.L., and Roth, M.B. (2014). Iodide Protects Heart Tissue from Reperfusion Injury. PLoS One *9*, e112458.

Joy, E.F., Bonn, J.D., and Barnard, A.J. (1973). Photometric determination of trace bromide in alkali metal chlorides. Analytical Chemistry *45*, 856-860.

Khan, K., Rudkin, A., Parry, D.A., Burdon, K.P., McKibbin, M., Logan, C.V., Abdelhamed, Z.I., Muecke, J.S., Fernandez-Fuentes, N., Laurie, K.J*., et al.* (2011). Homozygous mutations in PXDN cause congenital cataract, corneal opacity, and developmental glaucoma. Am J Hum Genet *89*, 464-473.

Khoshnoodi, J., Pedchenko, V., and Hudson, B.G. (2008). Mammalian collagen IV. Microsc Res Tech *71*, 357-370.

Khoshnoodi, J., Sigmundsson, K., Cartailler, J.P., Bondar, O., Sundaramoorthy, M., and Hudson, B.G. (2006). Mechanism of chain selection in the assembly of collagen IV: a prominent role for the alpha2 chain. J Biol Chem *281*, 6058-6069.

Kirk, K.L. (1991). Biochemistry of Inorganic Bromide. In Biochemistry of the Elemental Halogens and Inorganic Halides (Springer), pp. 109-120.

Klopman, G. (1968). Chemical reactivity and the concept of charge- and frontier-controlled reactions. Journal of the American Chemical Society *90*, 223-234.

Langeveld, J.P., Wieslander, J., Timoneda, J., McKinney, P., Butkowski, R.J., Wisdom, B.J., Jr., and Hudson, B.G. (1988). Structural heterogeneity of the noncollagenous domain of basement membrane collagen. J Biol Chem *263*, 10481-10488.

Lázár, E., Péterfi, Z., Sirokmány, G., Kovács, H.A., Klement, E., Medzihradszky, K.F., and Geiszt, M. (2015). Structure–function analysis of peroxidasin provides insight into the mechanism of collagen IV crosslinking. Free Radical Biology and Medicine *83*, 273-282.

Lee, J., Bandyopadhyay, J., Lee, J.I., Cho, I., Park, D., and Cho, J.H. (2015). A role for peroxidasin PXN-1 in aspects of C. elegans development. Mol Cells *38*, 51-57.

Lees, G.E., Helman, R.G., Kashtan, C.E., Michael, A.F., Homco, L.D., Millichamp, N.J., Ninomiya, Y., Sado, Y., Naito, I., and Kim, Y. (1998). A model of autosomal recessive Alport syndrome in English cocker spaniel dogs. Kidney Int *54*, 706-719.

Lerner, R.A., Glassock, R.J., and Dixon, F.J. (1967). The role of anti-glomerular basement membrane antibody in the pathogenesis of human glomerulonephritis. J Exp Med *126*, 989-1004.

Levental, K.R., Yu, H., Kass, L., Lakins, J.N., Egeblad, M., Erler, J.T., Fong, S.F., Csiszar, K., Giaccia, A., Weninger, W.*, et al.* (2009). Matrix crosslinking forces tumor progression by enhancing integrin signaling. Cell *139*, 891-906.

Levine, R.L., Mosoni, L., Berlett, B.S., and Stadtman, E.R. (1996). Methionine residues as endogenous antioxidants in proteins. Proc Natl Acad Sci U S A *93*, 15036-15040.

Levy, J.B., Hammad, T., Coulthart, A., Dougan, T., and Pusey, C.D. (2004a). Clinical features and outcome of patients with both ANCA and anti-GBM antibodies. Kidney Int *66*, 1535-1540.

Levy, J.B., Hammad, T., Coulthart, A., Dougan, T., and Pusey, C.D. (2004b). Clinical features and outcome of patients with both ANCA and anti-GBM antibodies. Kidney Int *66*, 1535-1540.

Levy, J.B., Turner, A.N., Rees, A.J., and Pusey, C.D. (2001). Long-term outcome of anti-glomerular basement membrane antibody disease treated with plasma exchange and immunosuppression. Ann Intern Med *134*, 1033-1042.

Li, H., Cao, Z., Zhang, G., Thannickal, V.J., and Cheng, G. (2012). Vascular peroxidase 1 catalyzes the formation of hypohalous acids: characterization of its substrate specificity and enzymatic properties. Free Radical Biology & Medicine *53*, 1954-1959.

Lionaki, S., Jennette, J.C., and Falk, R.J. (2007). Anti-neutrophil cytoplasmic (ANCA) and anti-glomerular basement membrane (GBM) autoantibodies in necrotizing and crescentic glomerulonephritis. Semin Immunopathol *29*, 459-474.

Liu, Y., Carson-Walter, E.B., Cooper, A., Winans, B.N., Johnson, M.D., and Walter, K.A. (2010). Vascular gene expression patterns are conserved in primary and metastatic brain tumors. Journal of neuro-oncology *99*, 13-24.

Ma, Z.-Q., Chambers, M.C., Ham, A.-J.L., Cheek, K.L., Whitwell, C.W., Aerni, H.-R., Schilling, B., Miller, A.W., Caprioli, R.M., and Tabb, D.L. (2011). ScanRanker: Quality assessment of tandem mass spectra via sequence tagging. Journal of Proteome Research *10*, 2896-2904.

Masuda, Y., Shimizu, A., Mori, T., Ishiwata, T., Kitamura, H., Ohashi, R., Ishizaki, M., Asano, G., Sugisaki, Y., and Yamanaka, N. (2001). Vascular endothelial growth factor enhances glomerular capillary repair and accelerates resolution of experimentally induced glomerulonephritis. Am J Pathol *159*, 599-608.

Mayeno, A.N., Curran, A.J., Roberts, R.L., and Foote, C.S. (1989). Eosinophils preferentially use bromide to generate halogenating agents. Journal of Biological Chemistry *264*, 5660-5668.

McCall, A.S., Cummings, C.F., Bhave, G., Vanacore, R., Page-McCaw, A., and Hudson, B.G. (2014). Bromine is an essential trace element for assembly of collagen IV scaffolds in tissue development and architecture. Cell *157*, 1380-1392.

Mertz, W. (1981). The essential trace elements. Science *213*, 1332-1338.

Miura, Y., Nakai, K., Suwabe, A., and Sera, K. (2002). Trace elements in renal disease and hemodialysis. Nuclear Instruments and Methods in Physics Research Section B: Beam Interactions with Materials and Atoms *189*, 443-449.

Mock, A., Warta, R., Geisenberger, C., Bischoff, R., Schulte, A., Lamszus, K., Stadler, V., Felgenhauer, T., Schichor, C., Schwartz, C.*, et al.* (2015). Printed peptide arrays identify prognostic TNC serumantibodies in glioblastoma patients.

Morgan, W., III, Yardley, J., Luk, G., Niemiec, P., and Dudgeon, D. Total parenteral nutrition and intestinal development: A neonatal model. Journal of Pediatric Surgery *22*, 541-545.

Morrissey, M.A., and Sherwood, D.R. (2015). An active role for basement membrane assembly and modification in tissue sculpting. Journal of Cell Science.

Nagy, P., Beal, J.L., and Ashby, M.T. (2006). Thiocyanate is an efficient endogenous scavenger of the phagocytic killing agent hypobromous acid. Chem Res Toxicol *19*, 587-593.

Nelson, R.E., Fessler, L.I., Takagi, Y., Blumberg, B., Keene, D.R., Olson, P.F., Parker, C.G., and Fessler, J.H. (1994). Peroxidasin: a novel enzyme-matrix protein of Drosophila development. EMBO J *13*, 3438-3447.

Nielsen, F.H. (1998). Ultratrace elements in nutrition: Current knowledge and speculation. The Journal of Trace Elements in Experimental Medicine *11*, 251-274.

Nitta, K., Uchida, K., Kimata, N., Honda, K., Horita, S., Hayashi, T., Ishizuka, T., Kobayashi, H., Kawashima, A., Yumura, W.*, et al.* (1999). Increased serum levels of vascular endothelial growth factor in human crescentic glomerulonephritis. Clin Nephrol *52*, 76-82.

Ntatsaki, E., Watts, R.A., and Scott, D.G. (2010). Epidemiology of ANCA-associated vasculitis. Rheum Dis Clin North Am *36*, 447-461.

Oe, P., Vis, R., Meijer, J., Van Langevelde, F., Allon, W., and Meer Cvd, V.H. (1981). Bromine deficiency and insomnia in patients on dialysis. Trace Element Metabolism in Man and Animals, TEMA-4 Australian Academy of Science, Canberra, 526-529.

Olson, S.W., Arbogast, C.B., Baker, T.P., Owshalimpur, D., Oliver, D.K., Abbott, K.C., and Yuan, C.M. (2011). Asymptomatic Autoantibodies Associate with Future Anti-glomerular Basement Membrane Disease. Journal of the American Society of Nephrology.

Olszowy, H.A., Rossiter, J., Hegarty, J., Geoghegan, P., and Haswell-Elkins, M. (1998). Background Levels of Bromide in Human Blood. Journal of Analytical Toxicology *22*, 225-230.

Ooi, J.D., Chang, J., O'Sullivan, K.M., Pedchenko, V., Hudson, B.G., Vandenbark, A.A., Fugger, L., Holdsworth, S.R., and Kitching, A.R. (2013). The HLA-DRB1*15:01-restricted Goodpasture's T cell epitope induces GN. J Am Soc Nephrol *24*, 419-431.

Ooi, J.D., Phoon, R.K., Holdsworth, S.R., and Kitching, A.R. (2009). IL-23, not IL-12, directs autoimmunity to the Goodpasture antigen. J Am Soc Nephrol *20*, 980-989.

Pastor-Pareja, J.C., and Xu, T. (2011). Shaping cells and organs in Drosophila by opposing roles of fat body-secreted Collagen IV and perlecan. Dev Cell *21*, 245-256.

Pattison, D.I., and Davies, M.J. (2004). Kinetic analysis of the reactions of hypobromous acid with protein components: implications for cellular damage and use of 3-bromotyrosine as a marker of oxidative stress. Biochemistry *43*, 4799-4809.

Pattison, D.I., Davies, M.J., and Hawkins, C.L. (2012). Reactions and reactivity of myeloperoxidase-derived oxidants: differential biological effects of hypochlorous and hypothiocyanous acids. Free Radical Research *46*, 975-995.

Pavelka, S., Babicky, A., and Vobecky, M. (2005). Biological half-life of bromide in the rat depends primarily on the magnitude of sodium intake. Physiol Res *54*, 639-644.

Pearson, R.G. (1968). Hard and soft acids and bases, HSAB, part II: Underlying theories. Journal of Chemical Education *45*, 643.

Pedchenko, V., Bondar, O., Fogo, A.B., Vanacore, R., Voziyan, P., Kitching, A.R., Wieslander, J., Kashtan, C., Borza, D.B., Neilson, E.G.*, et al.* (2010). Molecular architecture of the Goodpasture autoantigen in anti-GBM nephritis. N Engl J Med *363*, 343-354.

Peskin, A.V., Turner, R., Maghzal, G.J., Winterbourn, C.C., and Kettle, A.J. (2009). Oxidation of methionine to dehydromethionine by reactive halogen species generated by neutrophils. Biochemistry *48*, 10175-10182.

Peterfi, Z., Donko, A., Orient, A., Sum, A., Prokai, A., Molnar, B., Vereb, Z., Rajnavolgyi, E., Kovacs, K.J., Muller, V.*, et al.* (2009). Peroxidasin is secreted and incorporated into the extracellular matrix of myofibroblasts and fibrotic kidney. Am J Pathol *175*, 725-735.

Pickens, S.R., Volin, M.V., Mandelin, A.M., Kolls, J.K., Pope, R.M., and Shahrara, S. (2010). IL-17 Contributes to Angiogenesis in Rheumatoid Arthritis. The Journal of Immunology *184*, 3233-3241.

Piedade-Guerreiro, J., Carmo Freitas, M., and Martinho, E. (1987). Application of NAA in determining the inorganic contents of the fruit fly (Ceratitis capitata Wied.) and its artificial food. Journal of Radioanalytical and Nuclear Chemistry *110*, 531-537.

Piper, M.D.W., Blanc, E., Leitao-Goncalves, R., Yang, M., He, X., Linford, N.J., Hoddinott, M.P., Hopfen, C., Soultoukis, G.A., Niemeyer, C.*, et al.* (2014). A holidic medium for Drosophila melanogaster. Nat Meth *11*, 100-105.

Poschl, E., Schlotzer-Schrehardt, U., Brachvogel, B., Saito, K., Ninomiya, Y., and Mayer, U. (2004). Collagen IV is essential for basement membrane stability but dispensable for initiation of its assembly during early development. Development *131*, 1619-1628.

Price, R., and Spiro, R. (1977). Studies on the metabolism of the renal glomerular basement membrane. Turnover measurements in the rat with the use of radiolabeled amino acids. Journal of Biological Chemistry *252*, 8597-8602.

Radstake, T.R., van Bon, L., Broen, J., Hussiani, A., Hesselstrand, R., Wuttge, D.M., Deng, Y., Simms, R., Lubberts, E., and Lafyatis, R. (2009). The pronounced Th17 profile in systemic sclerosis (SSc) together with intracellular expression of TGFbeta and IFNgamma distinguishes SSc phenotypes. PLoS One *4*, e5903.

Robertson, W.E., Rose, K.L., Hudson, B.G., and Vanacore, R.M. (2014). Supramolecular organization of the alpha121-alpha565 collagen IV network. J Biol Chem *289*, 25601-25610.

Roth, A.J., Ooi, J.D., Hess, J.J., van Timmeren, M.M., Berg, E.A., Poulton, C.E., McGregor, J., Burkart, M., Hogan, S.L., Hu, Y.*, et al.* (2013). Epitope specificity determines pathogenicity and detectability in ANCA-associated vasculitis. The Journal of Clinical Investigation *123*, 1773-1783.

Rutgers, A., Slot, M., van Paassen, P., van Breda Vriesman, P., Heeringa, P., and Tervaert, J.W. (2005). Coexistence of anti-glomerular basement membrane antibodies and myeloperoxidase-ANCAs in crescentic glomerulonephritis. Am J Kidney Dis *46*, 253-262.

Ryu, S., Lee, J.H., and Kim, S.I. (2006). IL-17 increased the production of vascular endothelial growth factor in rheumatoid arthritis synoviocytes. Clinical Rheumatology *25*, 16-20.

Salama, A.D., Chaudhry, A.N., Ryan, J.J., Eren, E., Levy, J.B., Pusey, C.D., Lightstone, L., and Lechler, R.I. (2001). In Goodpasture's disease, CD4+ T cells escape thymic deletion and are reactive with the autoantigen α3 (IV) NC1. Journal of the American Society of Nephrology *12*, 1908-1915.

Samuel, T.K., Sinclair, J.W., Pinter, K.L., and Hamza, I. (2014). Culturing Caenorhabditis elegans in Axenic Liquid Media and Creation of Transgenic Worms by Microparticle Bombardment. e51796.

Seeman, J.I. (1983). Effect of conformational change on reactivity in organic chemistry. Evaluations, applications, and extensions of Curtin-Hammett Winstein-Holness kinetics. Chemical Reviews *83*, 83-134.

Shi, R., Hu, C., Yuan, Q., Yang, T., Peng, J., Li, Y., Bai, Y., Cao, Z., Cheng, G., and Zhang, G. (2011). Involvement of vascular peroxidase 1 in angiotensin II-induced vascular smooth muscle cell proliferation. Cardiovasc Res *91*, 27-36.

Soltani, A., Muller, H.K., Sohal, S.S., Reid, D.W., Weston, S., Wood-Baker, R., and Walters, E.H. (2012). Distinctive characteristics of bronchial reticular basement membrane and vessel remodelling in chronic obstructive pulmonary disease (COPD) and in asthma: they are not the same disease. Histopathology *60*, 964-970.

Song, J.J., Guyette, J.P., Gilpin, S.E., Gonzalez, G., Vacanti, J.P., and Ott, H.C. (2013). Regeneration and experimental orthotopic transplantation of a bioengineered kidney. Nat Med *19*, 646-651.

Soudi, M., Paumann-Page, M., Delporte, C., Pirker, K.F., Bellei, M., Edenhofer, E., Stadlmayr, G., Battistuzzi, G., Boudjeltia, K.Z., Furtmuller, P.G.*, et al.* (2015). Multidomain human peroxidasin 1 is a highly glycosylated and stable homotrimeric high spin ferric peroxidase. J Biol Chem *290*, 10876-10890.

Soudi, M., Zamocky, M., Jakopitsch, C., Furtmuller, P.G., and Obinger, C. (2012). Molecular evolution, structure, and function of peroxidasins. Chem Biodivers *9*, 1776-1793.

Srivastava, A. (2014). Determination of minor and trace elements concentration in kidney stones using elemental analysis techniques (Paper 7304: Missouri S&T).

Sullivan, S., Salapow, M.A., Breen, R., and Broide, D.H. (1994). Eosinophil Peroxidase Differs from Neutrophil Myeloperoxidase in Its Ability to Bind Antineutrophil Cytoplasmic Antibodies Reactive with Myeloperoxidase. International Archives of Allergy and Immunology *105*, 150-154.

Sundaramoorthy, M., Meiyappan, M., Todd, P., and Hudson, B.G. (2002). Crystal Structure of NC1 Domains: STRUCTURAL BASIS FOR TYPE IV COLLAGEN ASSEMBLY IN BASEMENT MEMBRANES. Journal of Biological Chemistry *277*, 31142-31153.

Sutton, C., Brereton, C., Keogh, B., Mills, K.H., and Lavelle, E.C. (2006). A crucial role for interleukin (IL)-1 in the induction of IL-17–producing T cells that mediate autoimmune encephalomyelitis. The Journal of experimental medicine *203*, 1685-1691.

Tabb, D.L., Fernando, C.G., and Chambers, M.C. (2007). MyriMatch: highly accurate tandem mass spectral peptide identification by multivariate hypergeometric analysis. Journal of Proteome Research *6*, 654-661.

Than, M.E., Henrich, S., Huber, R., Ries, A., Mann, K., Kühn, K., Timpl, R., Bourenkov, G.P., Bartunik, H.D., and Bode, W. (2002). The 1.9-Å crystal structure of the noncollagenous (NC1) domain of human placenta collagen IV shows stabilization via a novel type of covalent Met-Lys cross-link. Proceedings of the National Academy of Sciences *99*, 6607-6612.

Thorning, D., and Vracko, R. (1977). Renal glomerular basal lamina scaffold: embryologic development, anatomy, and role in cellular reconstruction of rat glomeruli injured by freezing and thawing. Lab Invest *37*, 105-119.

Trautner, M., and Wieth, J.O. (1968a). Renal excretion of chloride, bromide and thiocyanate during water diuresis. Acta Physiol Scand *74*, 606-615.

Trautner, M., and Wieth, J.O. (1968b). Renal excretion of chloride, bromide and thiocyanate during water diuresis. Acta physiologica Scandinavica *74*, 606-615.

Tsuge, K., Kataoka, M., and Seto, Y. (2000). Cyanide and thiocyanate levels in blood and saliva of healthy adult volunteers. Journal of Health Science *46*, 343-350.

Uauy, R., Olivares, M., and Gonzalez, M. (1998). Essentiality of copper in humans. The American journal of clinical nutrition *67*, 952S-959S.

van Leeuwen, F.R., Sangster, B., and Hildebrandt, A.G. (1987). The toxicology of bromide ion. CRC Critical Reviews in Toxicology *18*, 189-213.

van Leeuwen, F.X., and Sangster, B. (1987). The toxicology of bromide ion. Critical reviews in toxicology *18*, 189-213.

Van Logten, M.J., Wolthuis, M., Rauws, A.G., Kroes, R., Den Tonkelaar, E.M., Berkvens, H., and Van Esch, G.J. (1974). Semichronic toxicity study of sodium bromide in rats. Toxicology *2*, 257-267.

Vanacore, R., Ham, A.J., Voehler, M., Sanders, C.R., Conrads, T.P., Veenstra, T.D., Sharpless, K.B., Dawson, P.E., and Hudson, B.G. (2009). A sulfilimine bond identified in collagen IV. Science *325*, 1230-1234.

Vanacore, R., Pedchenko, V., Bhave, G., and Hudson, B.G. (2011). Sulphilimine cross-links in Goodpasture's disease. Clin Exp Immunol *164 Suppl 1*, 4-6.

Vanacore, R.M., Ham, A.J., Cartailler, J.P., Sundaramoorthy, M., Todd, P., Pedchenko, V., Sado, Y., Borza, D.B., and Hudson, B.G. (2008). A role for collagen IV cross-links in conferring immune privilege to the Goodpasture autoantigen: structural basis for the crypticity of B cell epitopes. J Biol Chem *283*, 22737-22748.

Velden, J., Paust, H.J., Hoxha, E., Turner, J.E., Steinmetz, O.M., Wolf, G., Jabs, W.J., Ozcan, F., Beige, J., Heering, P.J.*, et al.* (2012). Renal IL-17 expression in human ANCA-associated glomerulonephritis. Am J Physiol Renal Physiol *302*, F1663-1673.

Vracko, R. (1974). Basal lamina scaffold-anatomy and significance for maintenance of orderly tissue structure. Am J Pathol *77*, 314-346.

Walker, F. (1972a). Basement-membrane turnover in the rat. The Journal of pathology *107*, 119-121.

Walker, F. (1972b). Basement-membrane turnover in man. The Journal of pathology *107*, 123-125.

Walker, F. (1973). The origin, turnover and removal of glomerular basement-membrane. The Journal of pathology *110*, 233-244.

Wallaeys, B., Cornelis, R., Mees, L., and Lameire, N. (1986). Trace elements in serum, packed cells, and dialysate of CAPD patients. Kidney Int *30*, 599-604.

Walser, M., and Rahill, W.J. (1966a). Renal tubular reabsorption of bromide compared with chloride. Clinical Science (London) *30*, 191-205.

Walser, M., and Rahill, W.J. (1966b). Renal tubular reabsorption of bromide compared with chloride. Clin Sci *30*, 191-205.

Wang, X., Harris, R.E., Bayston, L.J., and Ashe, H.L. (2008). Type IV collagens regulate BMP signalling in Drosophila. Nature *455*, 72-77.

Watt, F.M., and Huck, W.T. (2013). Role of the extracellular matrix in regulating stem cell fate. Nature Reviews Molecular Cell Biology *14*, 467-473.

Weber, M., and Pullig, O. (1992). Different immunologic properties of the globular NC1 domain of collagen type IV isolated from various human basement membranes. Eur J Clin Invest *22*, 138-146.

Weber, S., Dolz, R., Timpl, R., Fessler, J.H., and Engel, J. (1988). Reductive cleavage and reformation of the interchain and intrachain disulfide bonds in the globular hexameric domain NC1 involved in network assembly of basement membrane collagen (type IV). Eur J Biochem *175*, 229-236.

Weber, S., Engel, J., Wiedemann, H., Glanville, R.W., and Timpl, R. (1984). Subunit structure and assembly of the globular domain of basement-membrane collagen type IV. Eur J Biochem *139*, 401-410.

Weiss, S.J., Test, S.T., Eckmann, C.M., Roos, D., and Regiani, S. (1986). Brominating oxidants generated by human eosinophils. Science *234*, 200-203.

Weng, Y.C., Sonni, A., Labelle-Dumais, C., de Leau, M., Kauffman, W.B., Jeanne, M., Biffi, A., Greenberg, S.M., Rosand, J., and Gould, D.B. (2012). COL4A1 mutations in patients with sporadic late-onset intracerebral hemorrhage. Ann Neurol *71*, 470-477.

Wolf, R.L., and Eadie, G.S. (1950a). Reabsorption of bromide by the kidney. American Journal of Physiology *163*, 436-441.

Wolf, R.L., and Eadie, G.S. (1950b). Reabsorption of bromide by the kidney. Am J Physiol *163*, 436-441.

Woods, A.E., Carlton, R.F., Casto, M.E., and Gleason, G.I. (1979). Environmental bromine in freshwater and freshwater organisms: factors affecting bioaccumulation. Bulletin of environmental contamination and toxicology *23*, 179-185.

Yan, X., Sabrautzki, S., Horsch, M., Fuchs, H., Gailus-Durner, V., Beckers, J., Hrabe de Angelis, M., and Graw, J. (2014). Peroxidasin is essential for eye development in the mouse. Hum Mol Genet *23*, 5597-5614.

Yang, R., Hellmark, T., Zhao, J., Cui, Z., Segelmark, M., Zhao, M.-h., and Wang, H.-y. (2007a). Antigen and Epitope Specificity of Anti–Glomerular Basement Membrane Antibodies in Patients with Goodpasture Disease with or without Anti-Neutrophil Cytoplasmic Antibodies. Journal of the American Society of Nephrology *18*, 1338-1343.

Yang, R., Hellmark, T., Zhao, J., Cui, Z., Segelmark, M., Zhao, M.H., and Wang, H.Y. (2007b). Antigen and epitope specificity of anti-glomerular basement membrane antibodies in patients with goodpasture disease with or without anti-neutrophil cytoplasmic antibodies. J Am Soc Nephrol *18*, 1338-1343.

Young, P.R., and Hsieh, L.-S. (1978). General base catalysis and evidence for a sulfurane intermediate in the iodine oxidation of methionine. Journal of the American Chemical Society *100*, 7121-7122.

Yurchenco, P.D. (2011). Basement Membranes: Cell Scaffoldings and Signaling Platforms. Cold Spring Harbor Perspectives in Biology *3*.

Zhavoronkov, A.A., Kakturskii, L.V., Anke, M., Groppel, B., and Mikhaleva, L.M. (1996). [Pathology of congenital bromine deficit (experimental observation)]. Arkh Patol *58*, 62-67.

Zou, J., Henderson, L., Thomas, V., Swan, P., Turner, A.N., and Phelps, R.G. (2007). Presentation of the Goodpasture autoantigen requires proteolytic unlocking steps that destroy prominent T cell epitopes. J Am Soc Nephrol *18*, 771-779.